THE KINETICS AND THERMODYNAMICS OF CLAY MINERAL REACTIONS

by
John Alan Chermak

Dissertation submitted to the Faculty of
Virginia Polytechnic Institute and State University
in partial fulfillment of the requirements of the degree of
DOCTOR OF PHILOSOPHY
In
Geology

APPROVED:

J. D. Rimstidt, Chairman

L. W. Zelazny

J. R. Craig

R. J. Bodnar

S. C. Eriksson

November, 1989
Blacksburg, Virginia

ABSTRACT

The diagenesis of rocks during burial occurs in response to changing temperature, pressure, and solution composition. Due to their geologic abundance, high surface area, and reactivity clay minerals are important participants in the diagenesis of clastic rocks. The kinetic and thermodynamic stability of clays is in general poorly understood. This dissertation research measured the rate of transformation of kaolinite to muscovite/illite and developed a method to estimate clay mineral thermodynamic stability.

Clastic rock diagenesis is controlled by the rates of silicate mineral growth and transformation. Marine mudstones commonly contain large proportions of kaolinite which reacts during diagenesis to form muscovite/illite and/or chlorite. Batch reactor experiments were used to measure the reaction rate of 1.5 kaolinite + K^+ = muscovite + H^+ + 1.5 H_2O using the initial rate method and a fitted form of the integrated rate equation. Experiments were performed at temperatures ranging from 250° to 307°C with solutions of 0.5 - 2.0 m KCl. These results can then be extrapolated to diagenetic temperatures using the Arrhenius equation.

In addition, a technique was developed to estimate the ΔG_f^o and ΔH_f^o of silicate minerals. Silicate minerals have been shown to act as a combination of basic polyhedral units (Hazen 1985 and 1988). This work showed that their thermodynamic properties could be modeled as the sum of polyhedral contributions. A multiple linear regression model was used to find the contribution of the oxide and hydroxide components (g_i and h_i) to the ΔG_f^o and ΔH_f^o of a selected group of aluminosilicate minerals at 298 K. The ΔG_f^o and ΔH_f^o of other silicate minerals can be estimated from a weighted sum of the contribution of each oxide and hydroxide component (g_i and h_i). These results can be

also used to estimate the ΔG_f^o of silicate minerals at higher temperatures (up to ≈600 K) by using the equation,

$$g_i(T) = h_i(298) - T\left(\frac{h_i(298) - g_i(298)}{298}\right).$$

ACKNOWLEDGEMENTS

I would like to express my gratitude and appreciation to my major advisor and friend, Dr. J. Donald Rimstidt for his help, encouragement, and guidance throughout my years at Virginia Polytechnic Institute and State University. Appreciation also goes to my committee members Dr. Lucian Zelazny (Dr. Z), Dr. Susan Eriksson, Dr. Bob Bodnar and Dr. Jim Craig for their review of this dissertation and helpful comments. A special thanks also goes to for his mechanical expertise and patience.

A project such as this can not be accomplished alone so I have many friends and colleagues to be grateful to, it is not possible to list them all, but many deserve recognition. Special thanks go to a few good friends in the geology department, whose presence and encouragement helped me keep my "sanity", they are ,

, , , ,

, , , , , and .

Good friends and drinking buddies I met while at VPI&SU include ,

, , , , ,

, , , , and as well as all the guys from the Greeks and Ruminators softball teams. Friends met throughout my academic career (all 22 years worth) include , ,

, , , , , , ,

, and . A special friend who taught me how to love and appreciate life and whose memory will never be forgotten is the late .

This research was supported by the Petroleum Research Fund (PRF # 18852-AC2), administered by the American Chemical Society, ARCO Oil and Gas Company, The

Geological Society of America, and the Grant-in-Aid of Research Program administered by the Scientific Reserch Society of Sigma Xi.

I am indebted to my family including my father , my mother , my brother , my sister , and my grandparents and , and and for their support throughout my academic career and all phases of this study, their numerous sacrifices throughout the years have made this work possible. My dissertation is dedicated to them.

TABLE OF CONTENTS

THE HYDROTHERMAL TRANSFORMATION RATE OF KAOLINITE TO MUSCOVITE/ILLITE 1
Abstract 2
Introduction 3
Experimental 6
Results 10
Discussion 35
Applications 39
Conclusions 43

ESTIMATING THE THERMODYNAMIC PROPERTIES (ΔG_f^o and ΔH_f^o) OF SILICATE MINERALS AT 298 K FROM THE SUM OF POLYHEDRAL CONTRIBUTIONS 46
Abstract 47
Introduction 48
Methods 50
Results 52
Discussion 56
Conclusions 67

ESTIMATING ΔG_f^o OF SILICATE MINERALS AT HIGH TEMPERATURES FROM THE SUM OF POLYHEDRAL CONTRIBUTIONS 71
Abstract 72
Introduction 73
Methods 73
Results 76
Discussion 79
Conclusions 83
REFERENCES 88
APPENDIX I 98

APPENDIX II 112
VITA 114

LIST OF FIGURES

Figure 1. Marine mudstone mineral abundance in % versus temperature. 4
Figure 2. 50 ml titanium hydrothermal reactor vessel. 7
Figure 3a. SEM photograph of starting Georgia kaolinite. 8
Figure 3b. SEM photograph of starting Indian Ruby muscovite. 9
Figure 4. Gamma plotted as a function of ionic strength. 14
Figure 5. Hydrogen ion concentration versus time at 289°C. 16
Figure 6. Two SEM photographs of product muscovite/illite. 17
Figure 7. Log r versus log m_{K+} at 250°C, 275°C, 289°C, and 307°C. 22
Figure 8. Ln k_+ versus 1/T. 24
Figure 9. Log K versus 1/T for the kaolinite/muscovite equilibrium. 26
Figure 10. Ln (K-Q) versus time at 289°C. 29
Figure 11. Ln k_- versus 1/T. 31
Figure 12. Log r versus log A_{Musc}. 34
Figure 13. Plot of kaolinite weight % versus reaction time at 300°C. 36
Figure 14. SEM photograph of iron bearing muscovite/illite product. 37
Figure 15. Time constant versus 1/T. 42
Figure 16. Log r versus 1/T. 44
Figure 1. Graph of the g_i versus ΔG_f^o at 298 K. 60
Figure 2. Graph of the h_i versus ΔH_f^o at 298 K. 61
Figure 3. Clay activity-activity diagram of the K_2O-Al_2O_3-SiO_2-H_2O system at 298 K. 66
Figure 4. Zeolite activity-activity diagram of the K_2O-Al_2O_3-SiO_2-H_2O system at 298 K. 68
Figure 1. Graph of the g_i versus ΔG_f^o at 600 K. 82
Figure 2. Clay activity-activity diagram of the K_2O-Al_2O_3-SiO_2-H_2O system at 400 K. 85
Figure 3. Clay activity-activity diagram of the K_2O-Al_2O_3-SiO_2-H_2O system at 448 K. 86

LIST OF TABLES

Table 1. Concentration and pH versus time. 11
Table 2. Gamma as a function of pH. 15
Table 3a. ICP results for the kaolinite to muscovite reaction. 18
Table 3b. ICP results for the kaolinite dissolution reaction. 20
Table 4. The fitted polynomial equation for the concentration versus time data. 21
Table 5. Forward rate constants. 23
Table 6. Ln (K-Q) versus time. 27
Table 7. Reverse rate constants. 30
Table 8. The effect of varying surface area on the rate of reaction. 32
Table 9. K as compared to k_+/k_-. 40
Table 1. Minerals used in the multiple linear regression model 51
Table 2. Values of g_i and h_i. 53
Table 3. Minerals in the model ΔG_f^o (measured) as compared to ΔG_f^o (predicted) at 298 K. 54
Table 4. Minerals in the model ΔH_f^o (measured) as compared to ΔH_f^o (predicted) at 298 K. 55
Table 5a. Minerals not in the model ΔG_f^o and ΔH_f^o (calorimetry) as compared to ΔG_f^o and ΔH_f^o (predicted) at 298 K. 57
Table 5b. Minerals not in the model ΔG_f^o (solubility) as compared to ΔG_f^o (predicted) at 298 K. 58
Table 6. ΔG_f^o and ΔH_f^o oxide or hydroxide as compared to g_i and h_i. 59
Table 7. Method of estimation. 63
Table 8. Data used for activity diagram calculations. 65
Table 1. The $g_i(T)$ for individual polyhedra components. 77
Table 2a, b. Measured ΔG_f^o versus predicted ΔG_f^o at 400, 500, and 600 K. . . . 78
Table 3. High temperature estimation method. 80
Table 4. ΔG_f^o oxide or hydroxide as compared to g_i at 400, 500, and 600 K. . . 81
Table 5. Data used for activity diagram calculations. 84

THE HYDROTHERMAL TRANSFORMATION RATE OF KAOLINITE TO MUSCOVITE/ILLITE

ABSTRACT

Batch reactor experiments were performed to measure the rate of the reaction:

$$1.5 \text{ kaolinite} + K^+ = \text{muscovite} + H^+ + 1.5 \text{ water}$$

at temperatures ranging from 250 to 307°C . In these experiments, the rate of kaolinite conversion to muscovite/illite was monitored as the rate of production of H^+. Runs were performed in small volume (50 ml) titanium hydrothermal reactors charged with well crystalline Georgia kaolinite, Indian Ruby muscovite, and 25 ml of KCl solution (0.5 - 2.0 m). Both solids and solutions were monitored at specific intervals throughout each experiment. The determined rate law is:

$$\left(\frac{dm_{H^+}}{dt}\right) = -\left(\frac{dm_{K^+}}{dt}\right) = \left[\frac{A_M}{M}\right](k_+ m_{K^+} - k_- m_{H^+})$$

where m_{K+} and m_{H+} are the concentrations of potassium ion and hydrogen ion, k_+ and k_- are the forward and reverse rate constants in kg m^{-2} sec^{-1}, A_M is the total surface area of the muscovite in m^2, and M is the mass of the solution in kg.

The initial rate method was used to find k_+, and k_- was found by fitting data to an integrated rate equation. Temperature functions for the rate constants are:

$$\ln k_+ = 12.90 - (1.87 \times 10^4/T), R^2 = 0.98, \text{ and}$$

$$\ln k_- = 6.03 - (1.21 \times 10^4/T), R^2 = 0.95$$

The activation energies (E_a) for the forward and reverse reaction are 155 ± 15 kJ mol^{-1} and 101 ± 10 kJ mol^{-1} respectively.

INTRODUCTION

When sandstones and mudstones are buried, diagenetic mineral transformations occur in response to the increased temperatures. Figure 1 shows schematically a compilation of observations of the diagenetic transformations expected in an average marine mudstone. Note that detrital kaolinite comprises ≈25% of these rocks at low temperatures and that an important fate of this kaolinite is its transformation to illite and eventually to phengite. The rate of transformation of kaolinite to muscovite/illite is the topic of this study. Field evidence for the kaolinite to illite transformation is discussed by Kulbicki and Millot (1969) and an overview of this process is found in Kisch (1983).

For a detailed discussion of the mineralogical differences, occurrences, and abundance of muscovite versus illite see Bailey (1988). In this paper muscovite is defined as a 2:1 phyllosilicate with substitution of aluminum for silica in the tetrahedral sheet. The charge deficiency that develops is then satisfied by potassium ions in the interlayer (K^+ = 1.0 per unit cell). Illite is defined as a 2:1 phyllosilicate with substitution in either the octahedral (iron or magnesium for aluminum) and/or the tetrahedral sheet (aluminum for silica). The resulting charge deficiency is then satisfied by potassium ion in the interlayer (K^+ = 0.7-0.9 per unit cell). As the grain size of muscovite decreases interlayer potassium decreases (K^+ = 0.7-0.9 per unit cell) and the mineral approaches the composition of an illite. Thus, in the pure K_2O - Al_2O_3 - SiO_2 -H_2O system (conditions of the experiments) muscovite and illite appear to be indistinguishable minerals and will be grouped as muscovite/illite.

The nature and rate of clay mineral reactions influence the generation and migration of petroleum and other basinal fluids, contribute to the formation of sedimentary ore deposits, and often control the composition of aqueous pore fluids which drive other diagenetic reactions. Many field studies have identified possible clay reactions which are

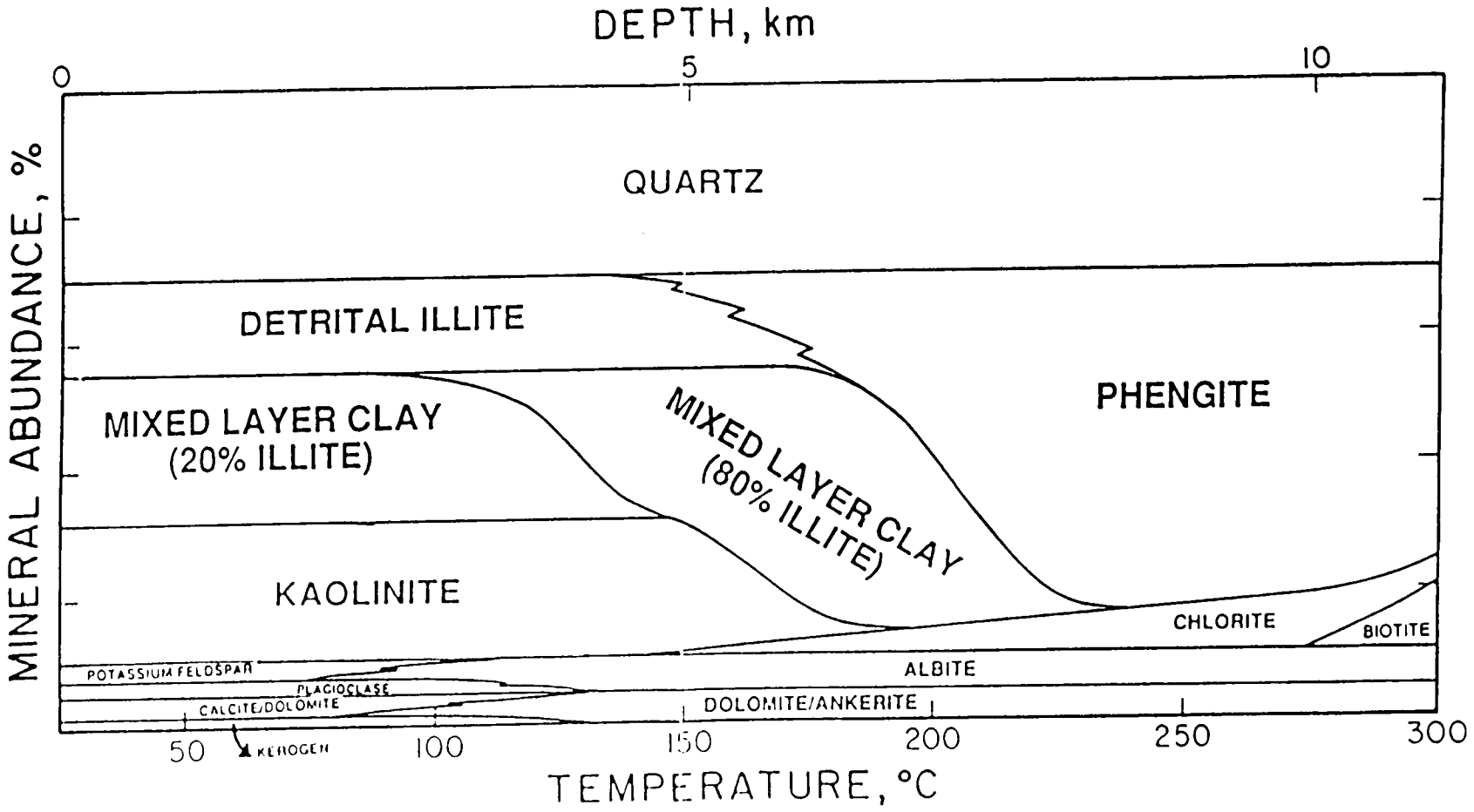

FIG. 1. A schematic diagram of mineral abundance in % versus temperature for a typical marine mudstone illustrating the diagenetic transformations that occur during burial diagenesis.

important in diagenetic regimes (Boles and Franks, 1979; Curtis, 1978; Helmhold and van de Kamp, 1985; Hutcheon et al., 1980). Despite attempts to use the mineralogy and distribution of clay minerals as indicators of paleotemperature or fluid flow, very little is known about the fundamental controls of clay mineral reaction types and rates because of the complex geochemistry of both the solid and fluid phases in natural systems.

Studies of clay mineral synthesis and transformation for conditions relating to diagenesis are mostly qualitative (DeKimpe and Gastuche, 1964; Hiltabrand et al., 1973; Dunoyer de Segonzac, 1970; Harder, 1978). There are only a few studies that have determined reaction kinetics (Bethke and Altaner, 1986; Eberl and Hower, 1976; Huang et al., 1986; Howard and Roy, 1985; Roberson and Lahann, 1981; Whitney and Northrop, 1988) and these concentrate on the smectite to illite reaction.

The equilibrium thermodynamics of the K_2O-Al_2O_3-SiO_2-H_2O system have been studied by Hess (1966), Hemley (1959), Giggenbach (1985), and Aargaard and Helgeson (1985). Associated phase diagrams and stability relations at temperatures up to 600°C are discussed, but, due to the very slow reaction rates of silicate minerals at low temperatures, equilibrium in rocks is rarely attained in nature. Therefore reaction kinetics must be considered in any models of burial diagenesis.

There are three fundamental types of equipment to perform rate experiments: batch reactors, plug flow reactors, and mixed flow reactors (Levenspiel, 1972; Hill, 1977, and Rimstidt and Dove, 1986). This study used batch reactor experiments to determine the transformation rate of kaolinite to muscovite/illite. In these experiments kaolinite ($Al_2Si_2O_5(OH)_4$) dissolves and muscovite/illite precipitates. We have determined the rate of transformation of kaolinite to muscovite/illite at temperatures of 250-307°C for varying KCl concentrations (0.5 - 2.0 m). The overall reaction is:

$$K^+ + 1.5\ Al_2Si_2O_5(OH)_4 = KAl_3S_3O_{10}(OH)_2 + H^+ + 1.5\ H_2O \qquad (1).$$

EXPERIMENTAL

Experiments were run in small volume (50 ml) titanium hydrothermal reactors (Figure 2). Several reactors were loaded with charges, sealed, and placed onto a rotisserie unit (≈2.5 rpm) inside a oven set at the desired run temperature. Individual reactors were removed at specific intervals, quenched in cold water and opened. Reaction times varied from 0.25 to 264 hours. The solution pH was measured at 25°C using a Ross combination pH electrode and the solids were separated from the solution by centrifugation and then decantion. The solids were washed with distilled/deionized water. The solids (both reactants and products) were characterized and analyzed by scanning electron microscopy and x-ray diffraction (suction on ceramic). Concentrations of Si^{4+} and Al^{3+} in run solutions were determined by inductively coupled plasma spectrophotometry (Sequential Jarrell-Ash Atomscan 2400).

Each reactor was charged with 0.25-4.0 grams of well crystalline Georgia kaolinite (description in van Olphen and Fripiat, 1979), obtained from the Clay Mineral Society, Indian Ruby muscovite (0.25-2.0 grams), and 25 ml of KCl solution (0.5-2.0 m) prepared from reagent grade KCl added to distilled/deionized water. Muscovite was added to insure that nucleation processes were not rate limiting. The specific surface area of reactants was calculated from a three point N_2 desorption BET isotherm determined using a Quantasorb surface area analyzer. The specific surface area (A_{sp}) for the kaolinite is 9.2 m^2/g and is 1.20 m^2/g for muscovite. The reactants were X-rayed to confirm purity. Figures 3a and b are scanning electron microscope (SEM) photographs of the starting kaolinite and muscovite.

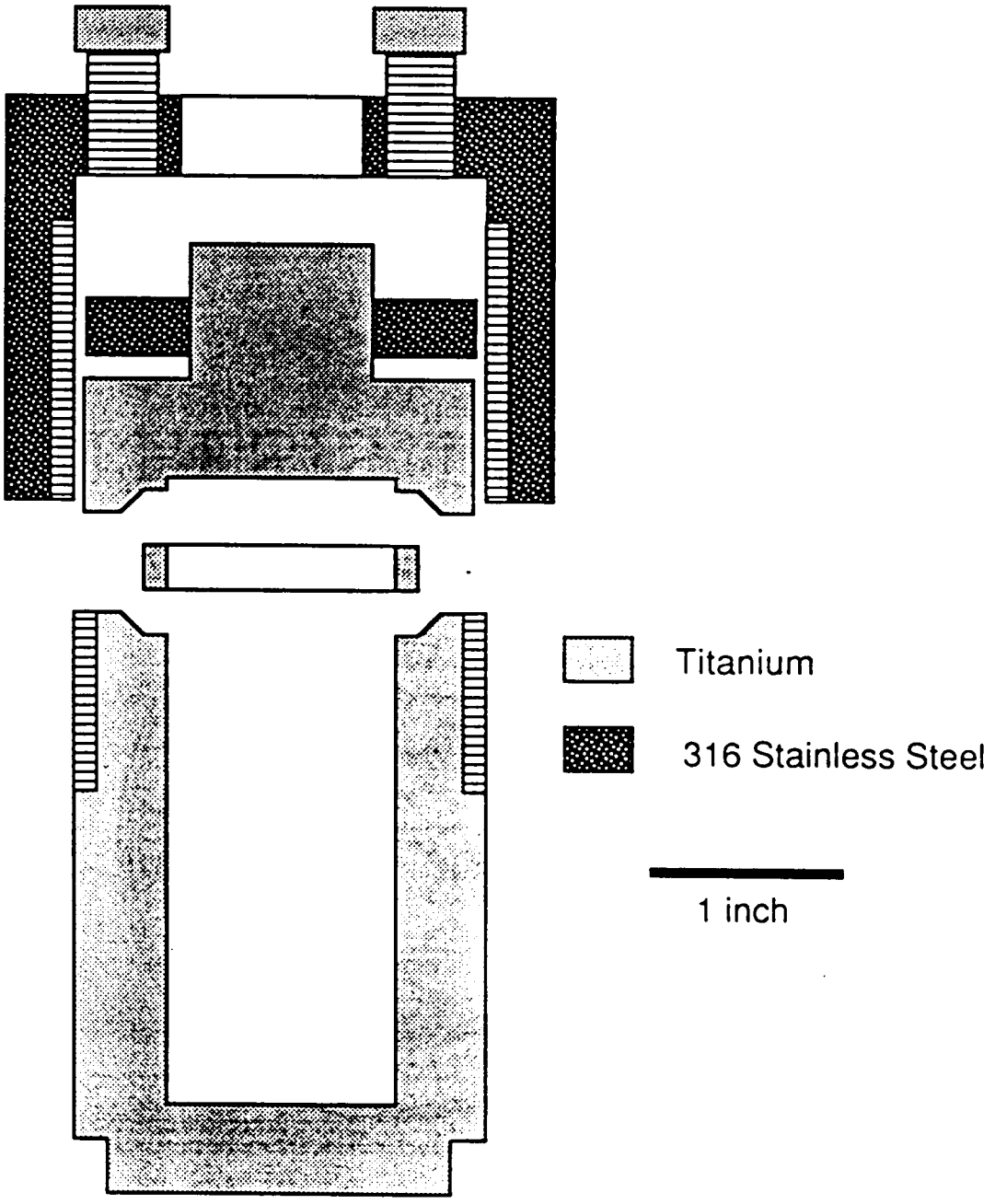

FIG. 2. Diagram of the 50 ml hydrothermal reactor vessel used for hydrothermal experiments. Notice that the body, seal, and head are made of titanium, and the thrust ring and cap are made of 316 stainless steel.

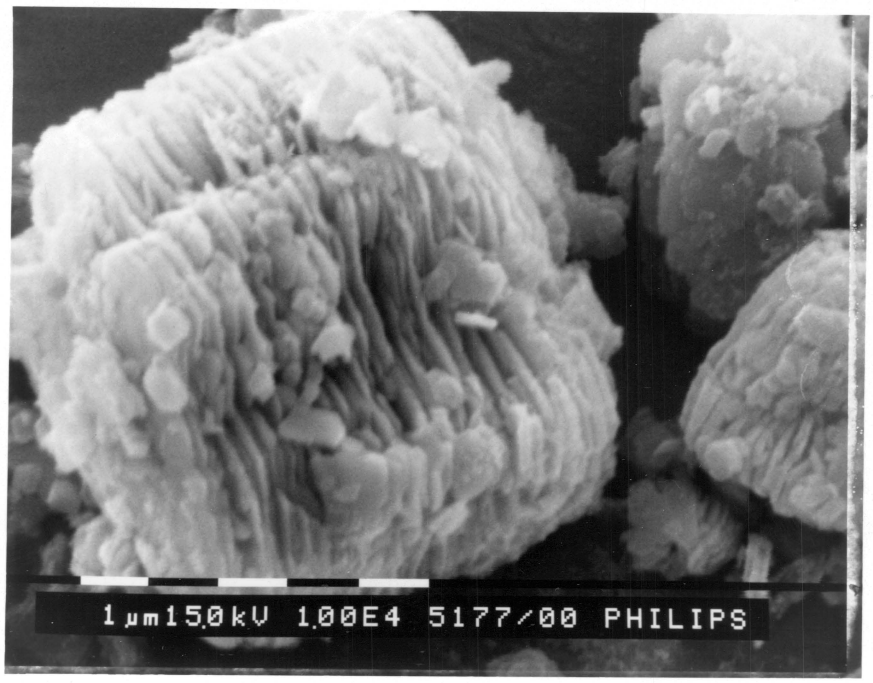

FIG. 3a. SEM photograph of well crystalline Georgia kaolinite run material; scale bar = 1 µm. Note the book-like morphology.

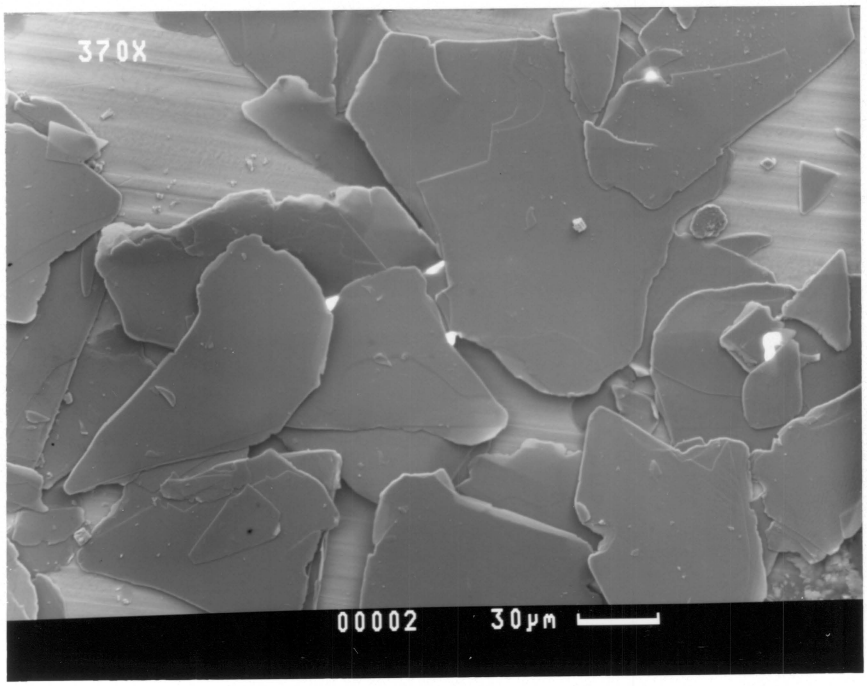

FIG. 3b. SEM photograph of Indian Ruby muscovite run material; scale bar = 30 µm. Note the typical platy nature.

RESULTS

Table 1 gives the pH versus time data collected at 250, 275, 290, and 307°C for eight experiments charged with 0.25 grams muscovite and 1.0 gram of kaolinite. The measured a_{H+} data were converted to m_{H+} by using the relation $a = m\gamma$ where a is the activity of H^+, m is the concentration of H^+ (moles/kg), and γ is the activity coefficient. γ was determined by preparing solutions of known m_{H+} (0.1 - 0.0001) and adding to these solutions known weights of KCl to produce solutions whose ionic strengths were equal to 0.5, 1.0, 2.0, and 4.0. The pH of these solutions was measured and gamma (γ) calculated. Figure 4 shows γ plotted versus ionic strength. pH was then found as function of γ at known KCl concentrations to enable the conversion of a_{H^+} to m_{H^+}. The fitted equations, shown in Table 2, are only valid at ionic strengths from 0.25 to 4.0. The m_{H^+} values in Table 1 were calculated from the γ's found by solving these equations. Figure 5 shows m_{H+} versus time for 2.0, 1.0, and 0.5 m experiment at 289°C.

At specific intervals throughout the experiment individual bombs were removed from the oven, opened, and their contents analyzed. X-ray diffraction analysis was used to confirm the presence of only kaolinite and muscovite/illite in the run solids. Figure 6 shows two SEM photographs of the muscovite/illite products showing textures similar to that of "hairy illite" (Bailey 1988). The presence of "hairy illite" at all temperatures was confirmed by SEM .

Silica and aluminum concentrations in selected runs were determined using a sequential inductively coupled plasma spectrophotometer (Atomscan 2400). Table 3a gives time, temperature, KCl, aluminum, and silica concentrations for four experiments. This table shows that silica and aluminum concentrations generally increase through time, with the aluminum data being a bit erratic. This increase in silica and aluminum concentrations can

Table 1. Concentration and pH versus time data at the run temperature and KCl concentration.

TIME hours	m_{KCl} molal	QUENCH pH	m_{H^+} molal
	250°C		
2.25	2.0	3.48	3.73×10^{-4}
5.75	2.0	3.43	4.14×10^{-4}
17.75	2.0	3.20	6.75×10^{-4}
92.75	2.0	2.95	1.16×10^{-3}
188.00	2.0	2.77	1.71×10^{-3}
264.75	2.0	2.70	1.99×10^{-3}
5.75	0.5	3.62	3.52×10^{-4}
92.75	0.5	3.42	5.44×10^{-4}
264.75	0.5	3.31	6.91×10^{-4}
	275°C		
2.00	2.0	3.41	4.32×10^{-4}
4.00	2.0	3.31	5.34×10^{-4}
7.08	2.0	3.21	6.60×10^{-4}
10.00	2.0	3.10	8.36×10^{-4}
13.00	2.0	3.02	9.93×10^{-4}
23.50	2.0	2.86	1.40×10^{-3}
29.92	2.0	2.82	1.53×10^{-3}
*167.50	2.0	2.40	3.86×10^{-3}
*217.25	2.0	2.32	4.60×10^{-3}
2.92	0.5	3.67	3.16×10^{-4}
4.50	0.5	3.58	3.84×10^{-4}
7.17	0.5	3.50	4.57×10^{-4}
10.92	0.5	3.43	5.32×10^{-4}
20.66	0.5	3.37	6.07×10^{-4}
118.00	0.5	3.12	1.05×10^{-3}

	289°C		
0.25	2.0	3.52	3.43×10^{-4}
2.00	2.0	3.22	6.46×10^{-4}
3.50	2.0	3.10	8.36×10^{-4}
4.00	2.0	3.11	8.18×10^{-4}
5.00	2.0	3.03	9.72×10^{-4}
7.75	2.0	2.95	1.16×10^{-4}
11.08	2.0	2.84	1.47×10^{-3}
23.00	2.0	2.64	2.27×10^{-3}
72.00	2.0	2.21	5.88×10^{-3}
72.00	2.0	2.20	6.02×10^{-3}
*167.75	2.0	2.06	8.23×10^{-3}
1.00	1.0	3.64	3.14×10^{-4}
3.92	1.0	3.36	5.73×10^{-4}
6.00	1.0	3.28	6.81×10^{-4}
9.08	1.0	3.16	8.84×10^{-4}
20.50	1.0	3.01	1.23×10^{-3}
31.00	1.0	2.89	1.60×10^{-3}
71.50	1.0	2.65	2.71×10^{-3}
*167.00	1.0	2.45	4.23×10^{-3}
*167.00	1.0	2.43	4.42×10^{-3}
1.50	0.5	3.64	3.37×10^{-4}
4.50	0.5	3.38	5.94×10^{-4}
8.87	0.5	3.26	7.71×10^{-4}
11.50	0.5	3.24	8.06×10^{-4}
22.25	0.5	3.18	9.19×10^{-4}
71.50	0.5	2.93	1.59×10^{-3}
167.00	0.5	2.77	2.29×10^{-3}
167.00	0.5	2.76	2.31×10^{-3}

		307°C	
2.50	2.0	3.08	8.73×10^{-4}
3.75	2.0	3.02	9.93×10^{-4}
5.00	2.0	2.94	1.18×10^{-3}
6.75	2.0	2.70	1.99×10^{-3}
8.00	2.0	2.58	2.59×10^{-3}
12.00	2.0	2.44	3.53×10^{-3}
20.25	2.0	2.18	6.29×10^{-3}
61.00	2.0	1.91	1.15×10^{-2}
*118.50	2.0	1.80	1.48×10^{-2}

* extent of reaction too great to be used in initial rate determination of k'_{+}.

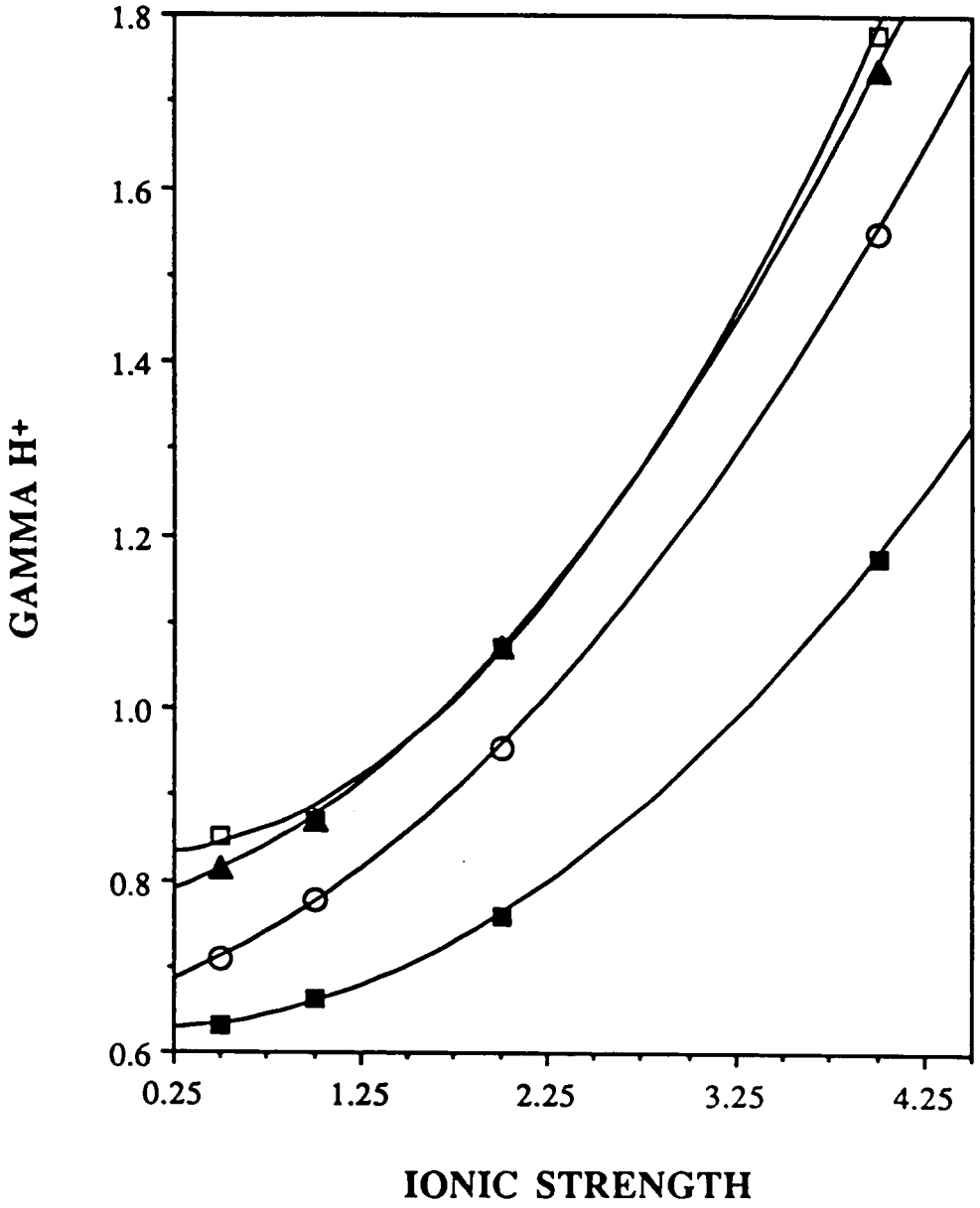

FIG. 4. Gamma (γ) plotted as a function of ionic strength at known hydrogen ion concentrations (open squares, $m_{H+} = 0.1$, solid triangles, $m_{H+} = 0.01$, open circles, $m_{H+} = 0.001$, and solid squares, $m_{H+} = 0.0001$). The determined polynomial equations are:
$\gamma = 0.625 - 2.52 \times 10^{-3} (I) + 3.50 \times 10^{-2} (I)^2$, $R^2 = 1.00$ for $m_{H+} = 0.0001$
$\gamma = 0.665 + 7.01 \times 10^{-2} (I) + 3.78 \times 10^{-2} (I)^2$, $R^2 = 1.00$ for $m_{H+} = 0.001$
$\gamma = 0.772 + 5.48 \times 10^{-3} (I) + 4.67 \times 10^{-2} (I)^2$, $R^2 = 1.00$ for $m_{H+} = 0.01$
$\gamma = 0.829 - 2.91 \times 10^{-3} (I) + 6.01 \times 10^{-2} (I)^2$, $R^2 = 1.00$ for $m_{H+} = 0.1$.

Table 2. The four equations used to determine gamma (γ) from a measured pH in a solution of known ionic strength.

$\gamma = 0.897 - 0.029\ (pH) - 0.00839\ (pH)^2$ for 0.5 m with an $R^2 = 0.99$
$\gamma = 0.837 + 0.063\ (pH) - 0.0254\ (pH)^2$ for 1.0 m with an $R^2 = 0.99$
$\gamma = 1.001 + 0.114\ (pH) - 0.0422\ (pH)^2$ for 2.0 m with an $R^2 = 1.00$
$\gamma = 1.714 + 0.138\ (pH) - 0.0699\ (pH)^2$ for 4.0 m with an $R^2 = 1.00$

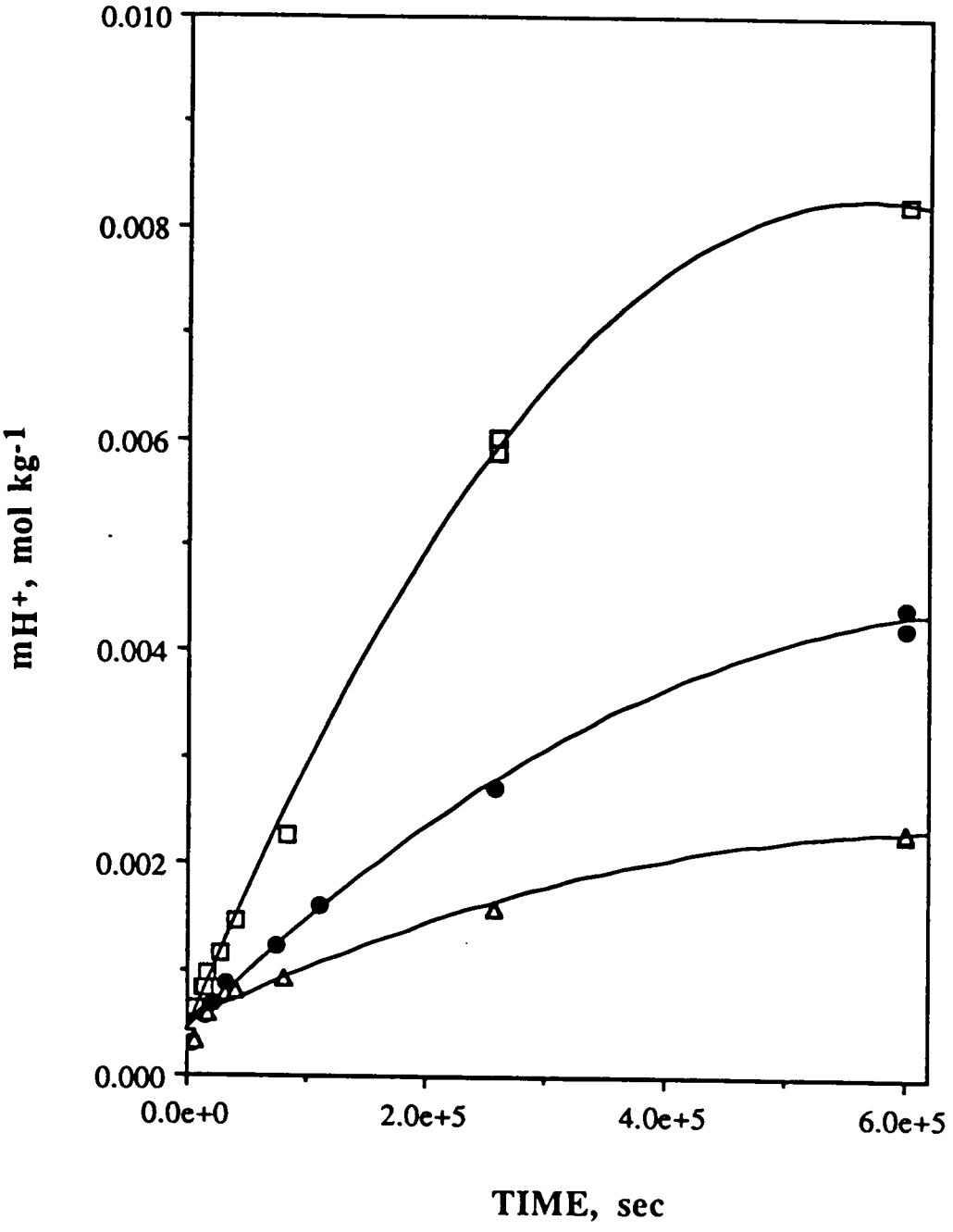

FIG. 5. A plot of hydrogen ion concentration versus time for experiments performed at 289°C with KCl concentrations of 2.0 m (open squares), 1.0 m (solid circles), and 0.5 m (open triangles).

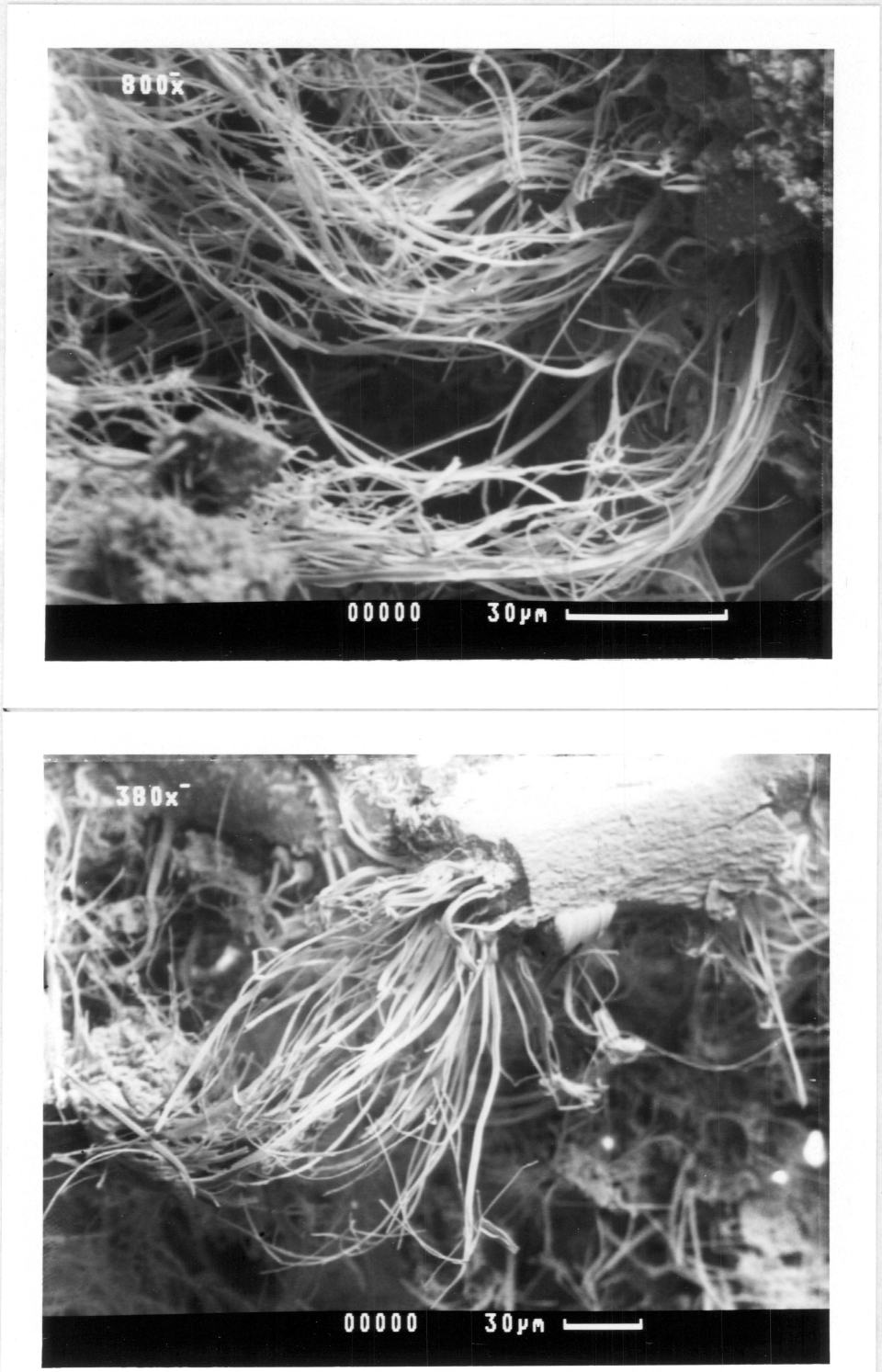

FIG. 6. SEM photographs of product muscovite/illite at two magnifications; scale bar = 30 µm. This experiment was run at 289°C, with 2 m KCl for 72 hours. Notice the fibrous nature of the muscovite/illite.

Table 3a. Time, temperature, KCl, aluminum, and silica concentrations for reaction (1), 1.5 kaolinite + K^+ = muscovite + H^+ + 1.5 water.

TIME hours	KCl molal	ALUMINUM ppm	SILICA ppm
		289°C	
1.50	0.50	0.114	137.9
4.50	0.50	0.457	174.6
8.87	0.50	0.535	190.6
11.50	0.50	0.164	178.0
22.25	0.50	0.354	204.0
71.50	0.50	0.610	215.4
1.00	1.0	0.383	133.2
3.92	1.0	0.409	192.1
6.00	1.0	0.485	200.8
9.08	1.0	0.648	213.2
20.50	1.0	0.612	231.0
31.00	1.0	0.736	230.2
71.50	1.0	0.674	254.4
167.00	1.0	0.843	268.8
0.25	2.0	0.524	141.1
2.00	2.0	0.643	206.4
4.00	2.0	0.827	220.4
7.75	2.0	0.827	240.6
11.08	2.0	0.961	261.6
23.00	2.0	1.208	274.4
72.00	2.0	1.831	285.8
167.75	2.0	2.428	320.4
		307°C	
3.75	2.0	3.220	279.0
12.00	2.0	4.422	357.8
20.25	2.0	4.144	371.6
118.50	2.0	6.500	368.4

be explained by simple dissolution of kaolinite partly in response to decreasing pH. Changing silica and aluminum concentrations had no direct effect on the rate interpretation because of their narrow range compared to orders of magnitude variation in hydrogen ion concentration. Table 3b gives time, temperature, pH, aluminum, and silica concentrations as a function of time for the simple dissolution of kaolinite reaction (m_{H^+} = 0.1, 0.01, and 0.001) at 289°C. Notice the increase in silica concentration and the erratic aluminum behavior as well as the constant solution pH with time.

The very small extent of reaction that occurred in these experiments is best quantified by monitoring solution chemistry. Analysis of m_{H^+} versus time data for rate determination was done by using both the initial rate method and an integrated form of the rate equation to determine k'_+ and k'_-, the apparent forward and reverse rate constants, respectively. Using the initial rate method, k'_+ was determined by fitting a polynomial equation of the form $m_{H^+} = a + bt + ct^2$; the equation was differentiated to give $dm_{H^+}/dt = b + 2ct$. The initial rate (dm_{H^+}/dt at time = 0) equals b. Results of this analysis are given in Table 4. A plot of log r versus log m_{K^+} (Figure 7) reveals that the reaction is first order (n = 0.9 - 1.0) in potassium ion. At log m_{K^+} = 0, log r = log k'_+ and k'_+ can then be converted to the forward rate constant k_+ by adjusting the results by a surface area (A) per mass of solution (M) term (Rimstidt and Barnes 1980). In our experiments the forward rate constant depends only on the surface area of muscovite (A_M) because it is much smaller than the surface area of kaolinite; this will be demonstrated later. Therefore $k'_+ = (A_M/M)\, k_+$, and $A_M/M = 12\ m^2\ kg^{-1}$. The forward rate constants for a system with a surface area of one square meter of muscovite and a one kilogram mass of solution are shown in Table 5. Figure 8 is an Arrhenius plot which reveals an activation energy (E_a) of 155 ± 15 kJ mol^{-1} for the forward reaction.

Table 3b. Time, temperature, KCl, aluminum, and silica concentrations for the dissolution of kaolinite at varying m_{H^+}.

TIME hours	m_{H^+} molal	QUENCH pH	ALUMINUM ppm	SILICA ppm
		289°C		
3.83	0.001	3.33	0.396	144.4
23.00	0.001	3.34	0.627	150.9
69.50	0.001	3.33	0.298	170.1
3.00	0.01	2.16	3.740	171.8
24.0	0.01	2.16	2.520	197.8
3.00	0.1	1.14	23.74	171.8
24.00	0.1	1.16	21.22	229.0
48.00	0.1	1.21	20.14	228.4

TABLE 4. The fitted polynomial equation and R^2 for each concentration versus time experiment. The b term is equal to the initial rate.

250°C, 2.0 m KCl
$m_{H^+} = 3.37 \times 10^{-4} + 7.55 \times 10^{-10}\, t - 4.01 \times 10^{-16}\, t^2$ $R^2 = 1.00$
250°C, 0.5 m KCl
$m_{H^+} = 4.01 \times 10^{-4} + 2.65 \times 10^{-9}\, t - 1.04 \times 10^{-15}\, t^2$ $R^2 = 0.99$
275°C, 2.0 m KCl
$m_{H^+} = 2.92 \times 10^{-4} + 1.72 \times 10^{-8}\, t - 5.15 \times 10^{-14}\, t^2$ $R^2 = 1.00$
275°C, 0.5 m KCl
$m_{H^+} = 3.06 \times 10^{-4} + 5.00 \times 10^{-9}\, t - 7.66 \times 10^{-15}\, t^2$ $R^2 = 0.99$
289°C, 2.0 m KCl
$m_{H^+} = 4.79 \times 10^{-4} + 2.34 \times 10^{-8}\, t - 9.01 \times 10^{-15}\, t^2$ $R^2 = 1.00$
289°C, 1.0 m KCl
$m_{H^+} = 3.72 \times 10^{-4} + 1.30 \times 10^{-8}\, t - 1.54 \times 10^{-14}\, t^2$ $R^2 = 0.99$
289°C, 0.5 m KCl
$m_{H^+} = 4.92 \times 10^{-4} + 5.52 \times 10^{-9}\, t - 4.19 \times 10^{-15}\, t^2$ $R^2 = 0.99$
307°C, 2.0 m KCl
$m_{H^+} = -3.80 \times 10^{-4} + 1.06 \times 10^{-7}\, t - 2.36 \times 10^{-13}\, t^2$ $R^2 = 1.00$

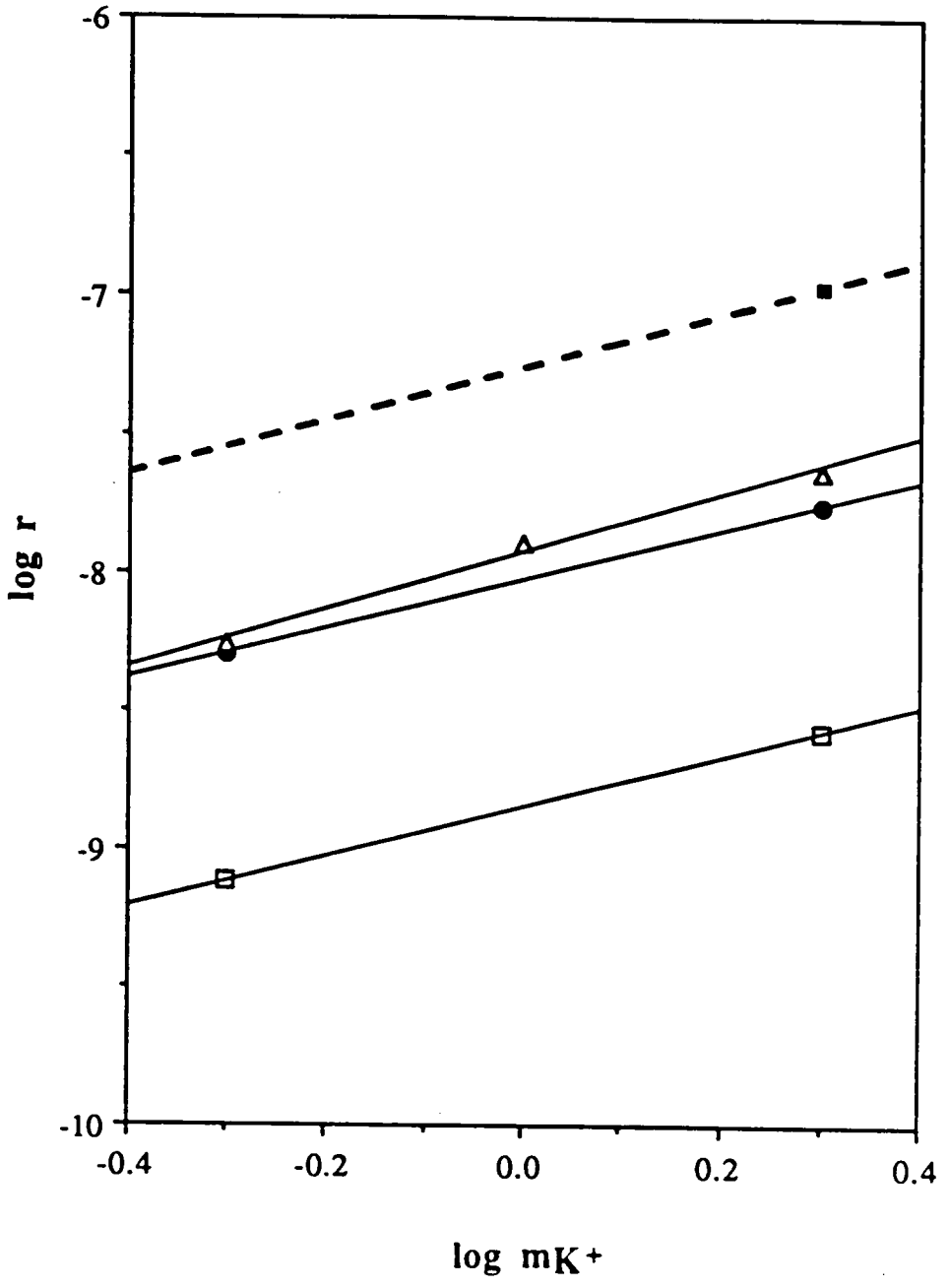

FIG. 7. Log r versus log m_{K+} at 250°C (open squares), 275°C (solid circles), 289°C (open triangles), and 307°C (solid squares). The fitted equations are $\log k'_{+} = -8.85 + 0.9 \log m_{K+}$ at 250°C, $\log k'_{+} = -8.03 + 0.9 \log m_{K+}$ at 275°C, $\log k_{+} = -7.92 + 1.0 \pm 0.1 \log m_{K+}$ at 289°C. The error calculated in the 289°C equation is the standard error of the reaction order (n).

Table 5. Forward rate constants k_+ and ln k_+ at temperature.

TEMP °C	k_+ sec^{-1}	ln k_+
250	$1.18 \pm 0.12 \times 10^{-10}$	-22.86
275	$7.78 \pm 0.80 \times 10^{-10}$	-20.97
289	$1.00 \pm 0.10 \times 10^{-9}$	-20.72
307	$4.48 \pm 0.30 \times 10^{-9}$	-19.22

Errors associated with k_+ are standard errors of the b term in the polynomial fit.

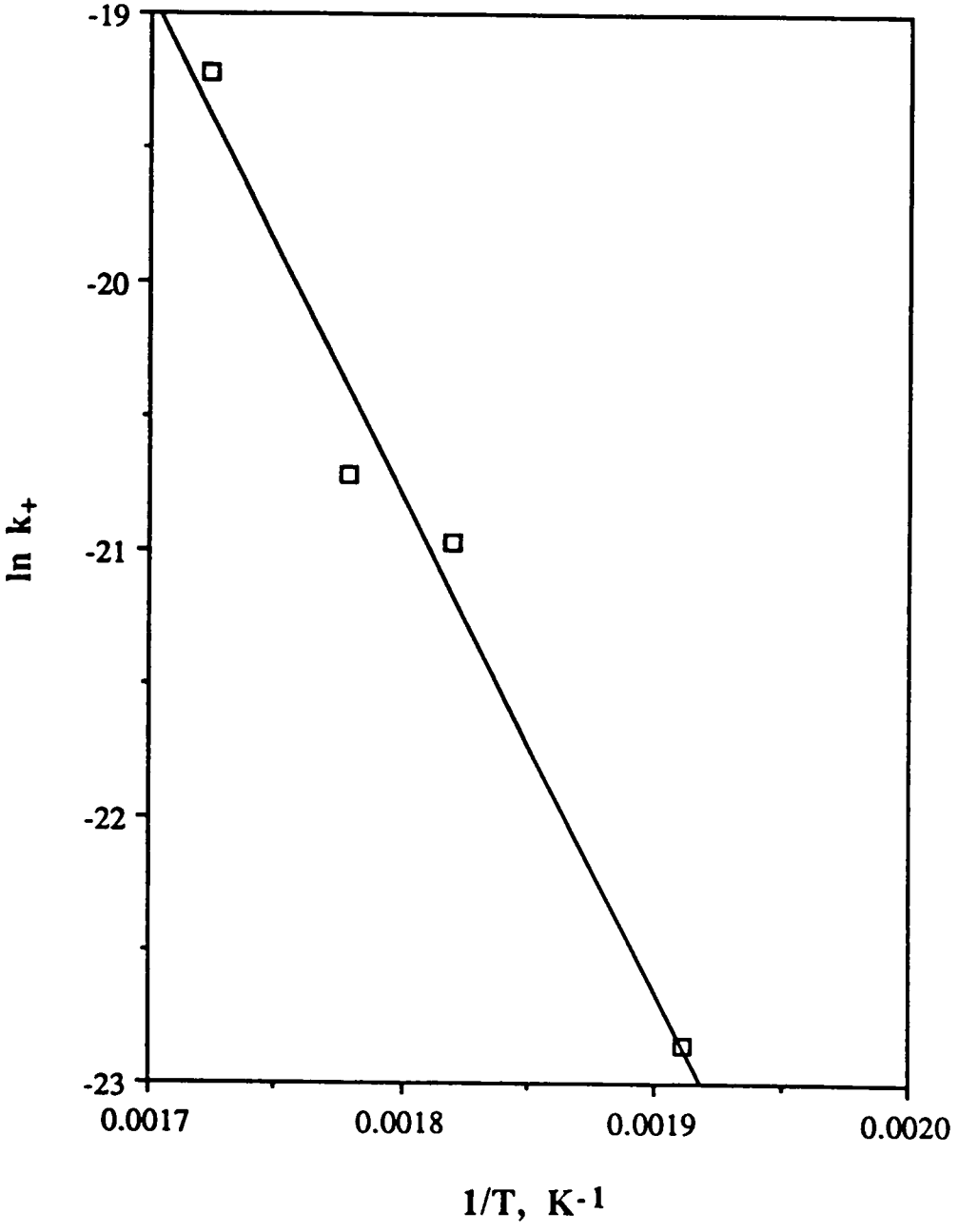

FIG. 8. Arrhenius plot showing ln k_+ versus 1/T for the data from the kaolinite to muscovite/illite reactions. The 307°C value was calculated from the measured 2.0 m point using a slope equal to one. The function relating k_+ to T is ln $k_+ = 12.90 - (1.87 \times 10^4/T)$ with an $R^2 = 0.98$.

In order to determine k_-', plots of ln (K - Q) versus time were constructed where K is the equilibrium m_{H^+}/m_{K^+} ratio, and Q is the ratio of m_{H^+}/m_{K^+} at time, t. The justification of this analysis is given in the discussion section. The choice of K was based on Hemley's (1959) measurement of the conditions for kaolinite/muscovite equilibrium. His data for 200 to 300°C were fit to an equation (Figure 9), where $\log K = 2.74 - (2798/T)$. Hemley observed that changing pressure had little effect on the equilibrium m_{H^+}/m_{K^+} ratio. The equilibrium m_{H^+}/m_{K^+} quotient is an approximate expression of K which should be a_{H^+}/a_{K^+}, but Hemley showed that this ratio is independent of KCl concentrations (0.65 - 4.0 m). Thus, the activity coefficient quotient $\gamma_{H^+}/\gamma_{K^+}$ appears to be nearly one within the range of the ionic strengths of these experiments. Thus the concentration ratios, K' and Q', are numerically equivalent to activity ratios K and Q. Table 6 gives the ln (K - Q) values as a function of time as well as the determined linear equations (with the associated R^2) where the slopes of these linear functions are equal to k_-'. A plot of ln (K - Q) versus T at 289°C and 1.0 and 0.5 m KCl is shown in Figure 10. The reverse rate constant (k_-) was determined by the relation $k_-' = (A_M/M)\, k_-$. The values of k_- for a system with a surface area of one square meter of muscovite and a one kilogram mass of solution are given in Table 7. Figure 11 is an Arrhenius plot for k_- showing that $E_a = 101 \pm 10$ kJ mol^{-1} for the reverse reaction.

The surface areas of both kaolinite and muscovite were varied to determine their effect on the rate. Table 8 lists pH and m_{H^+} versus time data from five experiments at 289°C and 2.0 m KCl with varying surface areas of muscovite and kaolinite. These experiments were short term and the results were analyzed by the initial rate method. The equation and R^2 for each polynomial fit is given in Table 8; the b term is equal to the initial rate (time = 0). Their was no effect on the rate of the reaction when the surface area, A_K, of kaolinite was varied from 2.30 to 36.84 m^2 (log rate = -7.56 ± 0.07). Changing the surface area,

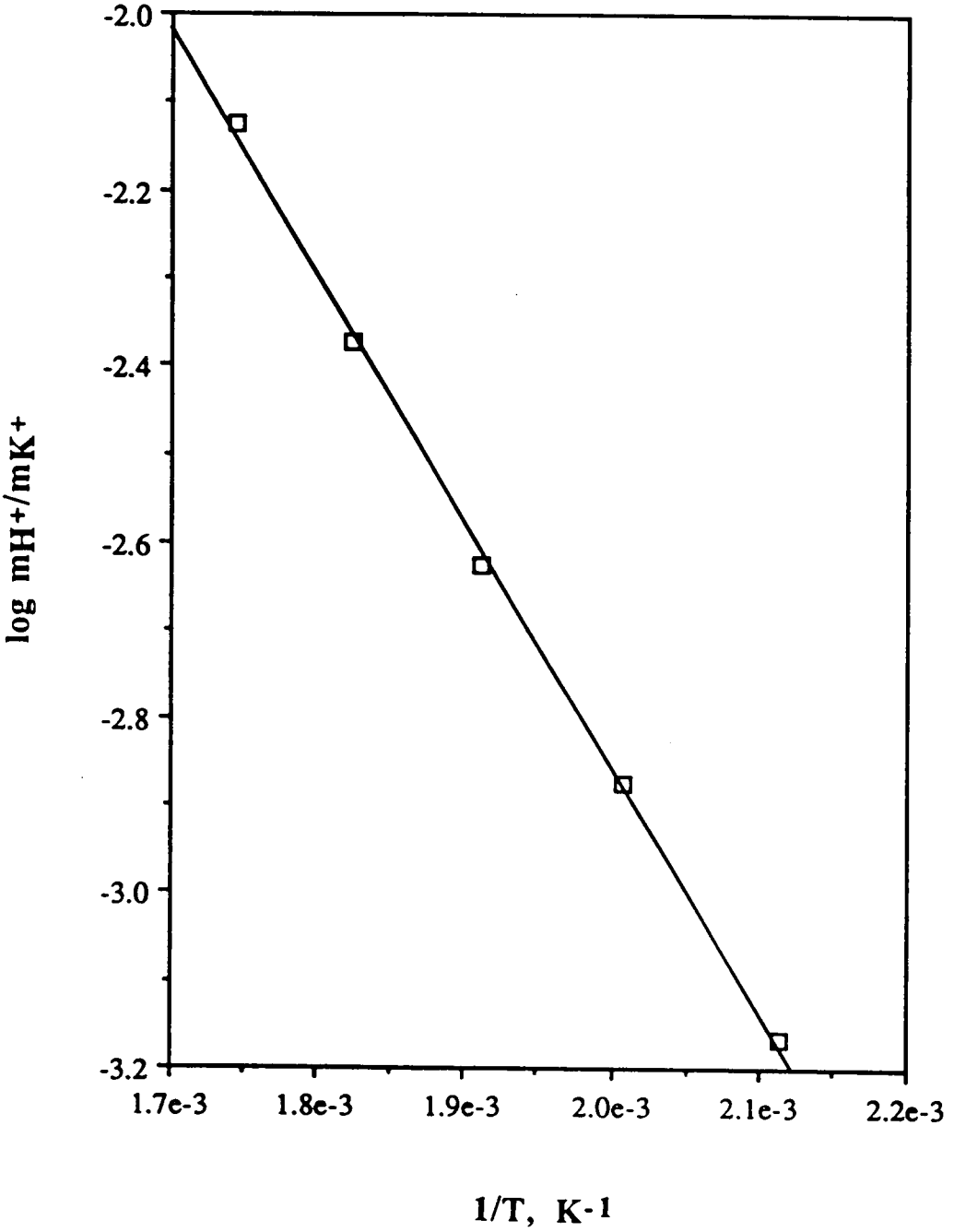

FIG. 9. Hemley's (1959) values for log K plotted versus 1/T for the kaolinite/muscovite equilibrium. The best fit equation is log K = 2.74 - (2798/T) with an $R^2 = 1.00$.

Table 6. Values of ln (K-Q) versus time at temperature and KCl concentration: straight line equations, R^2, and k' is the slope.

TIME hours	KCl molal	ln (K-Q)
	250°C	
2.25	2.0	-6.11
5.75	2.0	-6.12
17.75	2.0	-6.18
92.75	2.0	-6.31
188.00	2.0	-6.47
264.75	2.0	-6.57
$\ln (K-Q) = -6.13 - 4.80 \times 10^{-7}\ t$		$R^2 = 0.99$
5.75	0.5	-6.38
92.75	0.5	-6.64
264.75	0.5	-6.89
$\ln (K-Q) = -6.41 - 5.29 \times 10^{-7}\ t$		$R^2 = 0.97$
	275°C	
2.00	2.0	-5.51
4.00	2.0	-5.52
7.08	2.0	-5.54
10.00	2.0	-5.56
13.00	2.0	-5.58
23.50	2.0	-5.64
29.92	2.0	-5.66
167.50	2.0	-6.06
217.25	2.0	-6.23
$\ln (K-Q) = -5.53 - 8.97 \times 10^{-7}\ t$		$R^2 = 0.99$
2.92	0.5	-5.62
4.50	0.5	-5.66
7.17	0.5	-5.70
10.92	0.5	-5.74
20.66	0.5	-5.79
118.0	0.5	-6.13
$\ln (K-Q) = -5.66 - 1.13 \times 10^{-6}\ t$		$R^2 = 0.96$

289°C

0.25	2.0	-5.19
2.00	2.0	-5.22
3.50	2.0	-5.23
4.00	2.0	-5.23
5.00	2.0	-5.25
7.75	2.0	-5.26
11.08	2.0	-5.29
23.00	2.0	-5.38
72.00	2.0	-5.87
72.00	2.0	-5.90
167.75	2.0	-6.42

$\ln (K-Q) = -5.22 - 2.13 \times 10^{-6} t$ $R^2 = 0.98$

1.00	1.0	-5.21
3.92	1.0	-5.26
6.00	1.0	-5.28
9.08	1.0	-5.33
20.50	1.0	-5.40
31.00	1.0	-5.48
71.50	1.0	-5.80
167.00	1.0	-6.49
167.00	1.0	-6.62

$\ln (K-Q) = -5.23 - 2.20 \times 10^{-6} t$ $R^2 = 1.00$

1.50	0.5	-5.28
4.50	0.5	-5.39
8.87	0.5	-5.47
11.50	0.5	-5.49
22.25	0.5	-5.54
71.50	0.5	-5.96
167.00	0.5	-6.75
167.00	0.5	-6.78

$\ln (K-Q) = -5.35 - 2.36 \times 10^{-6} t$ $R^2 = 1.00$

307°C

2.50	2.0	-4.85
3.75	2.0	-4.86
5.00	2.0	-4.87
6.75	2.0	-4.93
8.00	2.0	-4.97
12.00	2.0	-5.04
20.25	2.0	-5.28
61.00	2.0	-6.00
118.5	2.0	-7.08

$\ln (K-Q) = -4.81 - 5.35 \times 10^{-6} t$ $R^2 = 1.00$

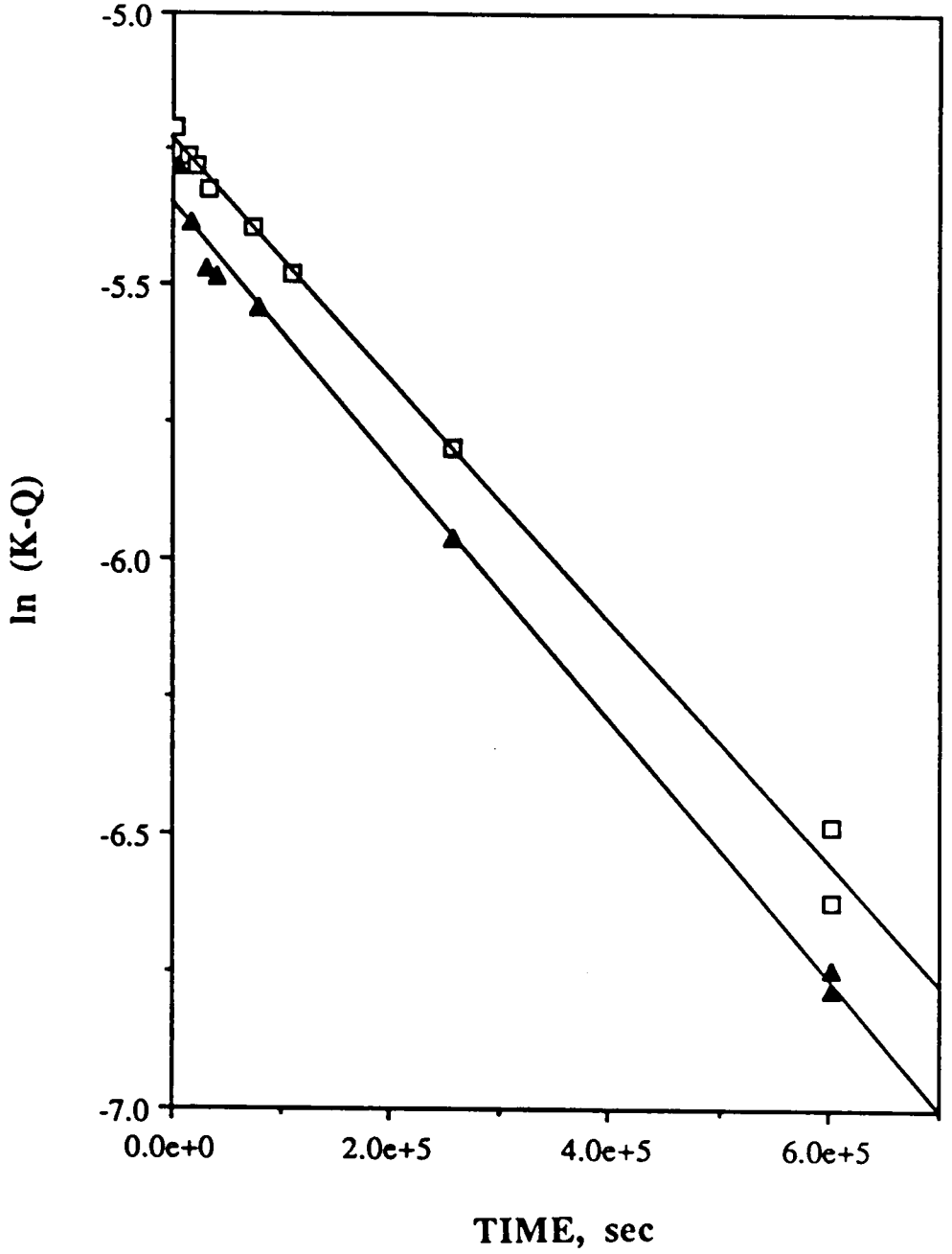

FIG. 10. A sample plot of ln (K-Q) versus time at 289°C and KCl concentrations of 1.0 m (open squares) and 0.5 m (solid triangles). Best fit equations for these data are given in Table 6.

Table 7. Reverse rate constants k_- and ln k_- at temperature.

TEMP °C	k_- sec^{-1}	ln k_-
250	$4.00 \pm 0.24 \times 10^{-8}$	-17.03
250	$4.42 \pm 0.84 \times 10^{-8}$	-16.93
275	$7.50 \pm 0.24 \times 10^{-8}$	-16.41
275	$9.45 \pm 0.94 \times 10^{-8}$	-16.17
289	$1.78 \pm 0.09 \times 10^{-7}$	-15.54
289	$1.83 \pm 0.04 \times 10^{-7}$	-15.51
289	$1.97 \pm 0.05 \times 10^{-7}$	-15.44
307	$4.46 \pm 0.08 \times 10^{-7}$	-14.62

Errors associated with k_- are standard errors of the slope of the linear fit.

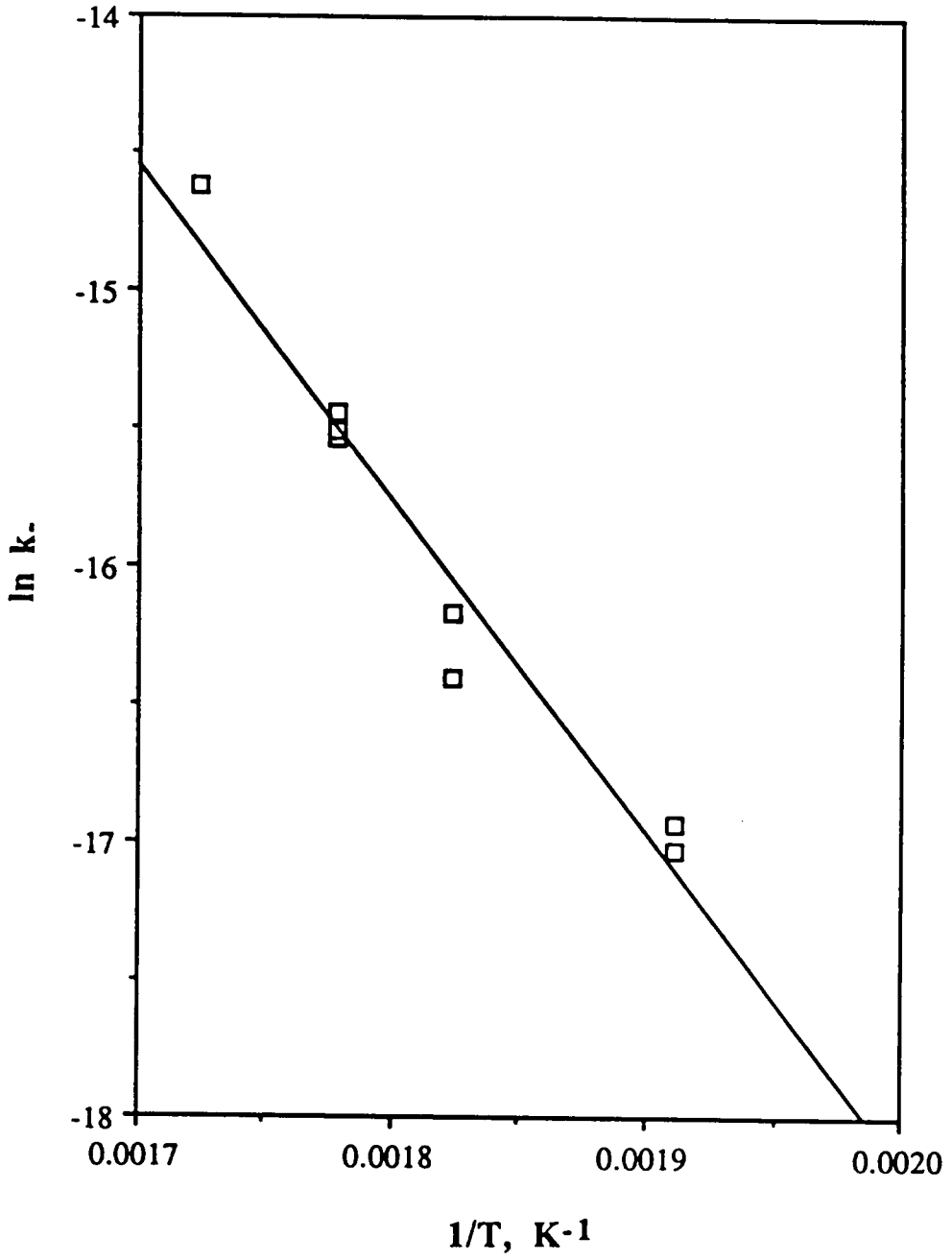

FIG. 11. Arrhenius plot showing ln k_- versus 1/T for the reverse rate constants for the kaolinite to muscovite/illite transformation. The best fit equation is $\ln k_- = 6.03 - (1.21 \times 10^4/T)$ with an $R^2 = 0.95$.

TABLE 8. Concentration and pH versus time data at 289°C and 2.0 m KCl. The best fit polynomial equation and R^2 is also given.

TIME hours	A_K (KAOL) m^2	A_M (MUSC) m^2	QUENCH pH	m_{H^+} moles/kg
3.50	2.30	0.30	3.24	6.195 e-4
5.00	2.30	0.30	3.15	7.508 e-4
7.00	2.30	0.30	3.04	9.510 e-4
9.00	2.30	0.30	2.94	1.180 e-3
20.00	2.30	0.30	2.67	2.126 e-3
$m_{H^+} = 2.26 \times 10^{-4} + 3.10 \times 10^{-8}\ t - 6.38 \times 10^{-14}\ t^2$ $R^2 = 1.00$				
2.00	36.84	0.30	2.92	1.232 e-3
5.00	36.84	0.30	2.79	1.635 e-3
7.00	36.84	0.30	2.78	1.671 e-3
20.00	36.84	0.30	2.52	2.956 e-3
$m_{H^+} = 1.07 \times 10^{-3} + 2.63 \times 10^{-8}\ t - 1.68 \times 10^{-15}\ t^2$ $R^2 = 0.99$				
0.25	9.20	0.30	3.52	3.427 e-4
2.00	9.20	0.30	3.22	6.464 e-4
3.50	9.20	0.30	3.10	8.358 e-4
4.00	9.20	0.30	3.11	8.181 e-4
5.00	9.20	0.30	3.03	9.717 e-4
7.75	9.20	0.30	2.95	1.155 e-3
11.08	9.20	0.30	2.84	1.466 e-3
23.00	9.20	0.30	2.64	2.270 e-3
72.00	9.20	0.30	2.21	5.884 e-3
72.00	9.20	0.30	2.20	6.017 e-3
$m_{H^+} = 4.79$ e-4 $+ 2.34 \times 10^{-8}\ t - 9.01 \times 10^{-15}\ t^2$ $R^2 = 1.00$				
1.75	9.20	1.20	3.11	8.181 e-4
3.50	9.20	1.20	2.77	1.708 e-3
7.75	9.20	1.20	2.49	3.159 e-3
10.75	9.20	1.20	2.46	3.375 e-3
18.00	9.20	1.20	2.28	5.033 e-3
$m_{H^+} = 2.98 \times 10^{-4} + 1.09 \times 10^{-7}\ t - 5.69 \times 10^{-13}\ t^2$ $R^2 = 0.98$				
1.50	9.20	2.40	2.98	1.082 e-3
3.50	9.20	2.40	2.57	2.648 e-3
5.25	9.20	2.40	2.43	3.607 e-3
7.00	9.20	2.40	2.41	3.770 e-3
7.08	9.20	2.40	2.35	4.307 e-3
9.00	9.20	2.40	2.28	5.033 e-3
$m_{H^+} = 5.89 \times 10^{-5} + 2.20 \times 10^{-7}\ t - 2.21 \times 10^{-12}\ t^2$ $R^2 = 0.97$				

A_M, of muscovite from 0.30 to 2.40 m^2 had a large effect on the overall rate (log rate varied -7.63 to -6.66). A plot of log A_M versus log r (Figure 12) shows the linear relationship, log r = -7.06 + 1.08 log A_M with an $R^2 = 1.0$; that is, the transformation rate is directly proportional to A_M. Thus, the transformation rate of kaolinite to muscovite/illite in our experiments depended only on the surface area of muscovite for this range of surface areas (A_M/A_K = 0.3 to 0.008) suggesting that the rate limiting step is associated with the precipitation of muscovite/illite. Note that if $A_K < A_M$, the rate would likely be a function of A_K.

Other rate experiments in the kaolinite-potassium feldspar-muscovite/illite-quartz system were attempted at temperatures ranging from 250-307°C. The first experiment was the reverse reaction, muscovite + H^+ + 1.5 H_2O $\Rightarrow$ kaolinite + K^+. Problems include highly variable quench pH's and the precipitation of potassium feldspar confirmed by x-ray diffraction at 307°C and m_{H^+} = 0.1-0.0001. The latter was a result of rapid dissolution of the kaolinite/muscovite mixture in acid solutions to release dissolved potassium and silica causing the solution compositions to move into the potassium feldspar stability field. Secondly, the rate of the reaction kaolinite + potassium feldspar + 3 H_2O $\Rightarrow$ muscovite + 2 H_4SiO_4 was investigated. These experiments show a drop in pH (2.5-1.5) with time, although according to the equation above, no hydrogen ion should be generated or consumed. This continuous pH drop indicates that the potassium feldspar did not react with H^+ as rapidly as it was released by the kaolinite to muscovite/illite transformation reaction (equation 1), so potassium feldspar dissolution was rate limiting in this experiment. The grain size of potassium feldspar ranged from 590 μm to 20 μm and extensive etch pit development was observed on the feldspar grains. These kaolinite plus potassium feldspar experiments were also run in 316 stainless steel reactors. These experiments showed that the presence of iron leached from the stainless

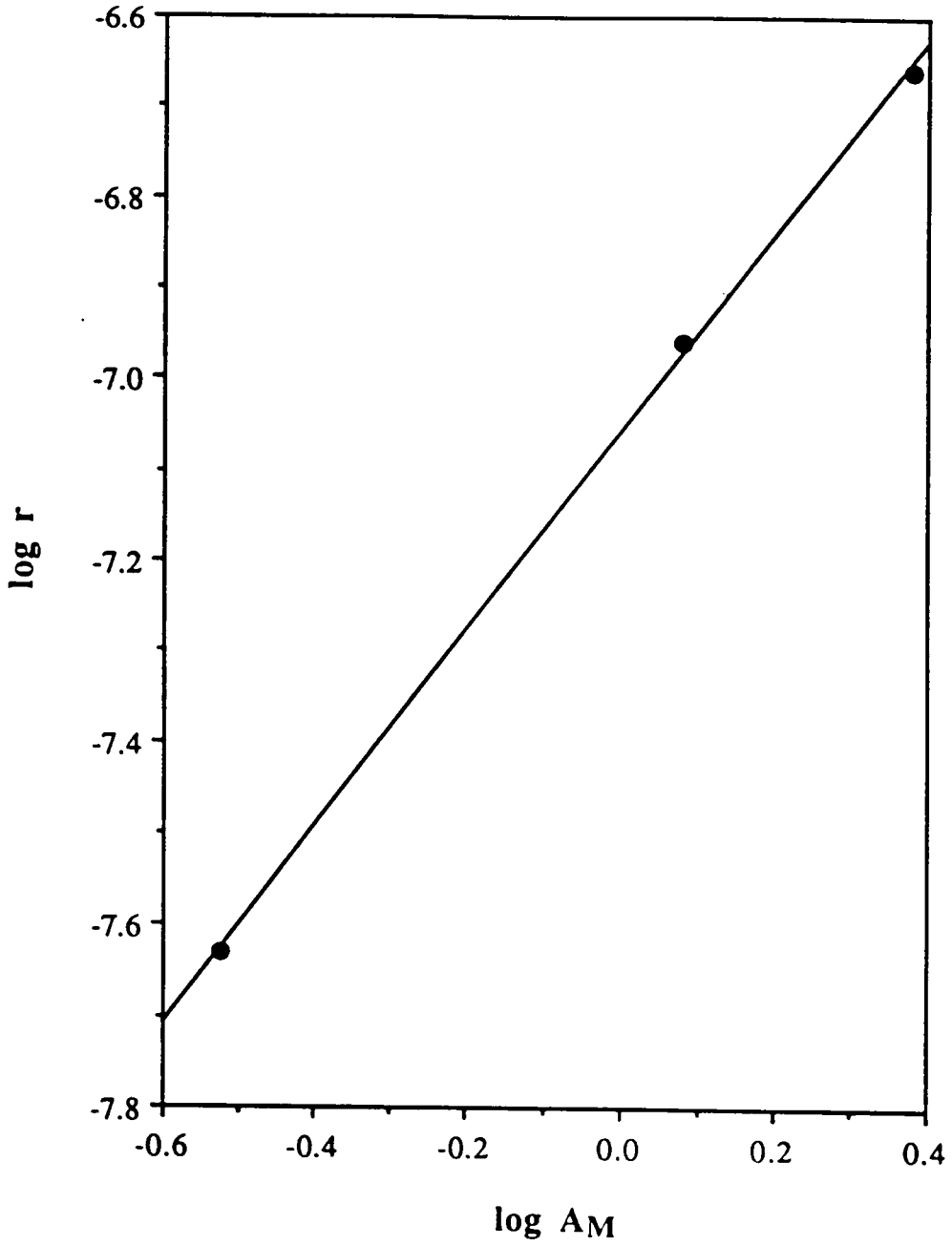

FIG. 12. Plot of log r versus log A_{Musc}. The best fit equation is log r = -7.06 + 1.08 (log A_{Musc}) with an R^2 = 1.00.

steel increased the rate of transformation dramatically. In the stainless steel reactors at 300°C and 2.0 m KCl, the conversion to muscovite/illite was complete in four days while in the titanium bombs nearly 30% kaolinite remained after 20 days (Figure 13). The presence of structural iron in the muscovite/illite product was confirmed by the damping of the 002 muscovite/illite x-ray diffraction peak. SEM observation showed that the product muscovite/illite in these experiments kept the original book-like morphology (Figure 14). Thirdly, the reaction kaolinite + $K^+ \Rightarrow$ muscovite was attempted without using any muscovite seed material. The absence of muscovite led to the nucleation of muscovite/illite as the rate limiting step so the m_{H^+} versus time data could not be fit by a simple polynomial equation. The rate was slow until nucleation occurred, then the rate accelerated as the surface area of the muscovite/illite increased by growth and further nucleation. Finally, the K^+ + 1.5 kaolinite = muscovite + H+ + 1.5 H_2O reaction was investigated at 93°C. After ≈6 months the presence of a fibrous muscovite/illite phase was confirmed by SEM. Data for these experiments are given in Appendix II.

DISCUSSION

The determination of the rate law began with the general form:

$$\left(\frac{dm_{H^+}}{dt}\right) = -\left(\frac{dm_{K^+}}{dt}\right) = \left(k'_{+}(m_{K^+})^n - k'_{-}(m_{H^+})^m\right) \qquad (2)$$

where the reaction orders n and m were unknown. The initial rate assumption is that at early times in the experiment there is no back reaction so the rate can be approximated as $\left(\frac{dm_{H^+}}{dt}\right) = \left(k'_{+}(m_{K^+})^n\right)$. Taking the logarithm of both sides gives

$$\log r = \log k'_{+} + n \log m_{K+} \qquad (3)$$

where r is the rate, k'_{+} is the apparent forward rate constant, n is the reaction order, and m_{K+} is the concentration of potassium ion in moles kg^{-1}. The rate (r) can be determined

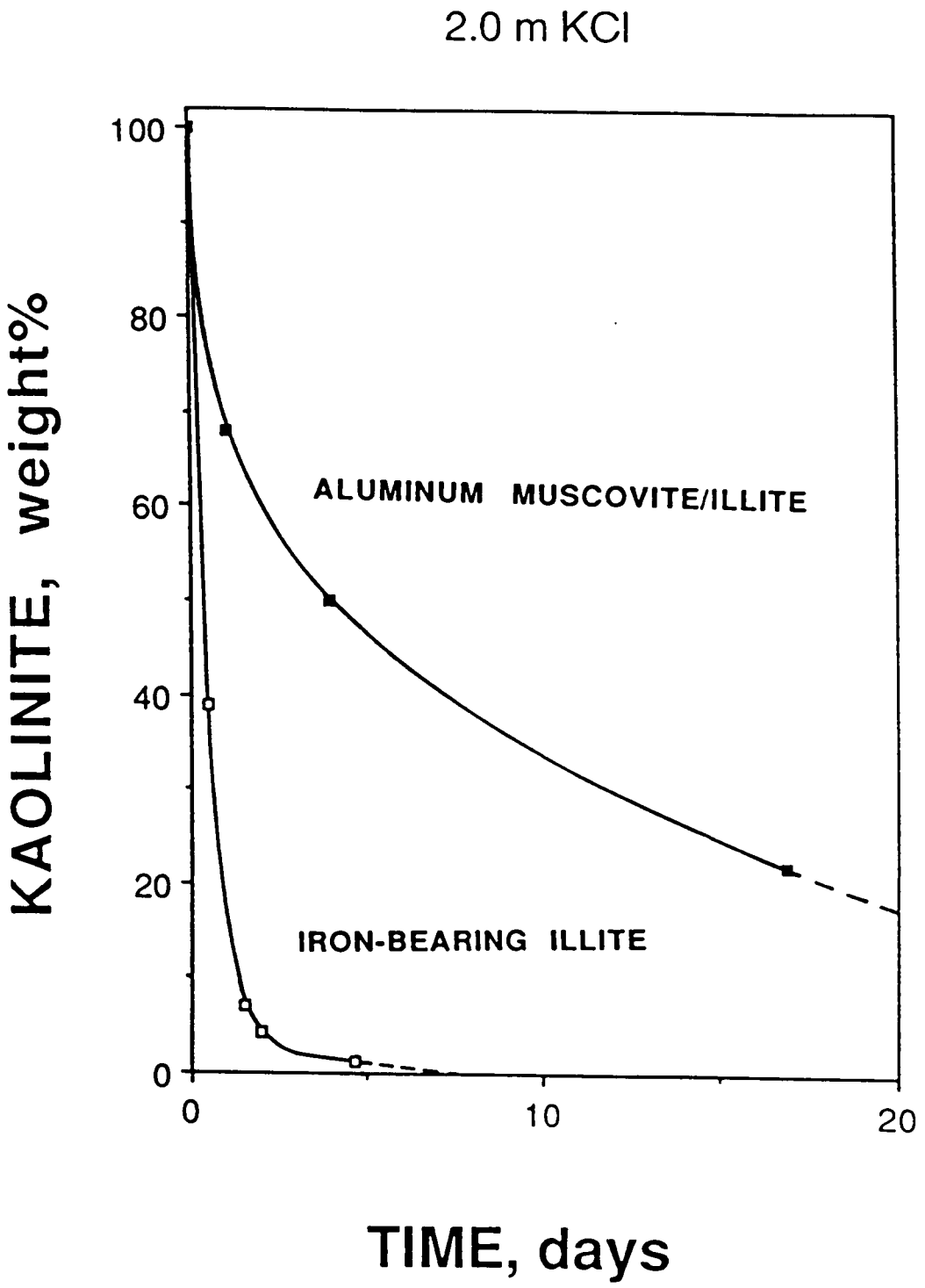

FIG. 13. Plot of kaolinite weight % versus reaction time at 300°C comparing experiments run in titanium reactors versus stainless steel reactors.

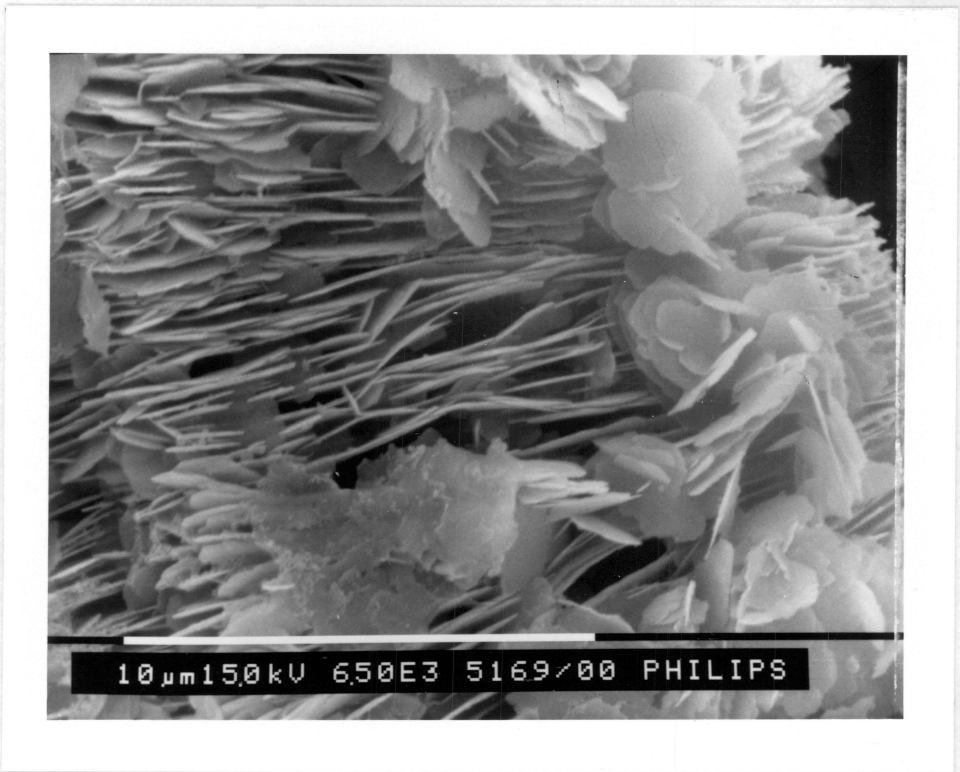

FIG. 14. SEM photograph of product muscovite/illite; scale bar = 10 µm. This experiment was run at 300°C, with 2 m KCl for 20 days. Notice the book like morphology. Note this experiment was contaminated with iron.

by using the initial rate method described in the results section. Log r can then be plotted versus the known log m_{K^+} to determine the reaction order n, and the apparent rate constant k'_+. The slopes of the lines in Figure 7 are 0.9, 0.9, and 1.0 ± 0.1 for experiments at 250°C, 275°C, and 289°C, respectively. Results were rounded to 1.0 for the reaction order in K^+ to simplify further analysis of the data. Furthermore, we assumed that if the reaction is first order in K^+ it is likely first order in H^+. Thus, both n and m in equation 2 were set equal to one in the next step of this analysis.

An integrated form of equation (2) was used to evaluate k'_-. This derivation is based on the observation that m_{K^+} is nearly constant over the duration of a single experiment. By holding m_{K^+} constant, equation (2) can be integrated as follows:

$$\int_{m_{H^+,1}}^{m_{H^+,2}} \left(\frac{dm_{H^+}}{k'_+ m_{K^+} - k'_- m_{H^+}} \right) = \int_{t_1}^{t_2} dt \qquad (4)$$

to give,

$$-\frac{1}{k'_-} \ln \frac{\left(k'_+(m_{K^+}) - k'_-(m_{H^+,2})\right)}{\left(k'_+(m_{K^+}) - k'_-(m_{H^+,1})\right)} = \Delta t \qquad (5)$$

The numerator and denominator of equation (5) can be decomposed by separating the bracketed term by $(m_{K^+} k'_-)$ to give,

$$-\left\{\frac{1}{k'_-}\right\}\left\{\ln\left[\frac{(m_{K^+}k'_-)\left(\frac{k'_+}{k'_-} - \frac{(m_{H^+,2})}{(m_{K^+})}\right)}{(m_{K^+}k'_-)\left(\frac{k'_+}{k'_-} - \frac{(m_{H^+,1})}{(m_{K^+})}\right)}\right]\right\} = \Delta t \qquad (6)$$

The first term in the square brackets cancel, k'_+/k'_- can be simplified to K by the principle of detailed balancing, and m_{H^+}/m_{K^+} equals the concentration product Q by definition. Therefore, a simple integrated form of the rate law is:

$$1/k'_- [\ln [(K - Q_2) / (K - Q_1)]] = \Delta t \qquad (7)$$

Multiplying equation (7) by k'_- and rearranging gives,

$$\ln (K - Q_2) = \ln (K - Q_1) - k'_- (\Delta t) \qquad (8)$$

Thus, the slope of the straight line produced by graphing ln $(K - Q_2)$ versus Δt has a slope of k'_-.

We can check the assumption of detailed balancing, ie. $k'_+/k'_- = k_+/k_- = K$ and the internal consistency of our analysis, by showing that the quotient k_+/k_-, of the semi-independently derived rate constants terms at 250, 275, 289, and 307°C agree well with Hemley's (1959) equilibrium constants (Table 9).

A general form of the integrated rate equation can be developed which then can be applied to natural systems. The derivation is similar to that in equations (4-8) except that we assumed that $m_{K^+} + m_{H^+} =$ constant. This more general form of the integrated rate law is

$$\ln (m_{K_1^+})(K - Q_1) - \ln (m_{K_2^+})(K - Q_2) = (k'_+ + k'_-)\Delta t \qquad (9)$$

where $m_{K_2^+}$ and $m_{K_1^+}$ are the final and initial potassium ion concentrations, K is the equilibrium constant, Q_2 and Q_1 are the final and initial m_{H^+}/m_{K^+} ratios, and k'_+ and k'_- are the apparent forward and reverse rate constants.

APPLICATIONS

There are two general uses for the rate law derived here. First, it can be used to model how quickly pore fluids in a rock will relax towards equilibrium after they have been perturbed by the addition of H^+ or K^+. Note that this analysis assumes a closed (batch reactor) system where the solution composition is instantaneously changed by the addition

Table 9. Comparison of the best fit ratio k_+/k_- values in Figures 6 and 9 to Hemly's measured equilibrium (K) data.

TEMP °C	log k_+/k_-	log K
250	-2.50	-2.61
275	-2.25	-2.36
289	-2.12	-2.24
307	-1.97	-2.08

of a dissolved component (H^+ or K^+). The second case considers the rate of mineral transformation in a system open to fluid flow (mixed flow reactor) where

$$\text{rate} = \left(\frac{dm_{H^+}}{dt}\right) = -\left(\frac{dm_{K^+}}{dt}\right) = \left(\frac{dn_{Musc.}}{dt}\right) = -\left(\frac{1}{1.5}\right)\left(\frac{dn_{Kaol.}}{dt}\right) \qquad (10)$$

The first case might apply when pore fluids in a formation were rapidly changed as a result of secondary or tertiary oil recovery technologies. The second case is helpful for understanding relatively long term diagenetic mineral transformations.

In a closed system, the time it takes solutions in contact with kaolinite - muscovite/illite to approach equilibrium at various temperatures can be expressed in terms of the time constant (t_c) (see discussion and derivation in Rimstidt and Barnes 1980). Rimstidt and Barnes (1980) found that $t_c = 1/k'_-$ for the silica water system; $t_c = 1/(k'_+ + k'_-)$ for the kaolinite to muscovite/illite reaction. Rimstidt and Barnes (1980) also showed that a first order reaction is essentially at equilibrium after $5t_c$. Figures 8 and 11 give the equations to determine the k_+ and k_- values as a function of temperature; these were transformed to k'_+ and k'_- by using $A_M/M = 12\ m^2/kg$ (surface area to mass ratio used in experiments to determine forward and reverse rate constants) and then assuming reasonable ranges of A_M/M. Figure 15 shows the t_c plotted versus temperature contoured in A_M/M ratios. This figure shows that at low temperatures (25 to 60°C) the rate of equilibration is very slow. For example, at 35°C and $A_M/M = 100$ the equilibration time ($5t_c$) would be ≈ 73,000 years, thus reaction kinetics must be considered in this regime.

When considering an open system, the differential rate law (equation 2) is modified by decomposing the numerator and denominator and separating $(m_{K^+})(k_-)$ to get:

$$\text{rate} = (A_M/M)\,(m_{K^+})(k_-)\,(K-Q) \qquad (11)$$

This situation can be viewed as a pore space with abundant kaolinite and muscovite/illite in a sandstone aquifer in contact with a flowing KCl solution. For conditions of this

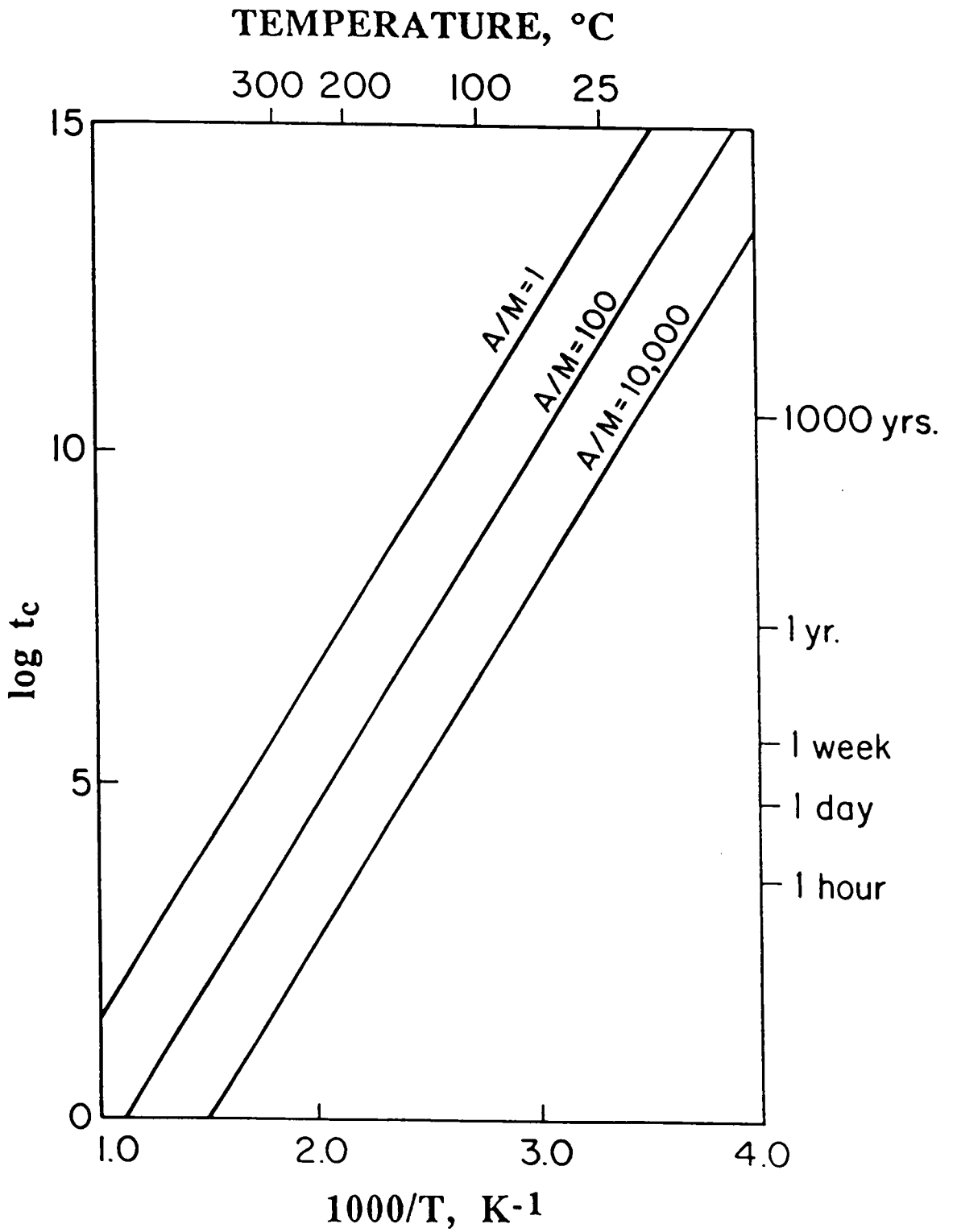

FIG. 15. The time constant (t_c) versus 1/T for the equilibration of the m_{K^+}/m_{H^+} ratio in a solution with kaolinite and muscovite/illite where the A_M/M (surface area of muscovite in m^2 divided by the mass of solution in kg) ratios vary from 1 to 10,000.

experiment (A_M/M = 12 $m^2 kg^{-1}$) m_{H+} = $1x10^{-6}$ and m_{KCl} = 2.0, 0.1, and 0.01 the rate (10) can then be predicted and is shown in Figure 16. For example at 100°C and 0.1 m_{KCl} the rate of hydrogen ion production is 10^{-16} mol kg^{-1} sec^{-1}. The rate read from this graph also equals the rate of formation of muscovite/illite (moles/sec) and 0.67 the rate of destruction of kaolinite, notice that the rate increases with increasing potassium concentration.

CONCLUSIONS

At 250 - 307°C the conversion of kaolinite to muscovite/illite,

$$K^+ + 1.5 \text{ kaolinite} = \text{muscovite} + H^+ + 1.5\ H_2O,$$

is fast enough to study conveniently using the hydrothermal experiments that we have designed. The 50 ml titanium batch reactors are well suited for for these hydrothermal experiments. Analysis of both solids and solutions is essential to aid in interpreting results. By monitoring the change in solution composition (m_{H^+}) very small extents of reaction were measured. The initial rate method as well as fitting data to the integrated form of the rate law were used to find the forward (k_+) and reverse (k_-) rate constants respectively. The reaction appears to be first order in both m_{H+} and m_{K+}, so the differential rate is

$$\left(\frac{dm_{H^+}}{dt}\right) = -\left(\frac{dm_{K^+}}{dt}\right) = \left[\frac{A_M}{M}\right](k_+ m_{K^+} - k_- m_{H^+}).$$

The forward reaction has an E_a = 155 ± 15 kJ mol^{-1} and the reverse reaction has an E_a = 101 ± 10 kJ mol^{-1}.

These experiments are analogs of the transformation of kaolinite to illite that commonly occurs during the burial diagenesis of clastic sedimentary rocks (Figure 1). The

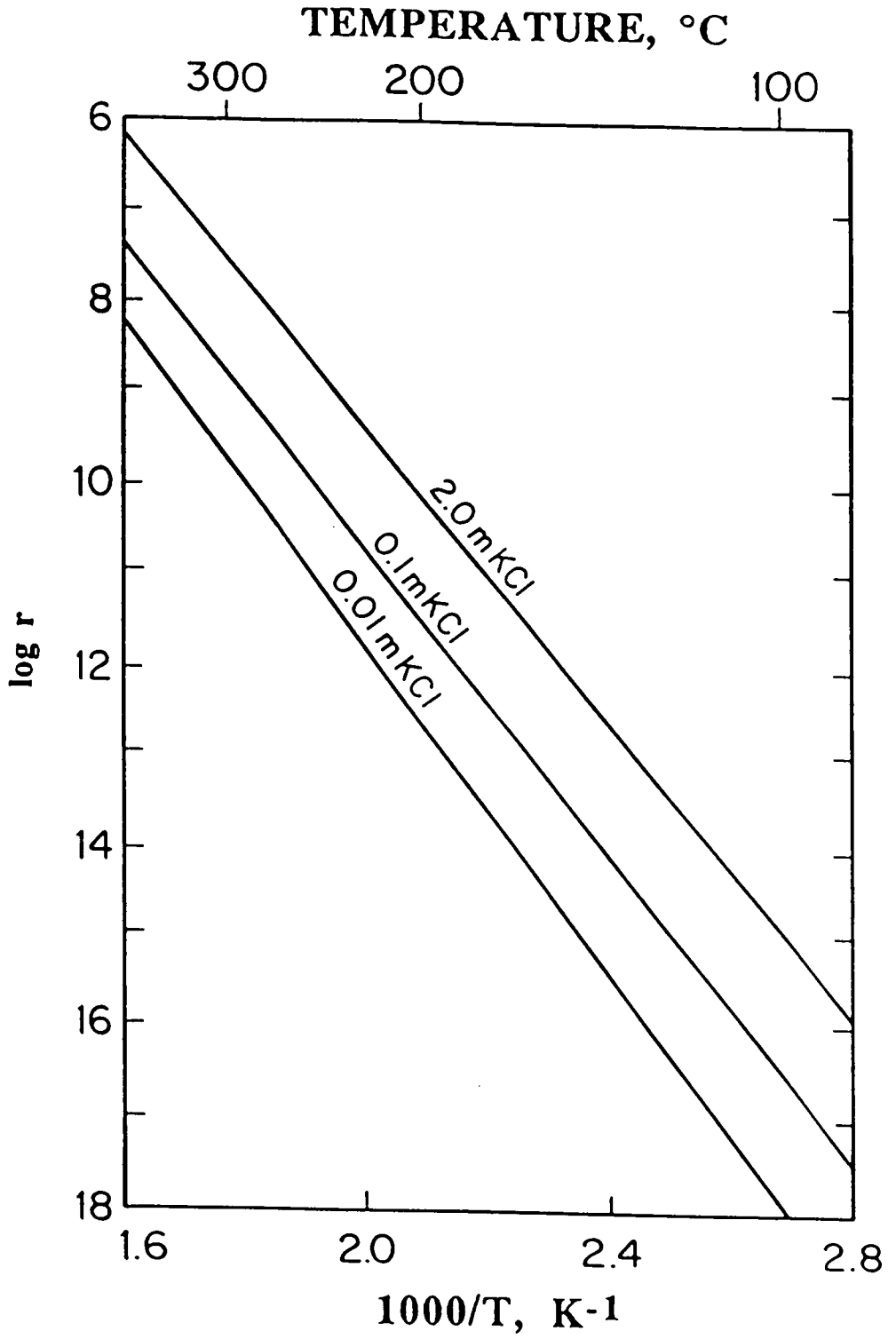

FIG. 16. Log r versus 1/T at $m_{H+} = 1 \times 10^{-6}$ and $m_{KCl} = 2.0$, 0.1, and 0.01.

morphologies of run products are equivalent to those of "hairy illite" which is commonly found in many sandstone pores (Bailey 1988).

The results of these experiments can be extrapolated to lower temperatures using the Arrhenius equation to predict transformation rates for diagenetic and hydrothermal conditions. These results are useful for predicting the rate of pore solution equilibration in closed systems as well as estimating rates of clay mineral transformation in open systems. However, they should be used cautiously because they were derived for the pure K_2O - Al_2O_3 - SiO_2 -H_2O system and we already know that the presence of ferrous/ferric iron in solution significantly accelerates the reaction rates. Further experiments are needed to determine effects of other cations (eg. Mg, Ca, and Na) on clay mineral transformation rates.

ESTIMATING THE THERMODYNAMIC PROPERTIES (ΔG_f^o and ΔH_f^o) OF SILICATE MINERALS AT 298 K FROM THE SUM OF POLYHEDRAL CONTRIBUTIONS

ABSTRACT

Many physical properties of silicate minerals can be modeled as a combination of basic polyhedral units (Hazen, 1985, 1988). It follows that their thermodynamic properties could be modeled as the sum of polyhedral contributions. We have determined, by multiple regression, the contribution of the $Al_2O_3(4)$ - $Al_2O_3(6)$ - $Al(OH)_3(6)$ - $SiO_2(4)$ - $MgO(6)$ - $Mg(OH)_2(6)$ - $CaO(6)$ - $CaO(8\text{-}Z)$ - $Na_2O(6\text{-}8)$ - $K_2O(8\text{-}12)$ - H_2O - $FeO(6)$ - $Fe(OH)_2(6)$ - $Fe_2O_3(6)$ components to the total ΔG_f^o and ΔH_f^o of a selected group of silicate minerals. Using these data we can estimate the ΔG_f^o and ΔH_f^o of other silicate minerals from a weighted sum of the contribution of each oxide and hydroxide component: $\Delta G_f^o = \sum n_i g_i$, and $\Delta H_f^o = \sum n_i h_i$ where n_i is the number of moles of the oxide or hydroxide per formula unit and g_i and h_i are the respective molar free energy, and enthalpy contribution of one mole of each oxide or hydroxide component. The technique outlined here can be used to estimate the thermodynamic properties of many silicate phases which are too complex or too impure to give reliable calorimetric measurements.

Experimentally measured ΔG_f^o and ΔH_f^o vs. predicted ΔG_f^o and ΔH_f^o for the minerals used in the model have associated average residuals of 0.26%, and 0.24% respectively. Thermodynamic properties of minerals not used in the model for which there are experimentally determined calorimetric data have average differences between measured and predicted values of 0.25% for ΔG_f^o for 18 minerals, 0.22% for ΔH_f^o for 20 minerals.

INTRODUCTION

Clay and zeolite minerals are very important phases in the near surface environment and the understanding of their thermodynamic properties is essential to modelling many geochemical processes. But, experimental measurements of the free energy of formation and enthalpy of formation (ΔG_f^o and ΔH_f^o, respectively) are few because they are difficult to perform. Problems associated with determining thermodynamic properties of clay and zeolite minerals include the chemical complexity and highly variable composition. The estimation technique for ΔG_f^o and ΔH_f^o developed here offers a reasonable way to approximate thermodynamic properties of clays and zeolites.

Many other techniques exist for estimating ΔG_f^o of silicate minerals (Nriagu, 1975; Chen, 1975; Tardy and Garrels, 1974, 1976, 1977, Karpov and Kashik, 1968; Mattigod and Sposito, 1978; La Iglesia and Aznar, 1986; Sposito, 1986) and ΔH_f^o (Kubaschewski and Alcock, 1979; Hemingway, 1982; Vieillard and Tardy, 1988). A complete discussion of each technique and associated errors here would be quite lengthy, therefore only a short summary will be presented. The data base used for most of the ΔG_f^o estimation techniques is based on solubility measurements of clay minerals. In these techniques, the estimation is based on the combined contributions of hydroxide components (i.e. $Si(OH)_4$, $Al(OH)_3$ etc.) rather than both hydroxide and oxide polyhedra. Karpov and Kashik used a multiple linear regression technique to estimate ΔG_f^o contribution of 36 different oxides to the overall ΔG_f^o of silicate minerals; however they ignored the hydroxide contributions. Tardy and Garrels (1976) developed an expression which describes the difference between ΔG_f^o of the simple oxide or hydroxide vs. ΔG_f^o of that same oxide or hydroxide within the silicate structure. This technique was extended further to include ΔH_f^o (Vieillard and Tardy, 1988). This basic technique of breaking down minerals into their "building block"

components is also used in S^oestimation (Robinson and Haas, 1983; Holland, 1989). Robinson and Haas's S^oestimates have small errors within the original data set but when applied outside the model data base, the estimates have much larger associated errors. The Robinson and Haas method of estimating entropy could be refined further if hydroxyls were viewed as parts of polyhedral units, and the simple oxide and hydroxide phases were removed from the model, as will be demonstrated later. Holland's estimation technique gives further refinement to the estimation of S^o by including a volume correction and considering magnetic contributions when estimating entropy.

This paper describes a multiple linear regression technique to determine the contribution of oxide and hydroxide components to the ΔG_f^o and ΔH_f^o of silicate minerals. The technique is based on the observation that silicate minerals have been shown to act as a combination of basic polyhedral units (Hazen, 1985). Using this polyhedral approach, volume, bulk modulus (Hazen, 1985), stable isotope fractionation (Savin and Lee, 1988) and refractive index (Bloss et al., 1983) can be modeled accurately. In turn, it seems reasonable that the thermodynamic properties of minerals could be estimated by summing the contributions of the individual polyhedra. We have determined, by multiple linear regression, the contribution of $Al_2O_3(4)$ - $Al_2O_3(6)$ - $Al(OH)_3(6)$ - $SiO_2(4)$ - $MgO(6)$ - $Mg(OH)_2(6)$ - $CaO(6)$ - $CaO(8\text{-}Z)$ - $Na_2O(6\text{-}8)$ - $K_2O(8\text{-}12)$ - H_2O - $FeO(6)$ - $Fe(OH)_2(6)$ - $Fe_2O_3(6)$ components to the total ΔG_f^o and ΔH_f^o of a selected group of silicate minerals. Where the (Z) in CaO(8-Z) represents coordination of these polyhedra in zeolite structures. We propose that the thermodynamic properties of many silicate phases which are too complex and too impure to give reliable calorimetric measurements can be estimated by summing the contributions of these components for the mineral of interest.

This approach has many advantages over other estimation techniques. First, thermodynamic properties of the minerals used to calibrate the model are based on

calorimetric and high temperature phase equilibrium measurements rather than on harder to determine solubility measurements. Second, it is conceptually simple and compelling to analyze a silicate mineral's properties in terms of the contributions of it's "building block" oxide and or hydroxide. Third, this technique is simple to implement because only the chemical formula and the coordination number of the polyhedra composing the mineral are needed. Finally, because of the large body of data available for use in the regression model, small errors in individual measurements have little effect on the estimated coefficients.

METHODS

A critically selected thermodynamic data base for 34 minerals was used (Table 1). The "building block" components for each mineral and the associated coordination numbers in the $Al_2O_3(4)$ - $Al_2O_3(6)$ - $Al(OH)_3(6)$ - $SiO_2(4)$ - $MgO(6)$ - $Mg(OH)_2(6)$ - $CaO(6)$ - $CaO(8\text{-}Z)$ - $Na_2O(6\text{-}8)$ - $K_2O(8\text{-}12)$ - H_2O - $FeO(6)$ - $Fe(OH)_2(6)$ - $Fe_2O_3(6)$ system was determined (Table 1). For example, the mineral kaolinite ($Al_2Si_2O_5(OH)_4$) is composed of 2 $SiO_2(4)$, 0.333 $Al_2O_3(6)$, and 1.333 $Al(OH)_3(6)$ polyhedra. When Al^{3+}, Fe^{3+}, Mg^{2+}, and Fe^{2+} are in six-fold coordination in the octahedral sheet of 1:1 and 2:1 phyllosilicate minerals, they were distributed as 0.6666 hydroxide and 0.3333 oxide, and 0.3333 hydroxide and 0.6666 oxide, respectively. This distribution is consistent with structural constraints on the distribution of oxide and hydroxide polyhedra (Weaver and Pollard, 1973). The number of $SiO_2(4)$ polyhedra for an individual mineral in the regression model was not allowed to exceed 5.0 to avoid over-weighting the contribution of a particular mineral. If the sum of the associated $SiO_2(4)$ polyhedra totaled more than five, one-half of the chemical formula was used. The rationale of this breakdown process was aided by a discussion of

Table 1. Minerals selected for the thermodynamic regression models and the relative contribution of their polyhedral components.

	Al_2O_3 (4)	Al_2O_3 (6)	$Al(OH)_3$ (6)	SiO_2 (4)	K_2O (8-12)	MgO (6)	$Mg(OH)_2$ (6)	H_2O	CaO (6)	CaO (8-Z)	Na_2O (6-8)	FeO (6)	$Fe(OH)_2$ (6)	Fe_2O_3 (6)
1 Kaolinite	0.0	0.33	1.33	2.0	0.0	0.0	0.0	0.0	0.0	0.0	0.0	0.0	0.0	0.0
2 Muscovite	0.5	0.67	0.67	3.0	0.5	0.0	0.0	0.0	0.0	0.0	0.0	0.0	0.0	0.0
3 Margarite	1.0	0.67	0.67	2.0	0.0	0.0	0.0	0.0	1.0	0.0	0.0	0.0	0.0	0.0
4 Talc	0.0	0.0	0.0	4.0	0.0	2.0	1.0	0.0	0.0	0.0	0.0	0.0	0.0	0.0
5 Pyrophyllite	0.0	0.67	0.67	4.0	0.0	0.0	0.0	0.0	0.0	0.0	0.0	0.0	0.0	0.0
6 Microcline	0.5	0.0	0.0	3.0	0.5	0.0	0.0	0.0	0.0	0.0	0.0	0.0	0.0	0.0
7 Low Albite	0.5	0.0	0.0	3.0	0.0	0.0	0.0	0.0	0.0	0.0	0.5	0.0	0.0	0.0
8 Anorthite	1.0	0.0	0.0	2.0	0.0	0.0	0.0	0.0	1.0	0.0	0.0	0.0	0.0	0.0
9 Analcime	0.5	0.0	0.0	2.0	0.0	0.0	0.0	1.0	0.0	0.0	0.5	0.0	0.0	0.0
10 Lawsonite	0.67	0.0	0.67	2.0	0.0	0.0	0.0	1.0	1.0	0.0	0.0	0.0	0.0	0.0
11 Ferrosilite	0.0	0.0	0.0	1.0	0.0	0.0	0.0	0.0	0.0	0.0	0.0	1.0	0.0	0.0
12 Fayalite	0.0	0.0	0.0	1.0	0.0	0.0	0.0	0.0	0.0	0.0	0.0	2.0	0.0	0.0
13 Leucite	0.5	0.0	0.0	2.0	0.5	0.0	0.0	0.0	0.0	0.0	0.0	0.0	0.0	0.0
14 Leonardite	1.0	0.0	0.0	4.0	0.0	0.0	0.0	3.5	0.0	1.0	0.0	0.0	0.0	0.0
15 Tremolite	0.0	0.0	0.0	4.0	0.0	2.0	0.5	0.0	0.0	1.0	0.0	0.0	0.0	0.0
16 Jadeite	0.0	0.5	0.0	2.0	0.0	0.0	0.0	0.0	0.0	0.0	0.5	0.0	0.0	0.0
17 Diopside	0.0	0.0	0.0	2.0	0.0	1.0	0.0	0.0	0.0	1.0	0.0	0.0	0.0	0.0
18 Merwinite	0.0	0.0	0.0	2.0	0.0	1.0	0.0	0.0	3.0	0.0	0.0	0.0	0.0	0.0
19 Monticellite	0.0	0.0	0.0	1.0	0.0	1.0	0.0	0.0	1.0	0.0	0.0	0.0	0.0	0.0
20 Grossular	0.0	1.0	0.0	3.0	0.0	0.0	0.0	0.0	0.0	3.0	0.0	0.0	0.0	0.0
21 Zoisite	0.0	1.33	0.33	3.0	0.0	0.0	0.0	0.0	0.0	2.0	0.0	0.0	0.0	0.0
22 Mordenite	0.47	0.0	0.0	5.06	0.0	0.0	0.0	3.47	0.0	0.29	0.18	0.0	0.0	0.0
23 Yugawaralite	0.5	0.0	0.0	3.0	0.0	0.0	0.0	2.0	0.0	0.5	0.0	0.0	0.0	0.0
24 Grunerite	0.0	0.0	0.0	4.0	0.0	0.0	0.0	0.0	0.0	0.0	0.0	3.0	0.5	0.0
25 Minnesotaite	0.0	0.0	0.0	4.0	0.0	0.0	0.0	0.0	0.0	0.0	0.0	2.0	1.0	0.0
26 Riebeckite	0.0	0.0	0.0	4.0	0.0	0.0	0.0	0.0	0.0	0.0	0.5	1.0	0.5	0.5
27 Chrysotile	0.0	0.0	0.0	2.0	0.0	1.0	2.0	0.0	0.0	0.0	0.0	0.0	0.0	0.0
28 Paragonite	0.5	0.67	0.67	3.0	0.0	0.0	0.0	0.0	0.0	0.0	0.5	0.0	0.0	0.0
29 Phlogopite	0.5	0.0	0.0	3.0	0.5	2.0	1.0	0.0	0.0	0.0	0.0	0.0	0.0	0.0
30 Laumontite	1.0	0.0	0.0	4.0	0.0	0.0	0.0	4.0	0.0	1.0	0.0	0.0	0.0	0.0
31 Nepheline	0.5	0.0	0.0	1.0	0.0	0.0	0.0	0.0	0.0	0.0	0.5	0.0	0.0	0.0
32 Greenalite	0.0	0.0	0.0	2.0	0.0	0.0	0.0	0.0	0.0	0.0	0.0	1.0	2.0	0.0
33 Prehnite	0.67	0.0	0.67	3.0	0.0	0.0	0.0	0.0	1.0	1.0	0.0	0.0	0.0	0.0
34 Acmite	0.0	0.0	0.0	2.0	0.0	0.0	0.0	0.0	0.0	0.0	0.5	0.0	0.0	0.5

Minerals used in ΔG_f^o model:1-27, 33, 34: Minerals used in ΔH_f^o model:1-32.

coordination numbers in silicates presented in Robinson and Haas (1983). A tabulation of the polyhedral coordination of oxide components of many silicate minerals is given by Smyth and Bish (1988).

The data were regressed to determine g_i and h_i (the contribution of one mole of component to the free energy and enthalpy of the mineral, respectively) for the models: $\Delta G_f^o = \Sigma\, n_i\, g_i$ (29 minerals) and $\Delta H_f^o = \Sigma\, n_i\, h_i$ (32 minerals) where n_i is the number of moles of component i. Entropy values (S^o) can be determined using the equation $\Delta G_f^o = \Delta H_f^o - T\Delta S_f^o$ where $\Delta S^o{}_f = S^o_{elements} - S^o$. S^o estimations from both a regression model $S^o = \Sigma\, n_i\, s_i$ (25 minerals) (Appendix II) and from the above equation were found to have much larger associated errors and to be more sensitive to the coordination than enthalpy and free energy values. We suggest using these techniques only for rough estimates of S^o. The technique of Holland (1989), gives more accurate estimates of S^o and can be used in conjunction with our ΔH_f^o model to produce an internally consistent set of ΔG_f^o, ΔH_f^o, and S^o values.

A few minerals showed poor agreement between measured and predicted values. Beware of minerals such as pyrope, akermanite, and wollastonite that have oxides with unusual coordination numbers because data for polyhedra with these coordination numbers are not specified by the model. Other minerals which resulted in poor fits to the model include Ca-Al pyroxene, forsterite, cordierite, andradite and gehlenite. We have no explanation for their inconsistency.

RESULTS

Tables 2 lists g_i and h_i and their errors derived from the model. Tables 3 and 4 show measured ΔG_f^o and ΔH_f^o versus those predicted using g_i and h_i from Table 2. The average

Table 2. The g_i and h_i of each polyhedral type.

Polyhedral unit	g_i kJ·mol^{-1}	Error kJ·mol^{-1}	h_i kJ·mol^{-1}	Error* kJ·mol^{-1}
Al_2O_3(4)	-1631.32	13.3	-1716.24	11.0
Al_2O_3(6)	-1594.52	15.3	-1690.18	15.9
$Al(OH)_3$(6)	-1181.62	13.2	-1319.55	12.2
SiO_2(4)	-853.95	4.6	-910.97	3.2
MgO(6)	-628.86	10.6	-660.06	7.9
$Mg(OH)_2$(6)	-851.86	10.2	-941.62	9.1
CaO(6)	-669.13	5.9	-696.65	5.2
CaO(8-Z)	-710.08	7.2	-736.04	7.1
Na_2O(6-8)	-672.50	26.0	-683.00	18.4
K_2O(8-12)	-722.94	27.4	-735.24	21.1
H_2O	-239.91	5.7	-292.37	4.6
FeO(6)	-266.29	6.8	-290.55	5.4
$Fe(OH)_2$(6)	-542.04	24.6	-596.07	8.2
Fe_2O_3(6)	-776.07	33.0	-939.18	35.6

* Standard error of the estimate

Table 3. Comparison of ΔG_f^o(measured) versus ΔG_f^o(predicted) for the 29 minerals used in the model and the associated errors.

Mineral	ΔG_f^o(measured) kJ·mol^{-1}	ΔG_f^o(predicted) kJ·mol^{-1}	Residuals kJ·mol^{-1}	% Residual
1 Kaolinite	-3799.4	-3814.9	15.5	0.41
2 Muscovite	-5595.5	-5589.7	-5.8	0.10
3 Margarite	-5854.8	-5859.1	4.3	0.07
4 Talc	-5536.1	-5525.4	-10.7	0.19
5 Pyrophyllite	-5265.9	-5266.6	0.6	0.01
6 Microcline	-3742.3	-3739.0	-3.4	0.09
7 Low albite	-3711.7	-3713.8	2.0	0.05
8 Anorthite	-4002.1	-4008.3	6.3	0.16
9 Analcime	-3091.7	-3099.7	8.0	0.26
10 Lawsonite	-4525.6	-4492.2	-33.4	0.74
11 Ferrosilite	-1117.1	-1120.2	-3.1	0.28
12 Fayalite	-1379.4	-1386.5	-7.2	0.52
13 Leucite	-2875.9	-2885.0	9.1	0.32
14 Leonardite	-6598.6	-6596.9	-1.7	0.03
15 Tremolite	-5814.0	-5809.5	-4.4	0.08
16 Jadeite	-2850.8	-2841.4	-9.4	0.33
17 Diopside	-3036.6	-3046.8	10.3	0.34
18 Merwinite	-4339.4	-4344.1	4.7	0.11
19 Monticellite	-2143.2	-2151.9	8.8	0.41
20 Grossular	-6295.3	-6286.6	-8.7	0.14
21 Zoisite	-6495.3	-6501.9	6.6	0.10
22 Mordenite	-6247.6	-6246.0	-1.6	0.03
23 Yugawaralite	-4193.9	-4212.4	18.5	0.44
24 Grunerite	-4494.4	-4485.7	-8.7	0.19
25 Minnesotaite	-4474.8	-4490.4	15.6	0.35
26 Chrysotile	-4034.0	-4040.5	6.5	0.16
27 Prehnite	-5816.4	-5816.3	-0.1	0.00
28 Riebeckite	-4699.9	-4677.4	-22.5	0.48
29 Acmite	-2409.7	-2432.2	22.5	0.93
			Average =	0.26

1, 4, 6, 7, 8, 9, 10, 12, 13, 14, 15, 16, 17, 18, 19 and 26 Robie et al. (1978); 2, 5, and 20 Krupka et al. (1979); 3, 21, and 27 Hemingway et al. (1982); 22 Johnson et al. (1986); these data were determined by calorimetry. 23 Zeng and Liou (1982); 11, 24, and 25 Miyano and Klein (1983); 28, and 29 Makarov et al. (1984); these data were determined from phase equilibrium reversals.

Table 4. Comparison of ΔH_f^o(measured) versus ΔH_f^o(predicted) for the 32 minerals used in the model and the associated errors.

Mineral	ΔH_f^o(measured) kJ·mol^{-1}	ΔH_f^o(predicted) kJ·mol^{-1}	Residual kJ·mol^{-1}	% Residual
1 Kaolinite	-4133.6	-4144.7	11.1	0.27
2 Muscovite	-5971.6	-5965.1	-6.5	0.11
3 Paragonite	-5941.5	-5939.0	-2.5	0.04
4 Margarite	-6239.6	-6241.3	1.7	0.03
5 Phologopite	-6213.9	-6220.4	6.5	0.10
6 Talc	-5915.9	-5905.6	-10.3	0.17
7 Pyrophyllite	-5639.8	-5650.4	10.6	0.18
8 Microcline	-3967.7	-3958.7	-9.0	0.22
9 Low Albite	-3935.1	-3932.5	-2.6	0.07
10 Anorthite	-4227.8	-4234.8	7.0	0.16
11 Analcime	-3309.8	-3313.9	4.1	0.12
12 Laumontite	-7277.2	-7265.6	-11.5	0.16
13 Lawsonite	-4863.9	-4834.8	-29.1	0.60
14 Ferrosilite	-1194.9	-1201.5	6.7	0.56
15 Fayalite	-1479.4	-1492.1	12.7	0.86
16 Leucite	-3038.7	-3047.7	9.0	0.30
17 Nepheline	-2092.1	-2110.6	18.5	0.88
18 Leonardite	-7123.2	-7119.4	-3.8	0.05
19 Tremolite	-6177.5	-6170.9	-6.7	0.11
20 Jadeite	-3029.4	-3008.5	-20.9	0.69
21 Diopside	-3210.8	-3218.0	7.3	0.23
22 Merwinite	-4566.8	-4571.9	5.2	0.11
23 Monticellite	-2262.7	-2267.7	5.0	0.22
24 Grossular	-6636.3	-6631.2	-5.1	0.08
25 Zoisite	-6891.1	-6898.4	7.3	0.10
26 Mordenite	-6756.2	-6765.7	9.5	0.14
27 Yugawaralite	-4518.1	-4543.8	25.7	0.57
28 Grunerite	-4824.2	-4813.6	-10.6	0.22
29 Minnesotaite	-4823.0	-4821.0	-2.0	0.04
30 Chrysotile	-4361.7	-4365.2	3.6	0.08
31 Greenalite	-3301.0	-3304.6	3.6	0.10
32 Riebeckite	-5043.6	-5043.6	0.0	0.00
			Average =	0.24

2, 7, 13, and 24 Krupka et al. (1979); 4, and 25 Hemingway et al. (1982); 5 Clemens et al. (1987); 6, 8, 9, 10, 11, 15, 16, 17, 18, 19, 20, 21, 22, 23, and 30 Robie et al. (1978); 26 Johnson et al. (1986); these data were determined by calorimetry. 1 Hemley et al. (1980); 3, and 12 Berman et al. (1985); 27 Zeng and Liou (1982); 14, 28, 29, and 31 Miyano and Klein (1983); 32 Makarov et al. (1984); these data were determined from phase equilibrium reversals.

difference between the predicted and the measured values is 0.26% for ΔG_f^o and 0.24% for ΔH_f^o and these differences are normally distributed. The average reported associated errors (2σ) for the experimentally determined thermodynamic values are 0.16% for ΔG_f^o and 0.13% for ΔH_f^o. Approximately 50% of the estimated values fall within the range of the error (2σ) reported for the experimentally determined data.

The accuracy of the models was tested by predicting the thermodynamic properties of minerals not used to develop the model. Table 5a compares the results of the model with calorimetrically determined thermodynamic data for 20 different minerals and gives associated differences. Average residuals for these minerals are: 0.25% for ΔG_f^o for 18 minerals and 0.22% for ΔH_f^o for 20 minerals. Table 5b shows that ΔG_f^o values derived from solubility measurements of clays agree with those predicted by this model with an average difference between the predicted and measured 0.54% for ΔG_f^o for 18 minerals.

DISCUSSION

A comparison of the g_i and h_i from these models to the ΔG_f^o and ΔH_f^o for the simple oxide or hydroxide components (Table 6) shows that there is a good correlation between g_i and ΔG_f^o (Fig. 1) and between h_i and ΔH_f^o (Fig. 2). These graphs show that free energy and enthalpy of formation of an oxide or hydroxide component in a silicate mineral generally is more negative than that of the simple oxide or hydroxide mineral by $\approx$ 36 $kJ \cdot mol^{-1}$ and $\approx$ 38 $kJ \cdot mol^{-1}$ respectively. The abundance of silicate minerals relative to free oxides and hydroxides in nature is consistent with this relationship.

The correlation lines in Figures 1 and 2 can be used to approximate a g_i or h_i for polyhedra not determined by this model. For example, experimental data for a mineral containing a $Fe(OH)_3$ polyhedron was not available to incorporate into these models but g_i

Table 5a. Measured ΔG_f^o and ΔH_f^o determined by calorimetry compared to their predicted values for 20 minerals.

Mineral	Chemical Formula	ΔG_f^o(pred) / ΔG_f^o(meas) kJ·mol^{-1}	%Difference	ΔH_f^o(pred) / ΔH_f^o(meas) kJ·mol^{-1}	%Difference
Nepheline (1)	$Na_{0.78}K_{0.22}AlSiO_4$	-2011.4 / ----	----	-2116.3 / -2110.3	0.28
Mesolite (2)	$Na_{0.676}Ca_{0.657}Al_{1.990}Si_{3.01}O_{10}\cdot 2.647H_2O$	-5530.6 / -5513.2	0.32	-5946.6 / -5947.1	0.01
Natrolite (2)	$Na_2Al_2Si_3O_{10}\cdot 2.0H_2O$	-5345.5 / -5316.6	0.54	-5716.9 / -5718.6	0.03
Scolecite (2)	$CaAl_2Si_3O_{10}\cdot 3.0H_2O$	-5623.0 / -5597.9	0.45	-6062.3 / -6049. 0	0.22
Stilbite (3)	$Na_{0.136}Ca_{1.02}K_{.006}Al_{2.180}Si_{6.820}O_{18}\cdot 7.33H_2O$	-10132.1 / -10143.0	0.11	-11025.2 / -11034.6	0.09
Ca-Olivine (4)	Ca_2SiO_4	-2192.2 / -2199.7	0.34	-2304.3 / -2316.5	0.53
Kyanite (4)	Al_2SiO_5	-2448.5 / -2444.0	0.18	-2601.2 / -2594.3	0.26
Prehnite (4)	$Ca_2Al_2Si_3O_{10}(OH)_2$	***** / -5816.4	****	-6189.5 / -6193.6	0.07
Hedenbergite (5)	$CaFeSi_2O_6$	-2684.3 / -2674.3	0.37	-2848.5 / -2837.6	0.38
Almandine (6)	$Fe_3Al_2Si_3O_{12}$	-4955.2 / -4951.3	0.08	-5294.7 / -5275.5	0.36
Oligoclase (7)	$Ca_{0.2}Na_{0.8}Al_{1.2}Si_{2.8}O_8$	-3772.7 / -3754.3	0.49	-3993.0 / -3977.3	0.39
Andesine (7)	$Ca_{0.4}Na_{0.6}Al_{1.4}Si_{2.6}O_8$	-3831.6 / -3818.3	0.35	-4053.5 / -4041.7	0.29
Labradorite (7)	$Ca_{0.5}Na_{0.5}Al_{1.5}Si_{2.5}O_8$	-3861.1 / -3848.9	0.32	-4083.7 / -4072.3	0.28
Bytownite (7)	$Ca_{0.8}Na_{0.2}Al_{1.8}Si_{2.2}O_8$	-3949.4 / -3959.7	0.26	-4174.4 / -4184.0	0.23
Merlionite (8)	$KAlSi_{1.94}O_{5.88}\cdot 1.69H_2O$	-3239.2 / -3241.4	0.07	-3487.1 / 3481.8	0.15
Merlionite (8)	$KAlSi_{1.81}O_{5.62}\cdot 1.69H_2O$	-3128.2 / -3123.3	0.16	-3368.7 / -3359.9	0.26
Merlionite (8)	$K_{0.80}Na_{0.20}AlSi_{1.94}O_{5.88}\cdot 1.81H_2O$	-3263.0 / -3272.2	0.28	-3517.0 / -3519.0	0.06
Merlionite (8)	$K_{0.91}Na_{0.09}AlSi_{1.81}O_{5.62}\cdot 1.79H_2O$	-3150.0 / -3144.6	0.17	-3395.6 / -3387.3	0.25
Merlionite (8)	$Na_{0.81}K_{0.19}AlSi_{1.94}O_{5.88}\cdot 2.13H_2O$	-3324.4 / -3325.8	0.04	-3594.6 / -3591.2	0.10
Merlionite (8)	$Na_{0.81}K_{0.19}AlSi_{1.81}O_{5.62}\cdot 2.18H_2O$	-3225.4 / -3225.3	0.00	-3490.8 / -3488.3	0.07
			Average = 0.25		Average = 0.22

------ not determined. *** value used in the model. 1 Robie et al. (1978); 2 Johnson et al. (1983); 3 O'Hare et al. (1986); 4 Hemingway et al. (1982); 5 Robie et al. (1987); 6 Chaterjee (1987); 7 Naumov et al. (1974); and 8 Donahoe et al. (1989).

Table 5b. ΔG_f^o determined from solubility measurements compared to predicted ΔG_f^o for 18 minerals along with the ΔH_f^o predicted by the model.

Mineral	Chemical Formula	ΔG_f^o(pred) / ΔG_f^o(meas) kJ·mol^{-1}	% Difference	ΔH_f^o(pred) kJ·mol^{-1}
Kerolite (9)	$Mg_3Si_4O_{10}(OH)_2 \cdot H_2O$	-5765.3 / -5828.03	1.07	-6198.0
Sepioilite (9)	$Mg_2Si_3O_{7.5}(OH) \cdot 3H_2O$	-4650.8 / -4692.80	0.89	-5070.9
Chlorite 1 (10)	$[Al_{1.44}Fe_{0.07}^{(3+)}Fe_{0.99}Mg_{3.24}]Al_{1.03}Si_{2.97}O_{10}(OH)_8$	-7819.8 / -7793.00	0.34	-8477.2
Chlorite 2 (10)	$[Al_{1.75}Fe_{0.12}^{(3+)}Fe_{2.61}Mg_{1.16}]\ Al_{1.16}Si_{2.84}O_{10}(OH)_8$	-7321.5 / -7319.00	0.03	-7952.3
Chlorite 3 (10)	$[Al_{1.60}Fe_{3.29}Mg_{1.05}]Al_{1.53}Si_{2.47}O_{10}(OH)_8$	-7282.0 / -7290.00	0.11	-7932.6
Chlorite 4 (10)	$[Al_{1.39}Fe_{0.21}^{(3+)}Fe_{0.57}Mg_{3.52}]Al_{1.01}Si_{2.99}O_{10}(OH)_8$	-7888.2 / -7869.00	0.24	-8553.5
Fithian Illite (11)	$K_{0.64}[Al_{1.54}Fe_{0.29}^{(3+)}Mg_{0.19}]Al_{0.49}Si_{3.51}O_{10}(OH)_2$	-5329.6 / -5443.40	2.09	-5715.0
G. Lake Illite(11)	$K_{0.59}[Al_{1.58}Fe_{0.24}^{(3+)}Mg_{0.15}]Al_{0.35}Si_{3.65}O_{10}(OH)_2$	-5299.2 / -5345.90	0.87	-5683.0
B. Bend Illite(11)	$K_{0.60}Na_{0.04}[Al_{1.43}Fe_{0.42}^{(3+)}Mg_{0.16}]\ Al_{0.52}Si_{3.48}O_{10}(OH)_2$	-5268.5 / -5333.34	1.21	-5656.5
Clay Spur (12)	$K_{0.02}Ca_{0.1}Na_{0.27}[Al_{1.52}Fe_{0.19}^{(3+)}Mg_{0.22}]\ Al_{0.06}Si_{3.94}O_{10}(OH)_2$	-5227.6 / -5226.40	0.02	-5612.8
Cheto (12)	$K_{0.02}Ca_{0.185}Na_{0.02}[Al_{1.52}Fe_{0.14}^{(3+)}Mg_{0.33}]\ Al_{0.07}Si_{3.93}O_{10}(OH)_2$	-5251.8 / -5245.30	0.12	-5639.4
K-Beidellite(13)	$K_{0.37}Ca_{0.01}Na_{0.07}[Al_{1.41}Fe_{0.415}^{(3+)}Fe_{0.055}^{(2+)}\ Mg_{0.205}]\ Al_{0.45}Si_{3.55}O_{10}(OH)_2$	-5234.5 / -5215.40	0.36	-5625.5
Mg-Beidellite(13)	$K_{0.095}Ca_{0.01}Na_{0.07}Mg_{0.135}\ [Al_{1.41}Fe_{0.415}^{(3+)}\ Fe_{0.055}^{(2+)}\ Mg_{0.205}]\ Al_{0.45}Si_{3.55}O_{10}(OH)_2$	-5219.3 / -5200.10	0.37	-5614.1
Smectite (14)	$Mg_{0.225}[Al_{1.345}Fe_{0.405}^{(3+)}Mg_{0.27}]Al_{0.30}Si_{3.70}O_{10}(OH)_2$	-5174.2 / -5214.70	0.78	-5568.5
Al-Belle F. (15)	$Al_{0.0883}[Al_{1.515}Fe_{0.225}^{(3+)}Mg_{0.29}]Al_{0.065}Si_{3.935}O_{10}(OH)_2$	-5193.9 / -5213.40	0.37	-5587.3
Mg-Belle F. (15)	$Mg_{0.1325}[Al_{1.515}Fe_{0.225}^{(3+)}Mg_{0.29}]\ Al_{0.065}Si_{3.935}O_{10}(OH)_2$	-5207.4 / -5222.80	0.29	-5600.1
Al-Aberdeen (15)	$Al_{0.1383}[Al_{1.29}Fe_{0.335}^{(3+)}Mg_{0.445}]Al_{0.18}Si_{3.82}O_{10}(OH)_2$	-5185.8 / -5200.00	0.27	-5581.0
Mg-Aberdeen(15)	$Mg_{0.2075}[Al_{1.29}Fe_{0.335}^{(3+)}Mg_{0.445}]Al_{0.18}Si_{3.82}O_{10}(OH)_2$	-5206.9 / -5218.70	0.23	-5601.0
		Average =	0.54	

9 Stoessel (1988); 10 Kittrick (1982); 11 Kittrick (1984); 12 Huang and Kellar (1973); 13 Misra and Upchurch (1976); 14 Carson et al. (1976); 15 Kittrick (1971 a, b, and c).

Table 6. ΔG_f^o and ΔH_f^o of the free oxide or hydroxide phases compared to g_i and h_i from the multiple linear regression model.

Oxide/Hydroxide	$\Delta G^o_{f\,oxide/hyd.}$ kJ·mol^{-1}	g_i kJ·mol^{-1}	$\Delta H^o_{f\,oxide/hyd.}$ kJ·mol^{-1}	h_i kJ·mol^{-1}
Al_2O_3(6)	-1582.23	-1594.52	-1675.70	-1690.18
$Al(OH)_3$	-1154.89	-1181.62	-1293.13	-1319.55
SiO_2	-856.29	-853.95	-910.70	-910.97
MgO	-569.20	-628.86	-601.49	-660.06
$Mg(OH)_2$	-833.51	-851.86	-924.54	-941.62
H_2O	-237.14	-239.91	-285.83	-292.37
CaO(6)	-603.49	-669.13	-635.09	-696.65
FeO	-251.16	-266.29	-272.04	-290.55
Fe_2O_3	-742.68	-776.07	-824.64	-939.18
$Fe(OH)_2$	-492.04	-542.04	-574.04	-596.07

All measured thermodynamic data from Robie et al. (1978), except for $Fe(OH)_2$ which is from Nordstrom et al. (1984).

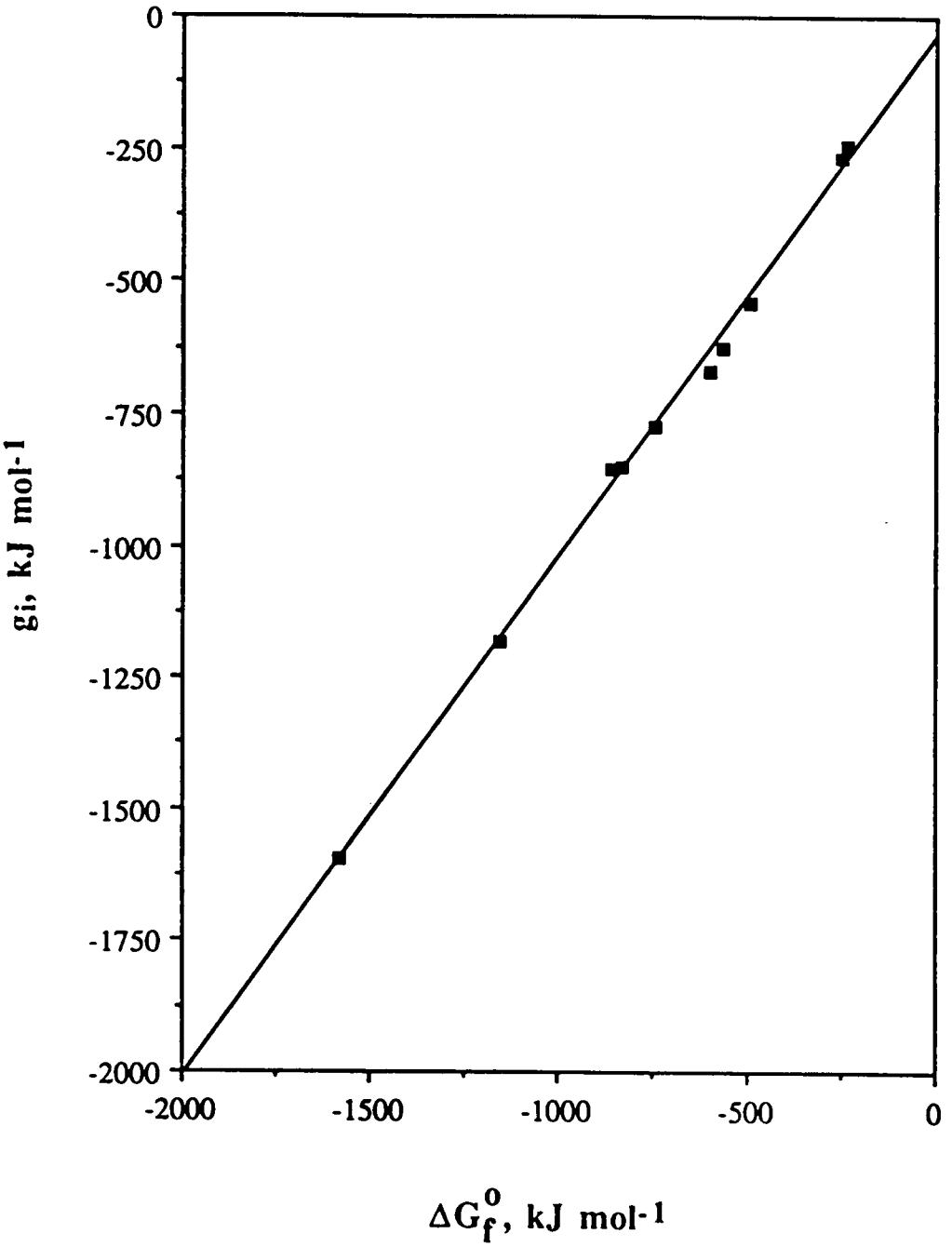

Fig. 1. Graph of the g_i (kJ·mol^{-1}) versus $\Delta G^o_{f\ \text{oxide/hydroxide}}$ (kJ·mol^{-1}) data from Table 6. The associated regression equation is $g_i = -35.55 + 0.990\ \Delta G^o_{f\ \text{oxide/hydroxide}}$ with an R value equal to 1.00.

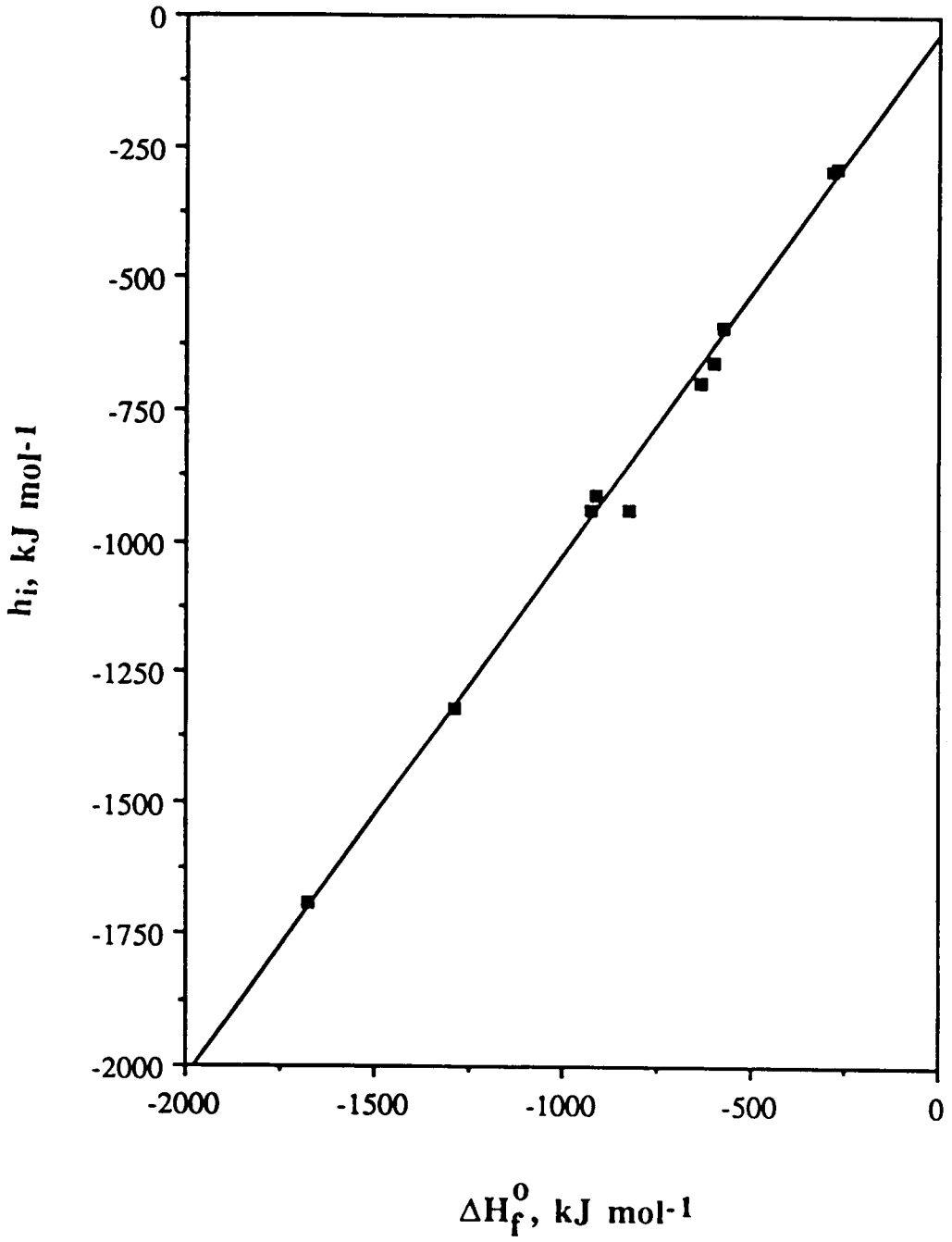

Fig. 2. Graph of the h_i (kJ·mol^{-1}) versus $\Delta H_{f\ \text{oxide/hydroxide}}^{o}$ (kJ·mol^{-1}) data from Table 6. The associated regression equation is $h_i = -38.29 + 0.995\ \Delta H_{f\ \text{oxide/hydroxide}}^{o}$ with an R value equal to 1.00.

and h_i can be approximated by using the experimentally determined $\Delta G_f^o[Fe(OH)_3]$ and $\Delta H_f^o[Fe(OH)_3]$. The values of ΔG_f^o = -696.50 kJ·mol^{-1}, and ΔH_f^o = -823.0 kJ·mol^{-1} (Wagman et al., 1982) can be used along with g_i = -35.6 + 0.990 ΔG_f^o and h_i = -38.3 + 0.995 ΔH_f^o to estimate g_i = -725.0 kJ·mol^{-1}, and h_i = -856.8 kJ·mol^{-1}. However, the errors associated with these estimates are unknown and may be large.

Table 7 describes the protocol to follow when estimating the thermodynamic properties of a silicate mineral using the model described above. It shows, as an example, the estimation of ΔG_f^o for an illite ($K_{0.75}(Al_{1.75}Mg_{0.25})Si_{3.5}Al_{0.5}O_{10}(OH)_2$). The estimated ΔG_f^o of this illite is -5463.0 kJ·mol^{-1}. Using an analogous procedure, it was found that ΔH_f^o = -5837.3 kJ·mol^{-1}. Note that the procedure for distributing the octahedral cations in step 2B is based on crystallographic constraints (Weaver and Pollard, 1973). On the other hand, the distribution of cations into the interlayer of chlorites (step 2C) is based on a thermodynamic argument, which results in the most negative (stable) ΔG_f^o for a given composition. Also, using ΔG_f^o and ΔH_f^o oxide/ hydroxide for cations in the chlorite interlayer is justified by the fact that chlorite interlayers act as simple oxide/hydroxide phases rather than as part of the silicate lattice. The presence of $Fe(OH)_2$ and $Mg(OH)_2$ in chlorite interlayers will be proposed later in this paper as a buffer to control the Fe^{2+} and Mg^{2+} contents of natural waters.

The difference between the thermodynamic properties of the oxide or hydroxide components in silicate minerals (g_i and h_i) and those components in simple minerals (ΔG_f^o and ΔH_f^o) is primarily a result of each interaction of the polyhedron with its nearest neighbors. For example, $Al(OH)_3$ in gibbsite is surrounded by six $Al(OH)_3$ polyhedra while an $Al(OH)_3$ polyhedron in the silicate minerals considered in this model is generally surrounded by, at most, only two $Al(OH)_3$ polyhedra with the other sites occupied by other tetrahedral components (generally SiO_2). The presence of these other components in the

Table 7. Method of estimation of ΔG_f^o and ΔH_f^o for a mineral in $kJ \cdot mol^{-1}$.

1. Determine chemical composition (analytical electron microscopy, microprobe, x-ray fluorescence, or wet chemical analysis).
2. Determine coordination based on known structures.
   A. For Ca-zeolite minerals with an unknown coordination number, the polyhedra is simply represented with a "z".
   B. For 1:1 phyllosilicate minerals distribute the octahedral cations as 0.6666 hydroxide and 0.3333 oxide. For 2:1 phyllosilicate minerals, the octahedral cations are distributed as 0.3333 hydroxide and 0.6666 oxide.
   C. For chlorites, distribute cations into the interlayer in the order $Al^{3+} > Fe^{2+} \geq Mg^{2+} > Fe^{3+}$ until the $(OH)_{interlayer\ total} = 8$. The remaining cations are then distributed into the octahedral sheet following the method in 2B.
3. Determine the number of polyhedra, n, of each component in the formula unit.
4. Multiply n by the g_i and h_i values (Table 2). The interlayer thermodynamic contribution for chlorites is then calculated by multiplying ΔG_f^o and ΔH_f^o of free oxide or hydroxide (Table 6) by the corresponding values of n determined in 2C.
5. Calculate ΔG_f^o and ΔH_f^o for the mineral of interest by summing the polyhedral contributions.

Example: Estimation of the ΔG_f^o of an illite.

1. Chemical formula = $K_{0.75}(Al_{1.75}Mg_{0.25})Si_{3.5}Al_{0.50}O_{10}(OH)_2$
2. In this structure the polyhedra are: $Al_2O_3(4)$, $Al_2O_3(6)$, $Al(OH)_3(6)$, $SiO_2(4)$, $MgO(6)$, $Mg(OH)_2(6)$, and $K_2O(8\text{-}12)$.
3. The number of each polyhedra are: $0.2500Al_2O_3(4)$, $0.5833Al_2O_3(6)$, $0.5833Al(OH)_3(6)$, $3.500SiO_2(4)$, $0.1666MgO(6)$, $0.08333Mg(OH)_2(6)$, and $0.3750K_2O(8\text{-}12)$.
4. $\Delta G_f^o = [0.2500\ (g_i\ [Al_2O_3(4)]) + 0.5833\ (g_i\ [Al_2O_3(6)]) + 0.5833\ (g_i\ [Al(OH)_3(6)]) + 3.500\ (g_i\ [SiO_2(4)]) + 0.1666\ (g_i\ [MgO(6)]) + 0.08333\ (g_i\ [Mg(OH)_2(6)]) + 0.3750\ (g_i\ [K_2O(8\text{-}12)])]$

   $\Delta G_f^o = [(0.2500)(-1631.32) + (0.5833)(-1594.52) + (0.5833)(-1181.62) + (3.500)(-853.95) + (0.1666)(-628.86) + (0.08333)(-851.86) + (0.3750)(-722.94)]$
5. $\Delta G_f^o = -5463.0\ kJ \cdot mol^{-1}$, ΔH_f^o can be determined the same way.

nearest neighbor sites clearly stabilizes the $Al(OH)_3$ in the silicates by the amount $g_i - \Delta G_f^o \approx 28$ kJ·mol^{-1}. The amount of this stabilization varies from site to site depending on the composition of the nearest neighbor shell, but the efficacy of the model presented here demonstrates that this stabilization value is fairly constant for a wide variety of sites in a wide range of silicate compositions, regardless of structure type. Conversely, however, this consideration means that the coefficients derived in this model are likely to be useful only for silicates. Notice that in Table 6 the only polyhedron in which $g_i > \Delta G_f^o$ is SiO_2, this is consistent with quartz being a very common mineral.

Thermodynamic data for ordered phases were chosen, whenever available, to create this model. As a result it seems likely that the estimated ΔG_f^o and ΔH_f^o values should be closest to those for a completely ordered mineral. Please note, however, that the variation in these values between ordered and disordered phases is generally smaller than the uncertainty of the estimate. For example, the differences between ΔG_f^o and ΔH_f^o for microcline versus sanadine is 0.07% and 0.20% respectively (Robie et al., 1978) while the uncertainity of our estimate of these values for microcline are on the order ±0.25%. A more sophisticated model will be necessary to develop enough resolution to account for order/disorder effects on these thermodynamic quantities.

This technique has a wide variety of applications in predicting thermodynamic properties of common zeolites and clays. First, the relative stability of clays in the K_2O - Al_2O_3 - SiO_2 - H_2O system will be discussed. Using the thermodynamic data in Table 8 a log a_{K^+}/a_{H^+} versus log $a_{H_4SiO_4}$ diagram at 298 K was constructed (Figure 3). Figure 3 shows the metastability of Al-montmorillonite and Al-illite, which agrees with the 298 K experimental data of Sass et al. (1987). In order to represent natural compositions more closely we determined the effect on ΔG_f^o of the substitution of various cations (Fe^{3+}, Fe^{2+}, and Mg^{2+}) into the montmorillonite and illite structures (Table 8). Figure 3 shows how

Table 8. ΔG_f^o data used in the calculation of the K_2O-Al_2O_3-SiO_2-H_2O diagrams.

Species	Chemical formula	ΔG_f^o kJ·mol^{-1}
1 Kaolinite	$Al_2Si_2O_5(OH)_4$	-3799.4
2 Pyrophyllite	$Al_2Si_4O_{10}(OH)_2$	-5265.9
3 Microcline	$KAlSi_3O_8$	-3742.3
4 Muscovite	$KAl_2(Si_3Al)O_{10}(OH)_2$	-5595.5
5 Water	H_2O	-237.1
6 Silicic acid	H_4SiO_4	-1309.2
7 Goethite	FeOOH	-488.7
8 Brucite	$Mg(OH)_2$	-833.5
9 Ferrous hydroxide	$Fe(OH)_2$	-492.0
10 Potassium ion	K^+	-282.7
11 Illite (Al)	$K_{0.75}Al_2(Si_{3.25}Al_{0.75})O_{10}(OH)_2$	-5508.9
12 Mont. (Al)	$K_{0.3}Al_{1.9}Si_4O_{10}(OH)_2$	-5282.5
13 Illite (Mg)	$K_{0.75}Al_{1.75}Mg_{0.25}(Si_{3.50}Al_{0.50})O_{10}(OH)_2$	-5463.0
14 Mont. (Mg)	$K_{0.30}Al_{1.70}Mg_{0.30}Si_4O_{10}(OH)_2$	-5308.3
15 Illite (Fe^{2+})	$K_{0.75}Al_{1.75}Fe_{0.25}(Si_{3.50}Al_{0.50})O_{10}(OH)_2$	-5376.7
16 Mont.(Fe^{2+})	$K_{0.30}Al_{1.70}Fe_{0.30}Si_4O_{10}(OH)_2$	-5204.8
17 Illite (Fe^{3+})	$K_{0.75}Al_{1.6}Fe_{0.4}(Si_{3.25}Al_{0.75})O_{10}(OH)_2$	-5338.9
18 Mont. (Fe^{3+})	$K_{0.30}Al_{1.5}Fe_{0.4}Si_4O_{10}(OH)_2$	-5112.4
19 Illite (Fe^{3+}, Mg)	$K_{0.75}Al_{1.35}Fe_{0.4}Mg_{0.25}(Si_{3.50}Al_{0.50})O_{10}(OH)_2$	-5293.0
20 Mont. (Fe^{3+}, Mg)	$K_{0.30}Al_{1.3}Fe_{0.4}Mg_{0.30}Si_4O_{10}(OH)_2$	-5138.3
21 Erionite	$KAlSi_3O_8 \cdot 3H_2O$	-4458.7
22 Phillipsite	$K_3Al_3Si_5O_{16} \cdot 6H_2O$	-9240.6
23 Clinoptilolite	$KAlSi_5O_{12} \cdot 4H_2O$	-6406.5

Sources: 1-3, 5, 7, 8, and 10 Robie et al. (1978); 4 Krupka et al. (1979); 6 Rimstidt (1984); 9 Nordstrom et al. (1984); and 11-23 this model.

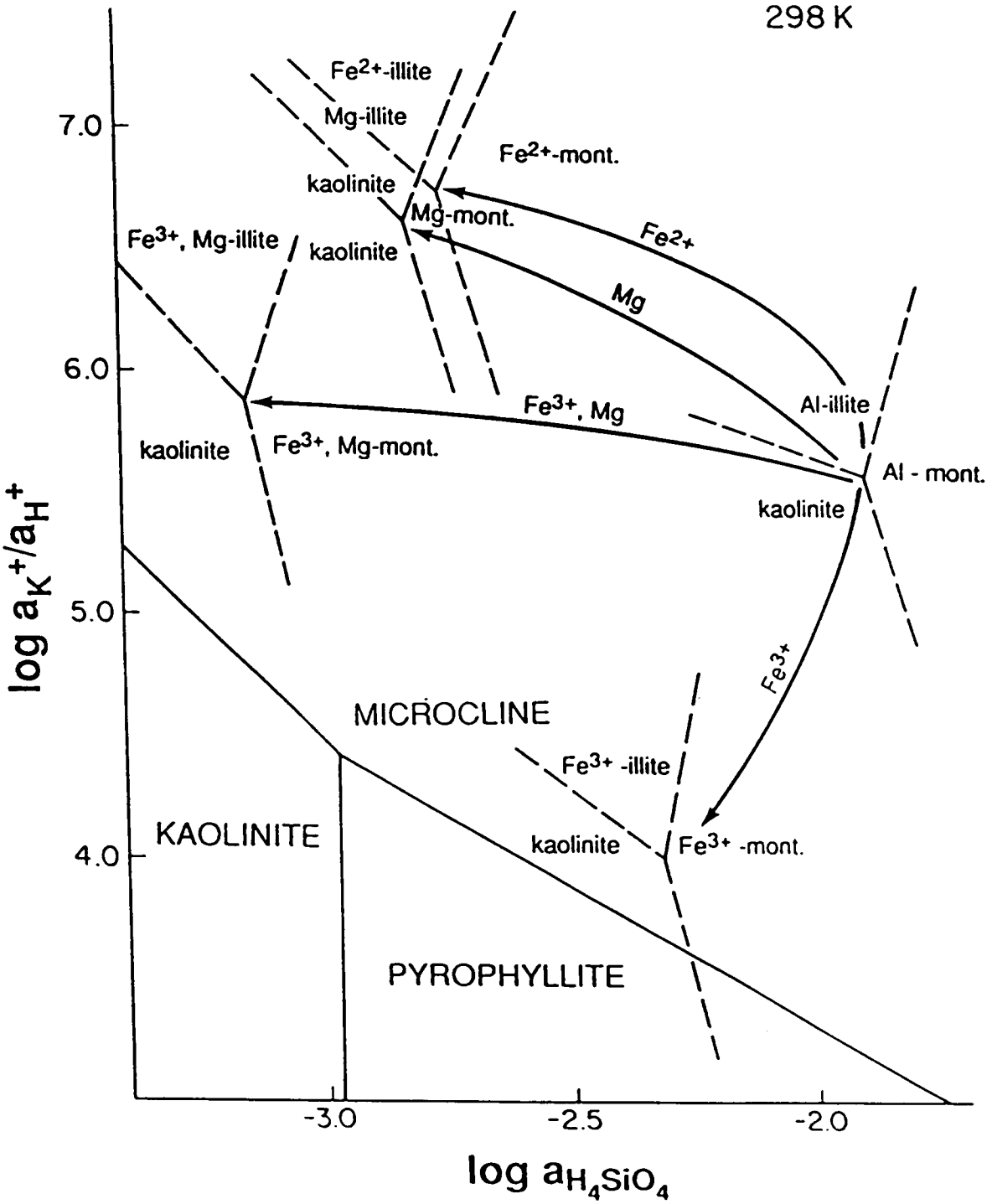

Fig. 3. Activity-activity diagram of the K_2O-Al_2O_3-SiO_2-H_2O system at 298 K showing the stable microcline-kaolinite-pyrophyllite triple point. This diagram also shows the effect of Mg^{2+}, Fe^{3+}, Fe^{2+}, and both Mg^{2+}-Fe^{3+} substitution (arrows) on the stability of the kaolinite-montmorillonite- illite triple point. Chemical compositions and thermodynamic data are given in Table 8.

these cation substitutions shift the kaolinite-montmorillonite-illite triple point. Notice that the ferric iron substitution seems to cause the greatest degree of stabilization of montmorillonite and illite. When writing reactions containing Fe^{3+}, Fe^{2+}, and Mg^{2+}, the concentrations of these cations in solution were assumed to be controlled by FeOOH, $Fe(OH)_2$, and $Mg(OH)_2$ solubilities. The choice of $Fe(OH)_2$ and $Mg(OH)_2$ as controls of Fe^{2+} and Mg^{2+} concentrations assumes the presence of chlorite interlayers containing these components, as previously discussed. If an amorphous ferric hydroxide phase controls the ferric iron concentration, the kaolinite-montmorillonite-illite triple point becomes even more stable relative to kaolinite, microcline, and pyrophyllite.

This technique was also used to estimate the ΔG_f^o of three K-zeolites: clinoptilolite, erionite, and phillipsite (Table 8). The results show that phillipsite is stable at SiO_2 concentrations <12 ppm, erionite between 12-16 ppm, and clinoptilolite >16ppm (Figure 4). Extensive zeolite formation (clinoptilolite, erionite, and phillipsite) at surface conditions (25°C) has been observed in altered volcanic tuffs (Hay 1986, and Sheppard and Gude 3d, 1973). Senkayi et al. (1987) observed the coexistence of opal CT-kaolinite-clinoptilolite at high silica concentrations, and Iijima (1978) reported that clinoptilolite and phillipsite are prominent in sediments in coexistence with interstitial water which has SiO_2 concentrations of between 6-42 ppm, and 5-21 ppm, respectively. The constructed activity diagram (Figure 4) is consistent with these natural observations.

CONCLUSIONS

The multiple linear regression technique presented here is a simple and effective way to estimate the ΔG_f^o and ΔH_f^o of silicate minerals. The only data needed for this estimation technique are the chemical composition and the coordination of the "building block"

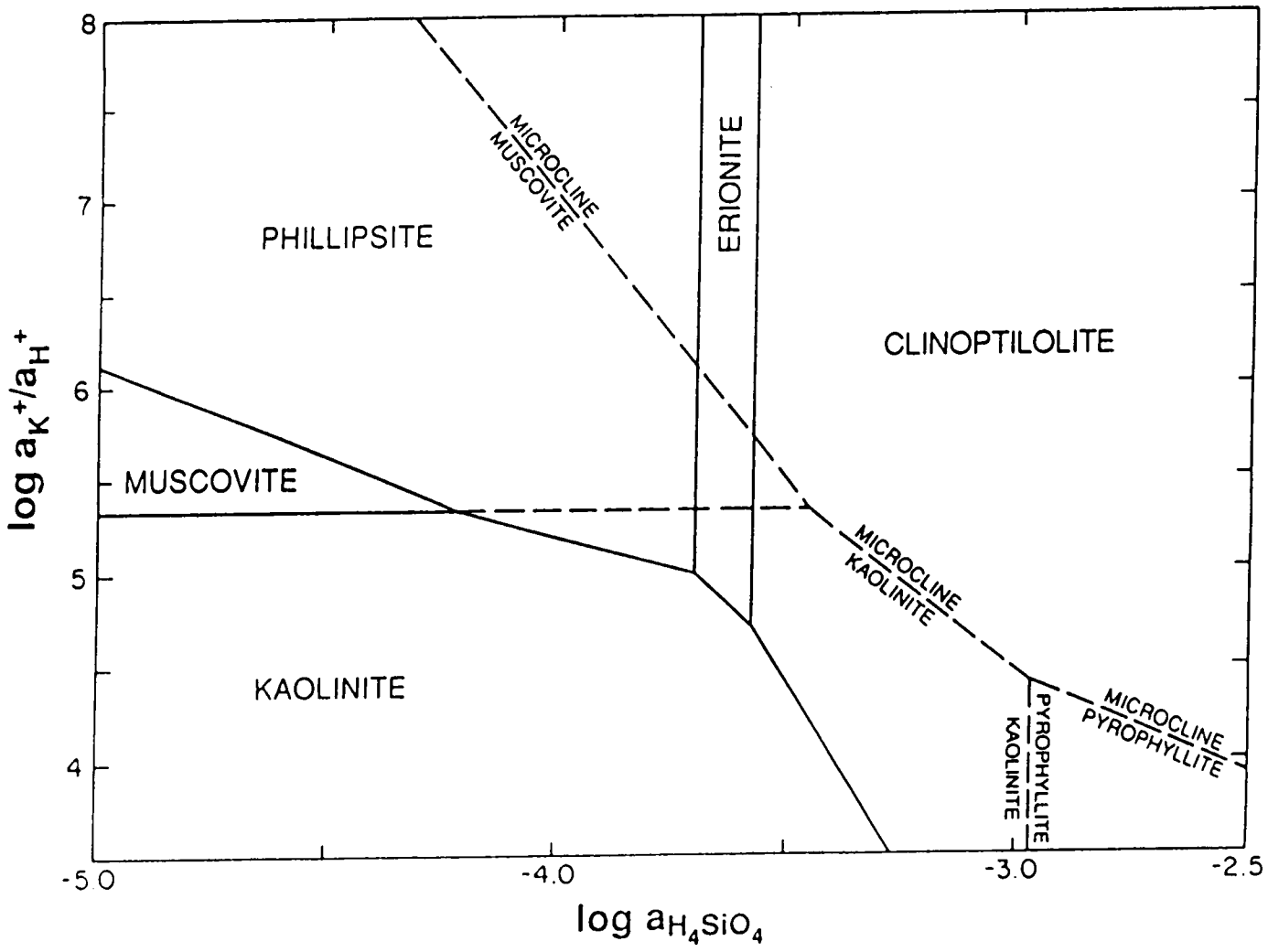

Fig. 4. Activity-activity diagram of the K_2O-Al_2O_3-SiO_2-H_2O system at 298 K showing three K-zeolite phases (phillipsite, erionite, and clinoptilolite). Thermodynamic data taken from Table 8.

polyhedra in the mineral of interest. The advantages of the technique include its simplicity (it can be programed into a microcomputer spreadsheet program), the fact that the model is based on calorimetric and high temperature phase equilibrium measurements rather than more difficult to perform solubility measurements, and its ability to model a wide range of silicate minerals. The technique gives results that agree quite well with a wide range of calorimetric and solubility data not used to derive the reported coefficients.

Although this technique seems to give reliable results for most cases, it should be used with some caution. We already know that the model presented here fails to predict accurately the thermodynamic properties of Ca-Al pyroxene, forsterite, cordierite, andradite, and gehlenite. There is no question that experimentally determined thermodynamic data are more accurate than these estimates and should be used in calculations when available. Furthermore, the user should always consider whether the predictions of this approach make sense in terms of their geologic/geochemical experience.

The overall usefulness of this model is demonstrated by showing a few examples in the K_2O - Al_2O_3 - SiO_2 - H_2O system. These activity-activity diagrams show that the clay mineral relations and the zeolite stability ranges determined using the estimated data agree well with experimental and geologic observations. Thus, the overall approach can be used to derive information on clay and zeolite mineral stabilities, and then to develop a better understanding of chemical reactions that occur during diagenesis. The ΔG^0_r values estimated from the model can be extrapolated to higher temperatures using estimated ΔH_r in the van't Hoff equation or by developing a similar model using higher temperature experimental data. In addition, it is likely that this technique could successfully model the thermodynamic properties of other complex mineral families (eg. sulfates, phosphates, arsenates and vanadates). Finally, this research extends the use of the "polyhedral approach" (Hazen, 1988) in modelling the thermodynamic properties of silicate minerals

from S^{o}(Robinson and Haas, 1983; Holland, 1989) to include ΔG_f^o and ΔH_f^o. The success of these "polyhedral models" strongly support the concept that the properties of silicate minerals are mostly determined by nearest neighbor interactions rather than by the longer range ordering used to classify these minerals into structure types.

ESTIMATING ΔG_f^0 OF SILICATE MINERALS AT HIGH TEMPERATURES FROM THE SUM OF POLYHEDRAL CONTRIBUTIONS

ABSTRACT

The technique that we developed to estimate ΔG_f^o of silicate minerals by summing the contribution of polyhedral components at 298 K (Chermak and Rimstidt 1989) can be extended to predict the free energy of formation of silicate minerals at higher temperatures. This approach is particularly useful for clays and zeolites which are geologically abundant and geochemically reactive but have few reported data for their ΔG_f^o at temperatures above 25°C. Multiple linear regression was used to find the contribution of the $Al_2O_3(4)$ - $Al_2O_3(6)$ - $Al(OH)_3(6)$ - $SiO_2(4)$ - $MgO(6)$ - $Mg(OH)_2(6)$ - $CaO(6)$ - $CaO(8\text{-}Z)$ -$Na_2O(6\text{-}8)$ - $K_2O(8\text{-}12)$ - H_2O - $FeO(6)$ - $Fe(OH)_2(6)$ - $Fe_2O_3(6)$ components to the total ΔG_f^o and ΔH_f^o at 298 K of a selected group of silicate minerals (Chermak and Rimstidt 1989). The g_i coefficients from this model can be extrapolated to higher temperatures using the equation $g_i(T) = h_i(298\ K) - T\left(\frac{h_i(298\ K) - g_i(298\ K)}{298}\right)$, where g_i and h_i are the respective molar free energy and enthalpy contribution of one mole of each oxide or hydroxide component at 298 K. The g_i of water was found to vary depending upon the cation with which it was associated. Therefore g_{water} was determined by two seperate multiple linear regressions, one for Na^+ and the other for Ca^{2+}. Experimentally measured ΔG_f^o versus predicted ΔG_f^o for 21 minerals used in the model have associated differences of 0.20%, 0.20%, and 0.22% at 400, 500, and 600 K respectively . Experimentally measured ΔG_f^o versus predicted ΔG_f^o for four, three, and two minerals not used in the model have associated differences of 0.33%, 0.33%, and 0.13% at 400, 500, 600 K respectively.

INTRODUCTION

Several techniques exist for estimating the ΔG_f^o of silicate minerals at 298 K (see the discussion in Chermak and Rimstidt 1989), but there are few techniques for estimating free energy of formation (ΔG_f^o) of silicate minerals at higher temperatures (Helgeson et al., 1979 and Helgeson et al., 1981). This paper describes a technique to determine the contribution of oxide and hydroxide components to the ΔG_f^o of silicate minerals at higher temperatures and these contributions can be used to estimate the ΔG_f^o of other minerals for which there are currently no data. These estimates can be used to understand silicate mineral equilibria in many different geologic processes such as diagenesis, hydrothermal alteration, and low grade metamorphism.

The technique is based on the observation that silicate minerals act as a combination of polyhedral units (Hazen 1985, 1988). Chermak and Rimstidt (1989) showed that the thermodynamic properties of selected silicate minerals could be estimated by summing the contributions of their individual oxide and hydroxide polyhedral building blocks. In this paper we show how the $g_{i(298)}$ and $h_{i(298)}$ values determined for $Al_2O_3(4)$ - $Al_2O_3(6)$ - $Al(OH)_3(6)$ - $SiO_2(4)$ - $MgO(6)$ - $Mg(OH)_2(6)$ - $CaO(6)$ - $CaO(8\text{-}z)$ -$Na_2O(6\text{-}8)$ - $K_2O(8\text{-}12)$ - $FeO(6)$ - $Fe(OH)_2(6)$ - $Fe_2O_3(6)$ polyhedra can be used to estimate the ΔG_f^o of silicate minerals containing these components at higher temperatures.

METHODS

A multiple linear regression technique was used to estimate the contribution (g_i and h_i) of the $Al_2O_3(4)$ - $Al_2O_3(6)$ - $Al(OH)_3(6)$ - $SiO_2(4)$ - $MgO(6)$ - $Mg(OH)_2(6)$ - $CaO(6)$ - $CaO(8\text{-}Z)$ - $Na_2O(6\text{-}8)$ - $K_2O(8\text{-}12)$ - H_2O - $FeO(6)$ - $Fe(OH)_2(6)$ - $Fe_2O_3(6)$ components to the total ΔG_f^o and ΔH_f^o of a selected group of silicate minerals (Chermak and Rimstidt 1989). The gi

and hi values from this regression model are used to estimate the ΔG_f^o and ΔH_f^o of other silicate minerals from a weighted sum of the contribution of each oxide and hydroxide component: $\Delta G_f^o = \Sigma\, n_i\, g_i$, and $\Delta H_f^o = \Sigma\, n_i\, h_i$, where n_i is the number of moles of the oxide or hydroxide per formula unit and g_i and h_i are the respective molar free energy, and enthalpy contribution of one mole of each oxide or hydroxide component.

Experimentally measured ΔG_f^o and ΔH_f^o vs. predicted ΔG_f^o and ΔH_f^o for the minerals used in the model have associated average residuals of 0.26%, and 0.24% respectively. For minerals not used in the model for which there are experimentally determined calorimetric data the average differences between measured and predicted values of ΔG_f^o for 18 minerals is 0.25% and 0.22% for ΔH_f^o for 20 minerals.

The basis for this estimation model is the development of a function to extrapolate the g_i values to higher temperatures. A temperature function, g_i (T), was found for each polyhedral component using the relation, G = H - TS, and the g_i (298 K) and h_i (298 K) values for oxide and hydroxide polyhedra reported in Chermak and Rimstidt (1989). The relationship of these variables at 298 K is

$$g_i\ (298\ K) = h_i\ (298\ K) - 298\ s_i\ (298\ K) \qquad (1)$$

where g_i (298 K) , h_i (298 K), and s_i (298 K) are the respective molar free energy, enthalpy, and entropy of formation from the elements of one mole of the polyhedral component at 298 K and one bar. Equation 1 can be rearranged to

$$s_i\ (298\ K) = \left(\frac{h_i\ (298\ K) - g_i\ (298\ K)}{298} \right) \qquad (2)$$

Assuming that $\Delta Cp,r$ (the change in heat capacity of reaction) from 298 K to temperature is equal to zero and using a standard thermodynamic relationship, equation (4-13) in Nordstrom and Munoz (1985)

$$g_i\,(T) - g_i\,(298) = -s_i\,(298)\,(T - 298) \qquad (3)$$

Substituting equation (2) into equation (3) gives

$$g_i\,(T) - g_i\,(298\ K) = -T\left(\frac{h_i\,(298\ K) - g_i\,(298\ K)}{298}\right) + 298\left(\frac{h_i\,(298\ K) - g_i\,(298\ K)}{298}\right) \qquad (4)$$

which can be simplified to find $g_i\,(T)$

$$g_i\,(T) = h_i\,(298\ K) - T\left(\frac{h_i\,(298\ K) - g_i\,(298\ K)}{298}\right) \qquad (5)$$

This is a linear function with an intercept of $g_i = h_i$ at 0 K and a slope of $[(h_i\,(298\ K) - g_i\,(298\ K)) / 298]$.

In addition, it was realized during the course of this study that the g_{H_2O} values published in Chermak and Rimstidt (1989) could be improved by accounting for the cation with which the water is associated. The g_{H_2O} values were revised as follows. Multiple linear regression (MLR) was used to calculate the values for $g_{water(298)}$ in association with Na^+ and Ca^{2+}. The $g_{water(298)}$ in Chermak and Rimstidt (1989) is for water associated with either Na^+ or Ca^{2+}, more accurate estimates of ΔG_f^o of hydrous phases were found when Na^+ and Ca^{2+} associated waters were regressed seperately. The same twenty-nine minerals (excluding the Ca^{2+} - H_2O associated minerals) used in Chermak and Rimstidt

(1989) were broken into their "building block" components and MLR was used to determine that g_{water} (298 K) = -230.82 kJ mol^{-1} for Na^+ associated water and g_{water} (298 K) = -240.57 kJ mol^{-1} for Ca^{2+} associated water. The g_i values of the other components did not change significantly in these new MLR.

RESULTS

Table 1 shows the g_i (T) functions for the polyhedral components considered in this model. Tables 2a and b show experimentally measured ΔG_f^o versus those predicted using the coefficients generated by the functions in Table 1. The average difference between the predicted and the measured values is 0.20% for ΔG_f^o at 400 K, 0.20% for ΔG_f^o at 500 K, and 0.22% for ΔG_f^o at 600 K. Note that only 298.15 K data were used to develop the estimation model for these phases. The accuracy of the model was tested by predicting the thermodynamic properties of some minerals not used to develop the model. Table 2b compares the model's results with calorimetrically determined thermodynamic data for four (400 K), three (500 K), and two (600 K) different minerals and gives associated differences. Average residuals for these minerals are: 0.33% for ΔG_f^o at 400 K, 0.33% for ΔG_f^o at 500 K, and 0.13% for ΔG_f^o at 600 K.

Multiple linear regression analysis was also used to determine the g_{water} (298) value for a mixed Na^+ and Ca^{2+} bearing mordenite (g_{water} = -237.93 kJ mol^{-1}). The percent site occupancy ($X_{Ca^{2+}}$ and X_{Na^+}) was then plotted against the value of g_{water} to determine the relation of g_{water} at any Na^+ and Ca^{2+} mole fraction combination. The calculated equation is,

$$g_{water} = -230.8 - 20.75\ (X_{Ca^{2+}}) + 11.00\ (X_{Ca^{2+}})^2 \qquad (6)$$

Table 1. g_i (T) in kJ mol^{-1}, for individual polyhedral components. Temperature in Kelvins.

Polyhedral component	Temperature Function $g_i(T) = h_i(298\ K) - T\left(\frac{h_i(298\ K) - g_i(298\ K)}{298}\right)$
$Al_2O_3(4)$	$g_{i(T)} = -1716.2 + 0.2848T$
$Al_2O_3(6)$	$g_{i(T)} = -1690.2 + 0.3209T$
$Al(OH)_3(6)$	$g_{i(T)} = -1319.6 + 0.4626T$
$SiO_2(4)$	$g_{i(T)} = -911.0 + 0.1913T$
$MgO(6)$	$g_{i(T)} = -660.1 + 0.1047T$
$Mg(OH)_2(6)$	$g_{i(T)} = -941.6 + 0.3011T$
$CaO(6)$	$g_{i(T)} = -696.7 + 0.0923T$
$CaO(8\text{-}Z)$	$g_{i(T)} = -736.0 + 0.0871T$
$Na_2O(6\text{-}8)$	$g_{i(T)} = -683.0 + 0.0352T$
$K_2O(8\text{-}12)$	$g_{i(T)} = -735.2 + 0.0413T$
$FeO(6)$	$g_{i(T)} = -290.6 + 0.0814T$
$Fe(OH)_2(6)$	$g_{i(T)} = -596.1 + 0.1812T$
$Fe_2O_3(6)$	$g_{i(T)} = -939.2 + 0.5471T$
$H_2O(Na)$	$g_{i(T)} = -283.2 + 0.1760T$
$H_2O(Ca)$	$g_{i(T)} = -293.0 + 0.1760T$

Table 2a.Comparison of measured ΔG_f^o versus predicted ΔG_f^o (kJ mol^{-1}) at 400, 500, and 600 K for minerals used in the model.

Mineral	ΔG_f^o (400) meas. / pred.	% difference	ΔG_f^o (500) meas. / pred.	% difference	ΔG_f^o (600) meas. / pred.	% difference
1 Kaolinite	-3689.9 / -3702.3	0.34	-3582.2 / -3591.7	0.26	-3474.8 / -3481.0	0.18
2 Muscovite	-5471.3 / -5461.5	0.18	-5344.0 / -5335.6	0.16	-5217.3 / -5209.7	0.14
3 Margarite	-5722.9 / -5728.5	0.10	-5593.4 / -5600.4	0.12	-5464.4 / -5472.2	0.14
4 Talc	-5406.0 / -5395.5	0.19	-5278.4 / -5267.9	0.20	-5151.4 / -5140.2	0.21
5 Pyrophyllite	-5140.0 / -5135.5	0.09	-5014.2 / -5006.8	0.15	-4888.9 / -4878.0	0.22
6 Microcline	-3664.6 / -3663.9	0.02	-3587.7 / -3590.2	0.07	-3511.0 / -3516.6	0.16
7 Low albite	-3634.9 / -3639.0	0.11	-3558.9 / -3565.6	0.19	-3483.1 / -3492.2	0.26
8 Anorthite	-3924.8 / -3930.9	0.16	-3849.0 / -3855.0	0.16	-3773.5 / -3779.0	0.14
9 Fayalite	-1345.4 / -1350.5	0.37	-1312.3 / -1315.1	0.21	-1279.6 / -1279.7	0.00
10 Leucite	-2820.3 / -2829.4	0.32	-2766.1 / -2774.9	0.32	-2712.5 / -2720.3	0.30
11 Tremolite	-5689.2 / -5686.1	0.05	-5567.1 / -5564.9	0.04	-5445.7 / -5443.7	0.04
12 Jadeite	-2789.3 / -2784.3	0.18	-2728.3 / -2728.3	0.00	-2667.5 / -2672.2	0.18
13 Diopside	-2977.0 / -2988.3	0.38	-2918.7 / -2930.9	0.42	-2860.6 / -2873.5	0.45
14 Merwinite	-4261.8 / -4266.2	0.11	-4186.0 / -4189.9	0.10	-4111.0 / -4113.5	0.06
15 Grossular	-6150.9 / -6168.9	0.29	-6029.7 / -6053.3	0.39	-5908.9 / -5937.8	0.48
16 Zoisite	-6359.7 / -6366.5	0.11	-6226.7 / -6233.5	0.11	-6094.1 / -6100.5	0.11
17 Grunerite	-4375.7 / -4373.7	0.04	-4266.0 / -4263.7	0.05	-4156.4 / -4153.7	0.06
18 Riebeckite	-4582.4 / -4552.3	0.66	-4466.9 / -4429.5	0.84	-4351.5 / -4306.7	1.00
19 Chrysotile	-3921.8 / -3929.5	0.20	-3811.8 / -3820.6	0.23	-3702.3 / -3711.7	0.25
20 Prehnite	-5687.3 / -5688.9	0.03	-5560.6 / -5563.8	0.06	-5434.6 / -5438.6	0.07
21 Analcime	-3001.8 / -3004.7	0.10	-2927.4 / -2932.7	0.18	-2853.3 / -2860.8	0.26
	Average =	0.20	Average =	0.20	Average =	0.22

1, 2, 4, 6-14, 19, and 21 Robie et al. (1978); 3, 5, 15, 16, and 20 Hemingway et al. (1982); 17 and 18 Makarov et al. (1984).

Table 2b. Comparison of measured ΔG_f^o versus predicted ΔG_f^o (kJ mol^{-1}) at 400, 500, and 600 K for minerals not used in the model.

Mineral	ΔG_f^o (400) meas. / pred.	% difference	ΔG_f^o (500) meas. / pred.	% difference	ΔG_f^o (600) meas. / pred.	% difference
1 Kyanite	-2392.5 / -2396.3	0.16	-2341.9 / -2345.1	0.14	-2291.4 / -2293.9	0.11
2 Ca-Olivine	-2159.8 / -2153.9	0.27	-2120.7 / -2116.4	0.20	-2081.8 / -2078.8	0.14
3 Natrolite	-5178.5 / -5199.1	0.40	-5041.9 / -5074.5	0.65		
4 Scolecite	-5443.7 / -5470.0	0.48				
	Average =	0.33	Average =	0.33	Average =	0.13

1 and 2 Hemingway et al. (1982); 3 and 4 Johnson et al. (1983).

if $X_{Ca^{2+}} = 1$, $g_{water} = -230.8 - 20.75 + 11.00 = -240.5$ kJ mol^{-1}. This equation could be refined further if more data were available. The h_{water} of Na^+ and Ca^{2+} was determined by using equation 1 and the slope of 0.176, which was determined by a plot of g_{water} (298 K) and h (298 K) versus temperature (Chermak and Rimstidt 1989).

Table 3 describes the algorithm to estimate the ΔG_f^o of a silicate mineral using the model described above. It shows, as an example, the estimation of ΔG_f^o for an illite ($K_{0.75}(Al_{1.75}\ Mg_{0.25})Si_{3.5}Al_{0.5}O_{10}\ (OH)_2$) at 500 K. The estimated ΔG_f^o of this illite is -5335.1 kJ mol^{-1} at 400 K, -5209.4 kJ mol^{-1} at 500 K, -5084.0 kJ mol^{-1} at 600 K.

DISCUSSION

It was found that the g_i coefficients predicted for higher temperatures by this model are well correlated with the ΔG_f^o of the free oxide or hydroxide components just as they are at 298 K (Chermak and Rimstidt 1989). For example, comparison was made of the g_i (T) from these models to the ΔG_f^o (Table 4) at 400, 500, and 600 K for the simple oxide or hydroxide components. Figure 1 is a plot of g_i (600 K) versus ΔG_f^o (600 K) where the corresponding equation of g_i (600 K) = -2.842 + 1.026 ΔG_f^o has an $R^2 = 0.999$. Equations for the regression lines at 400 and 500 K are g_i (400 K) = -39.76 + 0.982 ΔG_f^o $R^2 = 0.996$ and g_i (500 K) = -10.53 + 1.023 ΔG_f^o $R^2 = 0.998$. These correlation lines can be used to approximate a g_i (T) for polyhedra not determined by this model (Chermak and Rimstidt 1989). However, the errors associated with these estimates are unknown and may be large.

The slope of the line [(h_i (298 K) - g_i (298 K)) / 298] for each polyhedron is an indication of its change in stability as a function of temperature. The steeper the slope the more

Table 3. Method of estimation of ΔG_f^o at temperature for a mineral in $kJ \cdot mol^{-1}$.

1. Determine chemical composition (analytical electron microscopy, microprobe, x-ray fluorescence, or wet chemical analysis).
2. Determine coordination based on known structures.
   - A. For Ca-zeolite minerals with an unknown coordination number, the polyhedra is simply represented with a "z".
   - B. For 1:1 phyllosilicate minerals distribute the octahedral cations as 0.6666 hydroxide and 0.3333 oxide. For 2:1 phyllosilicate minerals, the octahedral cations are distributed as 0.3333 hydroxide and 0.6666 oxide.
   - C. For chlorites, distribute cations into the interlayer in the order $Al^{3+} > Fe^{2+} \geq Mg^{2+} > Fe^{3+}$ until the $(OH)_{interlayer\ total} = 8$. The remaining cations are then distributed into the octahedral sheet following the method in 2B.
3. Determine the number of polyhedra, n, of each component in the formula unit.
4. Determine the g_i (T) value at temperature of each polyhedra (Table 1).
   - A. When determining g_{water} (T) in zeolites
     1. Determine the mole fraction (X) of Na^+ and Ca^{2+}.
     2. Use ($X_{Ca^{2+}}$) in polynomial equation (5), to determine g_{water} (298 K)
     3. Determine h_{water} (298 K) using h_{water} (298 K) = g_{water} (298 K) + 298[0.176]
     4. g_{water} (T) = h_{water} (298 K) + 0.1760T.
5. Multiply n by the g_t values. The interlayer thermodynamic contribution for chlorites is then calculated by multiplying ΔG_f^o of free oxide or hydroxide at temperature (Table 4) by the corresponding values of n determined in 2C.
6. Calculate ΔG_f^o at temperature for the mineral of interest by summing the polyhedral contributions.

Example: Estimation of the ΔG_f^o of an illite at 500 K.

1. Chemical formula = $K_{0.75}(Al_{1.75}Mg_{0.25})Si_{3.5}Al_{0.50}O_{10}(OH)_2$
2. In this structure the polyhedra are: $Al_2O_3(4)$, $Al_2O_3(6)$, $Al(OH)_3(6)$, $SiO_2(4)$, $MgO(6)$, $Mg(OH)_2(6)$, and $K_2O(8\text{-}12)$.
3. The number of each polyhedra are: $0.2500Al_2O_3(4)$, $0.5833Al_2O_3(6)$, $0.5833Al(OH)_3(6)$, $3.500SiO_2(4)$, $0.1666MgO(6)$, $0.08333Mg(OH)_2(6)$, and $0.3750K_2O(8\text{-}12)$.
4. $\Delta G_f^o = [0.2500\ (g_{Al_2O_3(4)}\ (500\ K)) + 0.5833\ (g_{Al_2O_3(6)}\ (500\ K)) + 0.5833\ (g_{Al(OH)_3(6)}\ (500\ K)) + 3.500\ (g_{SiO_2(4)}\ (500\ K)) + 0.1666\ (g_{MgO(6)}\ (500\ K)) + 0.08333\ (g_{Mg(OH)_2(6)}\ (500\ K)) + 0.3750\ (g_{K_2O(8\text{-}12)}\ (500\ K))]$
   $\Delta G_f^o = [(0.2500)(-1573.8) + (0.5833)(-1529.8) + (0.5833)(-1088.3) + (3.500)(-815.3) + (0.1666)(-607.7) + (0.08333)(-791.1) + (0.3750)(-714.6)]$
5. $\Delta G_f^o = -5209.4\ kJ \cdot mol^{-1}$.

Table 4. Measured ΔG_f^o for each oxide/hydroxide compared to g_i (T) (kJ mol^{-1}).

Polyhedron	400 K		500 K		600 K	
	ΔG_f^o	g_i (400 K)	ΔG_f^o	g_i (500 K)	ΔG_f^o	g_i (600 K)
Al_2O_3(6)	-1550.2	-1602.3	-1518.6	-1573.8	-1487.2	-1545.3
$Al(OH)_3$(6)	-1107.7	-1134.6	-1061.1	-1088.3	-1014.9	-1042.0
SiO_2(4)	-837.7	-834.5	-819.4	-815.3	-801.2	-796.2
MgO(6)	-558.2	-618.2	-547.3	-607.7	-536.6	-597.3
$Mg(OH)_2$(6)	-802.3	-821.2	-771.9	-791.1	-741.7	-761.0
CaO(6)	-592.7	-659.7	-582.3	-650.5	-571.9	-641.3
FeO(6)	-244.2	-258.0	-237.6	-249.9	-231.1	-241.7
Fe_2O_3(6)	-714.9	-720.3	-688.1	-665.6	-661.9	-610.9

Thermodynamic data from Robie et al. 1978.

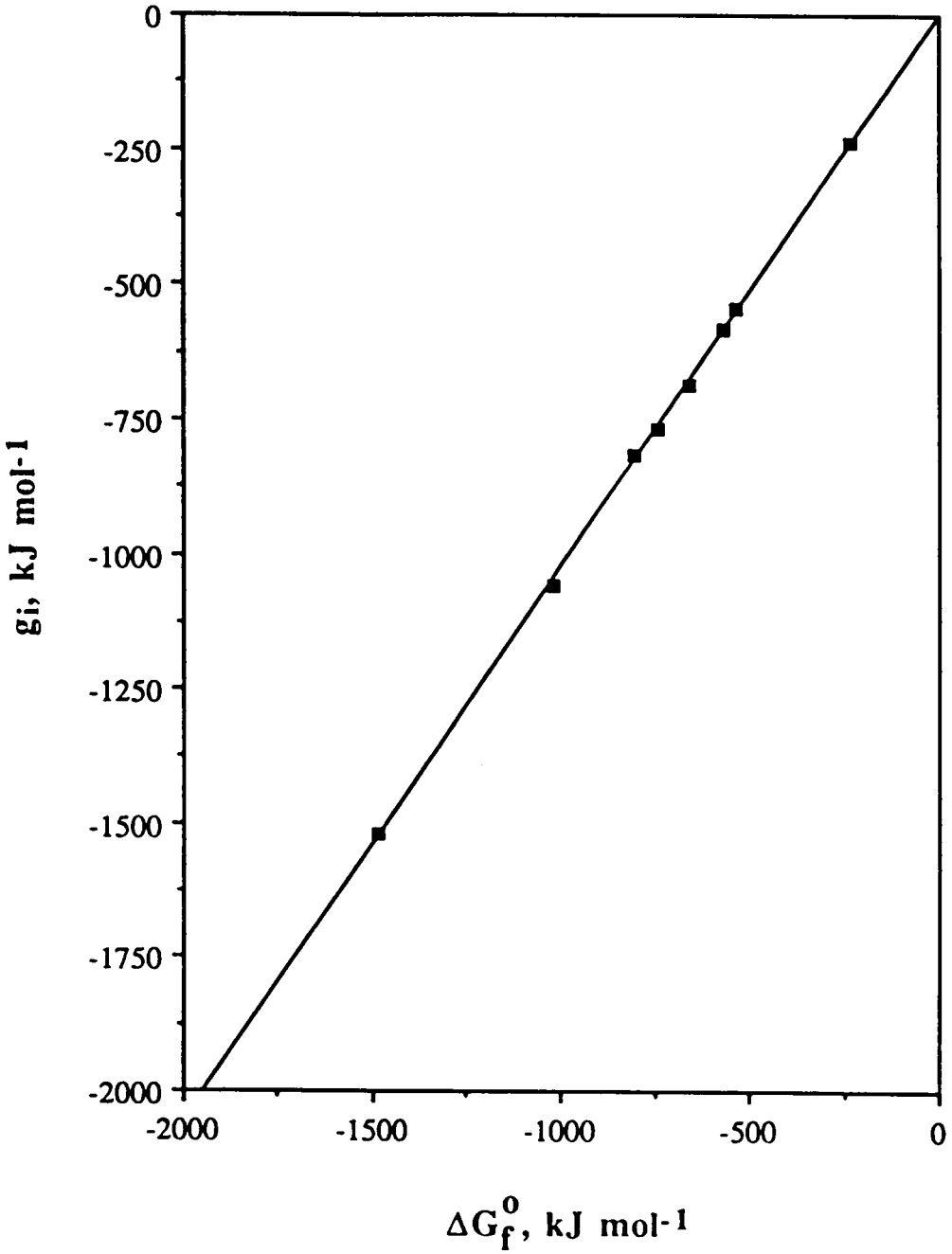

Fig. 1. Graph of the g_i (600 K) (kJ·mol^{-1}) versus ΔG_f^o oxide/hydroxide (kJ·mol^{-1}) data from Table 4.

unstable the component becomes in the silicate lattice relative to the elements with increasing temperature. The $Al(OH)_3$ and Fe_2O_3 polyhedra have the steepest associated slopes and the CaO (6, 8-Z), Na_2O (6-8), K_20 (8-12), and FeO(6) polyhedra have relatively shallow slopes.

Extrapolation of thermodynamic data from 298 K to higher temperatures using the assumption of constant becomes less reliable with increasing temperature. Differences between measured and predicted ΔG_f^o become larger (≈0.5%) at temperatures above 650 K. Possible reasons for this are that many of the minerals in the data base go through phase transitions between 700 - 900 K, and at higher temperatures the assumption that $\Delta Cp,r = 0$ is less accurate (Nordstrom and Munoz 1985). This model can still be used with caution above temperatures of 650 K but errors in estimates become larger.

Using the thermodynamic data in Table 5, we can illustrate the utility of this method by preparing activity/activity diagrams at 127°C and 175°C for the K_2O - Al_2O_3 - SiO_2 - H_2O system (Figures 2 and 3). The details of the construction of Figures 2 and 3 are given in Chermak and Rimstidt (1989). The substitution of iron and magnesium into the montmorillonite and illite structure at 127 and 175°C causes less of a shift in the kaolinite-montmorillonite-illite triple points than at 25°C diagram (Chermak and Rimstidt 1989). Similar to the 298 K diagram the montmorillonite and illite are still metastable at 127 and 175 K.

CONCLUSIONS

The technique presented here is a simple and effective way to estimate the ΔG_f^o of silicate minerals at high temperatures. The only data needed for this estimation technique are the chemical composition and the coordination of the "building block" polyhedra in the

Table 5. ΔG_f^o data used in the calculation of the K_2O-Al_2O_3-SiO_2-H_2O diagrams.

Species	Chemical formula	ΔG_f^o (400 K) kJ·mol^{-1}	ΔG_f^o (448 K) kJ·mol^{-1}
1 Kaolinite	$Al_2Si_2O_5(OH)_4$	-3689.9	-3638.1
2 Pyrophyllite	$Al_2Si_4O_{10}(OH)_2$	-5141.3	-5080.7
3 Microcline	$KAlSi_3O_8$	-3664.6	-3627.5
4 Muscovite	$KAl_2(Si_3Al)O_{10}(OH)_2$	-5471.3	-5410.3
5 Water	H_2O	-221.0	-213.5
6 Silicic acid	H_4SiO_4	-1258.3	-1234.6
7 Magnetite	Fe_3O_4	-977.7	-962.2
8 Hematite	Fe_2O_3	-714.9	-702.4
9 Brucite	$Mg(OH)_2$	-802.3	-787.8
10 Potassium ion	K^+	-292.4	-297.01
11 Illite (Al)	$K_{0.75}Al_2(Si_{3.25}Al_{0.75})O_{10}(OH)_2$	-5380.0	-5319.1
12 Mont. (Al)	$K_{0.3}Al_{1.9}Si_4O_{10}(OH)_2$	-5153.4	-5092.4
13 Illite (Mg)	$K_{0.75}Al_{1.75}Mg_{0.25}(Si_{3.50}Al_{0.50})O_{10}(OH)_2$	-5335.1	-5274.7
14 Mont. (Mg)	$K_{0.30}Al_{1.70}Mg_{0.30}Si_4O_{10}(OH)_2$	-5179.4	-5118.5
15 Illite (Fe^{2+})	$K_{0.75}Al_{1.75}Fe_{0.25}(Si_{3.50}Al_{0.50})O_{10}(OH)_2$	-5250.3	-5190.5
16 Mont.(Fe^{2+})	$K_{0.30}Al_{1.70}Fe_{0.30}Si_4O_{10}(OH)_2$	-5077.6	-5017.5

Sources: 1-4, 5, 7, 8 and 9 Robie et al. (1978); 6 Rimstidt (1984); 10 Naumov (1974); and 11-16 this model.

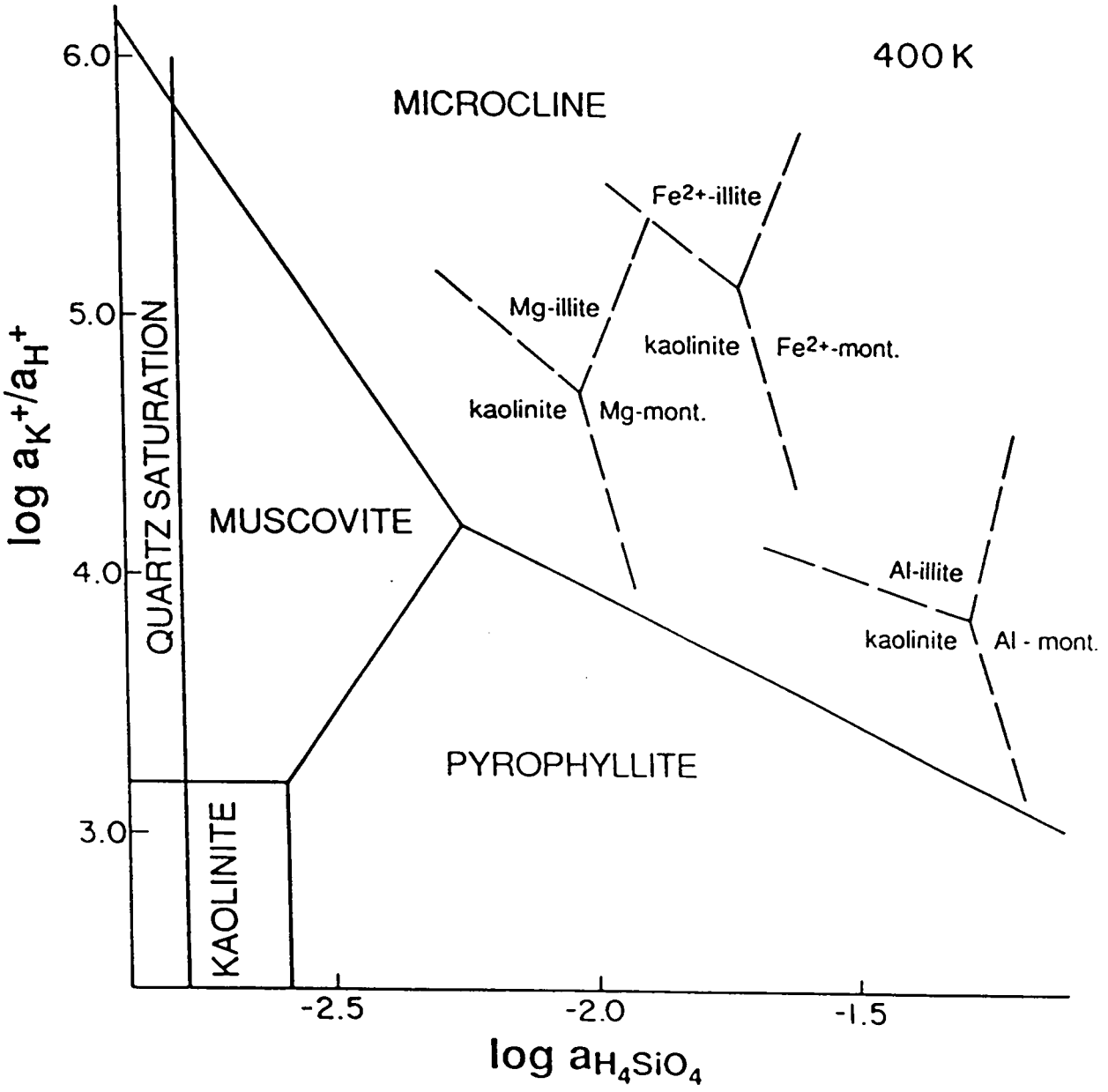

Fig. 2. Activity-activity diagram of the K_2O-Al_2O_3-SiO_2-H_2O system at 400 K. This diagram also shows the effect of Mg^{2+} and Fe^{2+} substitution on the stability of the kaolinite-montmorillonite-illite triple point.

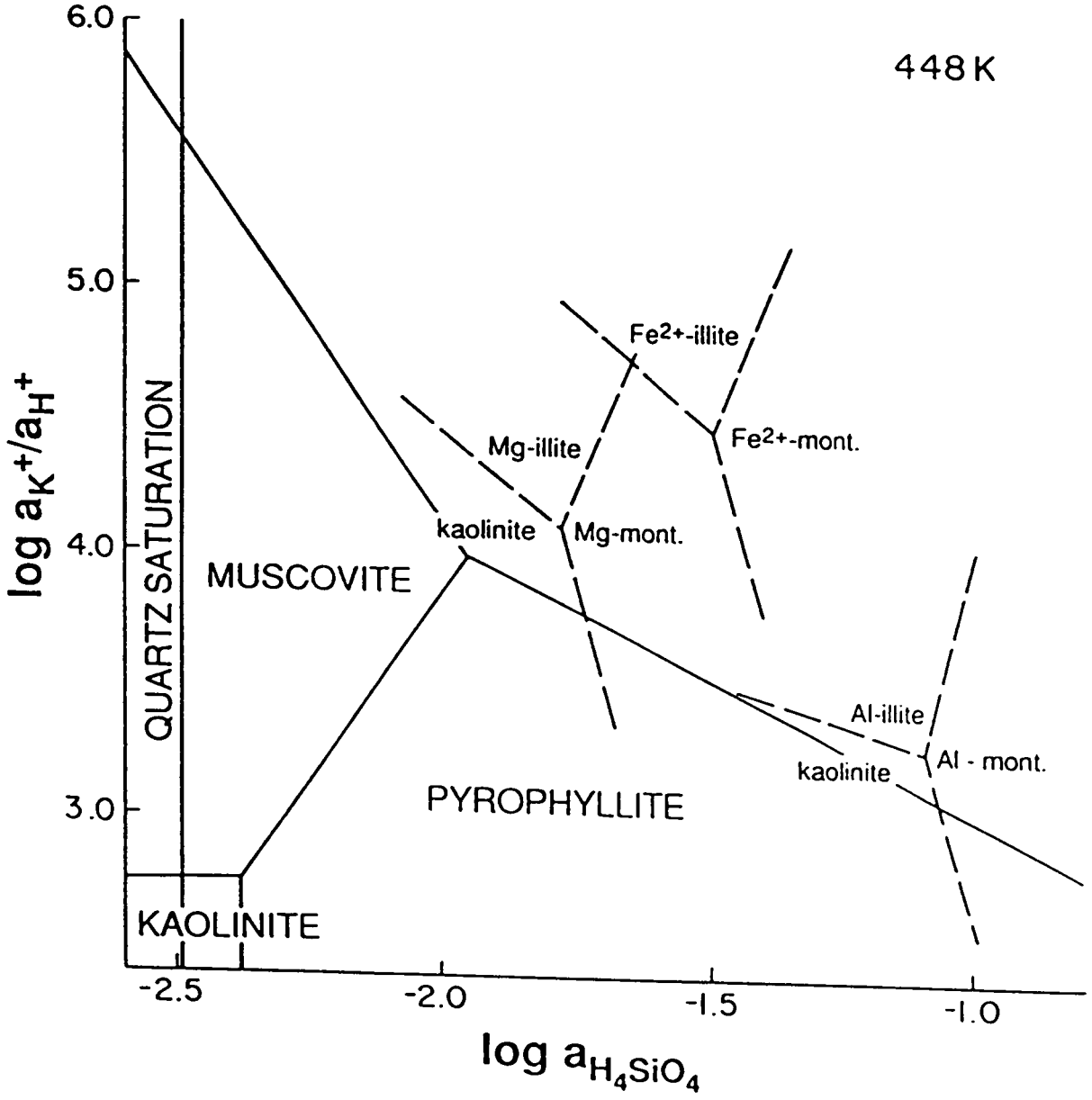

Fig. 3. Activity-activity diagram of the K_2O-Al_2O_3-SiO_2-H_2O system at 448 K. This diagram also shows the effect of Mg^{2+} and Fe^{2+} substitution on the stability of the kaolinite-montmorillonite-illite triple point.

mineral of interest. The approximate error associated with temperature estimates below ≈650 K ΔG_f^o is 0.25%. Estimates above temperatures of ≈650 K will likely have associated uncertainties > 0.5 %.

Although this technique seems to give reliable results for most cases, it should be used with some caution. There is no question that experimentally determined thermodynamic data are more accurate than these estimates and should be used when available. Furthermore, the user should always consider whether the predictions of this approach make sense in terms of their geologic/geochemical experience. Also note the other caveats discussed in Chermak and Rimstidt (1989).

In general, this technique to estimate the free energy of formation of silicate minerals is simple and reasonably accurate. This technique allows one to estimate values for the gibbs free energy of formation of minerals at higher temperatures since high temperature thermodynamic data is scarce or nonexistent . In addition the model could be expanded to a much wider range of compositions by adding minerals containing other components such as Li_2O, BeO, SrO, or $Fe(OH)_3$ to the regression data set.

REFERENCES

Aagaard P. and Helgeson H. C. (1983) Activity/composition relations among silicates and aqueous solutions: II. Chemical and thermodynamic consequences of ideal mixing of atoms on homological sites in montmorillonites, illites, and mixed layer clays, Clays and Clay Minerals 31, p. 207-217.

Bailey S. W. (1988) Micas, Reviews in Mineralogy 13, 583.

Berman, R.G., Brown, T.H., and Greenwood, H.J. (1985) An internally consistent thermodynamic data base for the minerals in the system Na_2O-K_2O-CaO-MgO-FeO-Fe_2O_3-Al_2O_3-SiO_2- TiO_2-H_2O-CO_2 . Atomic Energy of Canada Limited, Technical Record Tr-377.

Bethke C. M. and Altaner S. P. (1986) Layer-by-layer mechanism of smectite illitization and application to a new rate law. Clays and Clay Minerals 34, 136-145.

Bloss, F.D., Gunter, M., Su, S.C., and Wolfe, H.E. (1983) Gladstone-Dale constants: a new approach. Canadian Mineralogist, 21, 93-99.

Boles, J. R. (1977) Zeolites in low-grade metamorphic rocks. Mineralogical Society of America Reviews in Mineralogy, #4, F. A. Mumpton, Editor, 117-132.

Boles J. R. and Franks S.G. (1979) Clay diagenesis in the Wilcox sandstones of Southwest Texas: Implications of smectite diagenesis on sandstone cementation. Journal of Sedimentary Petrology, 49, p. 55-69.

Carson, C.D., Kittrick, J.A., Dixon, J.B., and McKee, T.R. (1976) Stability of soil smectite from a Houston black clay. Clays and Clay minerals, 24, 151-155.

Chaterjee, N. (1987) Evaluation of thermochemical data on Fe-Mg olivine, orthopyroxene, spinel, and Ca-Fe-Mg-Al garnet. Geochimica et Cosmochimica Acta, 51, 2515-2525.

Chen, C-H. (1975) A method of estimation of standard free energies of formation of silicate minerals at 298.15°K. American Journal of Science, 275, 801-817.

Chermak, J. A., and Rimstidt, J.D. (1989) Estimating the thermodynamic properties (ΔG^0_f and ΔH^0_f) of silicate minerals at 298K from the sum of polyhedral contributions. American Mineralogist 74, 1023-1031.

Clemens, J.D., Circone, S., Navrotsky, A., and McMillan, P.F. (1987) Phlogopite: High temperature solution calorimetry, thermodynamic properties, Al-Si and stacking disorder, and phase equilibria. Geochimica et Cosmochimica Acta, 51, 2569-2578.

Curtis C. D. (1978) Possible links between sandstone diagenesis and depth related geochemical reactions occurring in enclosed mudstones. Journal Geological Society of London 135, p. 107-117.

DeKimpe C. and Gastuche M. C. (1964) Low-temperature synthesis of kaolin minerals. American Mineralogist 49, p. 1-16.

Dunoyer de Segonzac G. D. (1970) The transformation of clay minerals during diagenesis and low-grade metamorphism: A review. Sedimentology 15, p. 281-346.

Donahoe, R.J., Hemingway, B.S., and Liou, J.G. (1989) Thermochemical data for merlionite: low temperature heat capacities and entropy at 298.18 K of six synthetic samples having varying Si-Al and Na-(Na+K) ratios. American Mineralogist.

Donahoe, R.J., Hemingway, B.S., and Liou, J.G. (1989) Thermochemical data for merlionite: low temperature enthalpies of formation at 298.18 K of six synthetic samples having varying Si-Al and Na-(Na+K) ratios. American Mineralogist.

Donahoe, R.J., Hemingway, B.S., and Liou, J.G. (1989) Thermochemical data for merlionite: low temperature free energies at 298.18 K of six synthetic samples having varying Si-Al and Na-(Na+K) ratios. American Mineralogist.

Eberl D. and Hower J. (1976) Kinetics of illite formation. Geological Society of America Bulletin 87, p. 1326-1330.

Giggenbach W. F. (1985) Construction of thermodynamic stability diagrams involving dioctahedral potassium clay minerals, Chemical Geology 49, 231-242.

Harder H. (1978) Synthesis of iron layer silicate minerals under natural conditions. Clays and Clay Minerals 26, p. 65-72.

Hay, R.L. (1986) Geologic occurrence of zeolites and some associated minerals. Pure and Applied Chemistry, 58, #10, 1339-1342.

Hazen, R.M. (1985) Comparative Crystal chemistry and the polyhedral approach. In Microscopic and Macroscopic, Reviews in Mineralogy, 14, Keiffer S.W., and Navrotsky A., Editors, 317-345.

Hazen, R.M. (1988) A Useful Fiction: Polyhedral modelling of mineral properties. American Journal of Science, 288-A, 242-269.

Helgeson, H. C.,Kirkham, D. H., and Flowers, G. C. (1981) Theoretical prediction of the thermodynamic behavior of aqueous electrolytes at high pressures and temperatures: IV. Calculation of activity coefficients, osmotic coefficients, and apparent molal and standard and relative partial molal properties to 600°C and 5kb. American Journal of Science, 281, 1249-1516p.

Helmhold K. P. and van de Kamp P. C. (1985) Diagenetic mineralogy and controls on albitization and laumontite formation in Paleogene arkoses, Santa Ynez Mountains, California. Clastic Diagenesis, AAPG Memoir 37, p. 239-276.

Hemingway, B.S. (1982) Thermodynamic properties of calcium aluminates. Journal of Physical Chemistry, 86, 2802-2803.

Hemingway, B.S., Haas, J. L. Jr., and Robinson, G. R. Jr. (1982) Thermodynamic properties of selected minerals in the system Al_2O_3-CaO-SiO_2-H_2O at 298.15 K and 1bar pressure and at higher temperatures. U.S. Geological Survey Bulletin 1544.

Hemley J. J. (1959) Some mineralogical equilibria in the system K_2O-Al_2O_3-SiO_2-H_2O, American Journal of Science 257, p. 241-270.

Hemley, J.J., Montoya, J.W., Marinenko, J.W., and Luce, R.W. (1980) Equilibria in the system Al_2O_3-SiO_2-H_2O and some general implications for alteration/ mineralization processes. Economic Geology, 75, 210-228.

Hess P. C. (1966) Phase equilibria of some minerals in the K_2O-Na_2O-Al_2O_3-SiO_2-H_2O system at 25°C and 1 atmosphere, American Journal of Science 264, p. 289-309.

Hill Jr. C. G. (1977) An Introduction to Chemical Engineering Kinetics and Reactor Design. John Wiley and Sons, New York, 594 pp.

Hiltabrand R. R. Ferrell R. E. and Billings G. K. (1973) Experimental diagenesis of Gulf Coast argillaceous sediment. AAPG Bulletin 57, p. 338-348.

Holland, T.J.B. (1989) Dependence of entropy on volume for silicate and oxide minerals: A review and a predictive model. American Mineralogist, 74, 5-13.

Howard J. J. and Roy D. M. (1985) Development of layer charge and kinetics of experimental smectite alteration. Clays and Clay Minerals 33, 81-88.

Huang, W.H., and Kellar, W.D. (1973) Gibbs free energies of formation calculated from dissolution data using specific mineral analyses-III. Clay minerals. American Mineralogist 58, 1023-1028.

Huang W. L. Bishop A. M. and Brown R. W. (1986) The effect of fluid/rock ratio on feldspar dissolution and illite formation under reservoir conditions. Clay Minerals 21, 585-601.

Hutcheon I. Oldershaw A. and Ghent E. D. (1980) Diagenesis of Cretaceous sandstones of the Kootenay formation at Elk Valley (Southeastern B.C.) and Mt. Allan (S.W. Alberta). Geochemica et Cosmochimica Acta 44, p. 1425-1435.

Iijima, A. (1978) Geological occurrences of zeolite in marine environments. Natural Zeolites, Occurrence, Properties and Use. Sand L.B. and Mumpton F.A. Eds., Pergamon Press, 175-198.

Johnson, G.K., Flotow, H.E., and O'Hare, P.A.G. (1983) Thermodynamic studies of zeolites: natrolite, mesolite and scolecite. American Mineralogist, 68, 1134-1145.

Johnson, G.K., Tasker, I.R., and Flotow, H.E.(1986) Thermodynamic studies of zeolites: mordenite and dehydrated mordenite. Clay Mineral Society Abstracts, Jackson, Mississippi, p. 18.

Karpov, I.K., and Kashik, S.A. (1968) Computer calculation of standard isobaric-isothermal potentials of silicates by multiple regression from a crystallochemical classification. Geochemistry International, 5, 706-713.

Kisch H. J. (1983) Mineralogy and petrology of burial diagenesis (burial metamorphism) and incipient metamorphism in clastic rocks. In Larsen , G. and Chilanger, G.V. (eds.) Diagenesis in Sediments and Sedimentary Rocks 2, Elsevier, Amsterdam, p. 289-493.

Kittrick, J.A. (1971a) Stability of montmorillonites-I. Belle Fourche and clay spur montmorillonite. Soil Science Society of America Proceedings, 35, 140-145.

Kittrick, J.A. (1971b) Montmorillonite equilibria and the weathering environment. Soil Science Society of America Proceedings, 35, 815-820.

Kittrick, J.A. (1971c) Stability of montmorillonites-II. Aberdeen montmorillonite. Soil Science Society of America Proceedings, 35, 820-823.

Kittrick, J.A. (1982) Solubility of two high-Mg and two high-Fe chlorites using multiple equilibria. Clays and Clay Minerals, 30, 167-179.

Kittrick, J.A. (1984) Solubility measurements of phases in three illites. Clays and Clay Minerals, 32, 115-124.

Krupka, K.M., Robie, R.A., and Hemingway, B.S. (1979) High-temperature heat capacities of corundum, periclase, anorthite, $CaAl_2Si_2O_8$ glass, muscovite, pyrophyllite, $KAlSi_3O_8$ glass, grossular, and $NaAlSi_3O_8$ glass. American Mineralogist, 64, 86-101.

Kubaschewski, O. and Alcock, C.B. (1979) Metallurgical Thermochemistry. Permagon Press Inc..

Kulbicki G. and Millot G. (1969) L'evolution de la fraction argileuse des gres petroliers cambro-ordoviciens du Sahara central. Bull. Serv. Carte Geol. Alsace-Lorraine 13, p. 147-156 (in French).

La Iglesia, A., and Aznar, A.J. (1986) A method of estimating the Gibbs energies of formation of zeolites. Zeolites 6, 26-29.

Levenspeil O. (1972) Chemical Reaction Engineering, 2nd ed.. John Wiley and Sons, New York, 578 pp.

Makarov, T.I., Sidorov, Y.I., and Naumov, V.B. (1984) Formation conditions for iron minerals in ultrabasic-alkali metasomites. Geochemistry International, 21, 148-160.

Mattigod, S.V., and Sposito, G. (1978) Improved method for estimating the standard free energies of formation ($\Delta G_{f\,298.15}$) of smectites. Geochimica et Cosmochimica Acta, 42, 1753-1762.

Misra, U.K., and Upchurch, W.J. (1976) Free energy of formation of beidellite from apparent solubility measurements. Clays and Clay Minerals, 24, 327-331.

Miyano, T., and Klein, C. (1983) Phase relations of orthopyroxene, olivine, and grunerite in high-grade metamorphic iron-formation. American Mineralogist, 68, 699-716.

Naumov, G.B., Ryzhenko, B.N., and Khodakovski, I.L. (1974) Handbook of Thermodynamic Data. N.T.I.S. Report No. U.S. Geological Survey-WRD-74-001.

Nordstrom, D.K., Valentine, S.D., Ball, J.W., Plummer, L.N., and Jones, B.F. (1984) Partial compilation and revision of basic data in the WATEQ programs. U.S. Geological Survey Water-Resources Investigation Report 84-4186, 10-14.

Nordstrom, D. K., and Munoz, J. L., (1985) Geochemical Thermodynamics. The Benjamin/Cummings Publishing Co., Inc., 477pp.

Nriagu, J.O. (1975) Thermochemical approximations for clay minerals. American Mineralogist, 60, 834-839.

O'Hare, P.A.G., Johnson, G.K., Tasker, I.R., Howell, D.A., and Wise, W.S. (1986) Thermochemistry of geothermal materials. U.S. Department of Energy, Summaries of Physical Research in the Geosciences, 5-6.

Rimstidt J. D. and Barnes H. L. (1980) The kinetics of silica-water reactions, Geochemica et Cosmochimica Acta 44, p. 1683-1699.

Rimstidt, J.D. (1984) Quartz solubility at low temperatures. GSA Programs with Abstracts, 16(6), 635.

Rimstidt J. D. and DOVE P. M. (1986) Mineral/solution reaction rates in a mixed flow reactor: Wollastonite Hydrolysis, Geochemica et Cosmochimica Acta 50, p. 2509-2516.

Roberson H. E. and Lahann R. W. (1981) Smectite to illite conversion rates: Effects of solution chemistry. Clays and Clay Minerals 29, 129-135.

Robie, R.A., Bin, Z., Hemingway, B.S., and Barton, M.D. (1987) Heat capacity and thermodynamic properties of andradite garnet, $Ca_3Fe_2Si_3O_{12}$, between 10 and 1000 K and revised values for $\Delta G°_f$ (298.15 K) of hedenbergite and wollastonite. Geochimica et Cosmochimica Acta, 51, 2219-2224.

Robie, R.A., Hemmingway, B.S., and Fischer, J.R. (1978) Thermodynamic properties of minerals and related substances at 298.15 K and 1 bar pressure and at higher temperatures. U.S. Geological Survey Bullein 1452.

Robinson, G.R., Jr., and Haas, J.L., Jr. (1983) Heat capacity, relative enthalpy, and calorimetric entropy of silicate minerals: an empirical method of prediction. American Mineralogist, 68, 541-553.

Sass, B.M., Rosenberg, P.E., and Kittrick, J.A. (1987) The stability of illite/smectite during diagenesis: An experimental study. Geochimica et Cosmochimica Acta, 51, 2103-2115.

Savin, S.M., and Lee, M. (1988) Isotopic studies of phyllosilicates. Hydrous Phyllosilicates, Bailey S.W. Ed., Reviews in Mineralogy, 19, 189-219.

Senkayi, A.L., Ming, D.W., Dixon, J.B., and Hossner, L.R. (1987) Kaolinite, opal CT, and clinoptilolite in altered tuffs interbedded with lignite in the Jackson Group, Texas. Clays and Clay Minerals, 35, 281-290.

Sheppard, R.A., and Gude 3d, A.J. (1973) Zeolite and associated authigenic silicate minerals in tuffaceous of the big sandy formation. U.S. Geological Survey Professional Paper, 830.

Senkayi, A. L., Ming, D. W., Dixon, J. B., and Hossner, L. R. (1987) Kaolinite, opal CT, and clinoptilolite in altered tuffs interbedded with lignite in the Jackson Group, Texas. Clays and Clay Minerals, 35, 281-290.

Sheppard, R. A., and Gude III, A. J. (1973) Zeolite and associated authigenic silicate minerals in tuffaceous of the big sandy formation. U.S. Geological Survey Professional Paper, 830.

Smyth, J.R., and Bish, D.L. (1988) Crystal Structures and Cation Sites of the Rock Forming Minerals. Allen and Unwin, Boston.

Sposito, G. (1986) The polymer model of thermochemical clay mineral stability, Clays and Clay Minerals, 34, 198-203.

Stoessel, R.K. (1988) 25°C and 1 atm dissolution experiments of sepiolite and kerolite. Geochimica et Cosmochimica Acta, 52, 365-374.

Tardy, Y., and Garrels, R.M. (1974) A method of estimating the Gibbs energies of formation of layer silicates. Geochimica et Cosmochimica Acta, 38, 1101-1116.

Tardy, Y., and Garrels, R.M. (1976) Prediction of Gibbs energies of formation -I. Relationships among Gibbs energies of formation of hydroxides, oxides and aqueous ions. Geochimica et Cosmochimica Acta, 40, 1051-1056.

Tardy, Y., and Garrels, R.M. (1977) Prediction of Gibbs energies of formation -II. Monovalent and divalent metal silicates. Geochimica et Cosmochimica Acta, 41, 87-92.

van Olphen H. and Fripiat J. J. (1979) Data handbook for clay materials and other non-metallic minerals. Pergamon Press, 346 pp.

Viellard, P., and Tardy, Y. (1988) Estimation on enthalpies of formation of minerals based on their refined crystal structures. American Journal of Science, 997-1040.

Wagman, D.D., Evans, W.H., Parker, V.B., Schumm, R.H., Halow, I., Bailey, S.M., Churney, K.L., and Nuttall, R.L. (1982) The NBS tables of chemical thermodynamic properties. Journal of Physical and Chemical Reference Data, 11.

Whitney G. and Northrop H. R.(1988) Experimental investigation of the smectite to illite reaction: Dual reaction mechanisms and oxygen-isotope systematics. American Mineralogist 73, p. 77-90.

Zeng, Y., and Liou, J.G. (1982) Experimental investigation of yugawaralite-wairakite equilibrium. American Mineralogist, 67, 937-943.

APPENDIX I

EXPERIMENTAL DATA (BATCH REACTOR)

Stainless Steel 1 (SS1): 25 ml bombs, 300°C, 10 ml of 0.5 m KCl, 1 g well crystalline Georgia kaolinite (Gkaol) with a surface area (SA) = 9.2 m^2/g, 0.25 g Brazilian quartz (Bq) ranging from 0.42 - 0.05 mm, 1.86 g Wards microperthite potassium feldspar (kspar) ranging from 0.59 - 0.15 mm.

time, hours	pH
12.00	4.62
24.00	4.45
36.00	4.62
46.42	4.70
46.42	4.60
50.72	4.33
100.82	4.49
142.00	4.70
217.83	4.63
265.17	4.43
314.33	4.60
357.58	4.51
643.75	4.58
701.75	4.61
721.00	4.58
721.00	4.62
1436.33	4.68

comments - differential scanning calorimetry analysis (DSC), x-ray diffraction (XRD), and scanning electron microscopy (SEM), bombs were not shaken. Clay coatings on feldspar grains ≈ 65% conversion after 1436.33 hours.

SS2: 25 ml bombs, 300°C, 10 ml of 2.0 m KCl, 1 g Gkaol, 0.25 g Bq , 1.86 g kspar ranging from 0.59 - 0.15 mm and < 0.15 mm.

kspar 0.59 - 0.15 mm		kspar < 0.15 mm	
time, hours	pH	time, hours	pH
24.00	2.90	99.17	3.97
190.50	5.85	165.33	4.78
459.75	5.50	404.75	5.53
459.75	5.54	813.00	5.59
813.00	5.55		
813.00	5.56		

comments - differential scanning calorimetry analysis (DSC), x-ray diffraction (XRD), and scanning electron microscopy (SEM) bombs were not shaken. Etch pits on kspar, illite with booklike morphology, a lot of iron in solution (yellow), 100% conversion in 4 days.

SS3: 25 ml bombs, 250°C, 10 ml of 0.5 m KCl, 1 g Gkaol, 0.25 g Bq , 5.0 g kspar < 0.15 mm.

time, hours	pH
12.00	5.90
33.92	5.69
81.83	5.66
226.75	5.55
263.00	5.39
349.58	5.30
470.00	5.23
562.67	5.23

comments - differential scanning calorimetry analysis (DSC), x-ray diffraction (XRD), and scanning electron microscopy (SEM) bombs were not shaken.

Begin rotisserie experiments

SS4: 50 ml bombs, 300°C, 20 ml of 0.5 m KCl, 2 g Gkaol, 0.50 g Bq , 5.0 g kspar 0.59 - 0.42 mm.

time, hours	pH
12.00	4.31
37.58	4.36
85.25	4.46
111.00	4.50
216.00	4.83
278.50	4.77
668.00	4.95
1436.25	4.83
1436.25	4.81

comments - differential scanning calorimetry analysis (DSC), x-ray diffraction (XRD), and scanning electron microscopy, bombs were shaken, ≈ 55% conversion after 1436.25 hours.

SS5: 50 ml bombs, 300°C, 20 ml of 2.0 m KCl, 2 g Gkaol, 0.50 g Bq, 5.0 g kspar 0.59 - 0.42 mm.

time, hours	pH
12.33	3.41
36.33	4.50
48.00	4.90
60.67	5.33
69.25	5.43
97.25	5.48
111.75	5.79

comments - differential scanning calorimetry analysis (DSC), x-ray diffraction (XRD), and scanning electron microscopy, bombs were shaken, rates limited by kspar dissolution, yellow solution due to dissolved iron and x-ray evidence for presence in illite.

Begin using titanium bombs.

Ti1: 50 ml bombs, 305°C, 20 ml of 2.0 m KCl, 2 g Gkaol, 0.50 g Bq, 5.0 g kspar 0.59 - 0.42 mm.

time, hours	pH
24.00	2.14
96.00	1.97
167.50	1.88
274.00	1.84
545.50	1.65
788.00	1.62
788.00	1.60

comments - Large pH drop, rate limited by kspar dissolution.

Ti2: 50 ml bombs, 246°C, 20 ml of 0.5 and 2.0 m KCl, 2 g Gkaol, 0.50 g Bq, 5.0 g kspar 0.59 - 0.42 mm.

0.5 m KCl		2.0 m KCl	
time, hours	pH	time, hours	pH
4.25	3.72	4.25	3.52
16.75	3.60	16.75	3.46
24.00	4.08	24.00	3.62
43.45	3.56	43.45	3.30, 3.29
48.00	3.68	48.00	3.39
72.00	3.63	72.00	3.47
112.67	3.64	112.67	3.39
352.67	3.61	352.67	3.61

comments - pH data erratic.

Ti3: 50 ml bombs, 210°C, 20 ml of 0.5 and 2.0 m KCl, 2 g Gkaol, 0.50 g Bq, 5.0 g kspar 0.59 - 0.42 mm.

0.5 m KCl		2.0 m KCl	
time, hours	pH	time, hours	pH
360.00	3.96	360.00	3.56
840.00	3.68	840.00	3.64
1440.00	3.63	1440.00	3.83
3240.00	4.03	3240.00	3.76

comments - pH data erratic and changing with time.

Ti4: 50 ml bombs, 305°C, 20 ml of 0.5 and 2.0 m KCl, 2 g Gkaol, 0.50 g Bq, 5.0 g kspar 0.42 - 0.02 mm.
comments - large pH drop regardless of grain size of kspar; feldspar dissolution is rate-limiting.

Ti5: 50 ml bombs, 246°C, 25 ml of 0.5 and 2.0 m KCl, 0.3 g Gkaol

0.5 m KCl		2.0 m KCl	
time, hours	pH	time, hours	pH
2.00	4.81	2.00	5.18
4.15	4.55	4.00	4.62
		8.50	4.26

Ti6: 50 ml bombs, 307°C, 25 ml of 2.0 m KCl, 1.0 g Gkaol

time, hours	pH
2.00	3.43
2.00	3.43
4.75	3.13
4.75	3.14
7.00	2.84
9.00	2.66
11.00	2.49
13.00	2.32
22.75	2.13
26.00	2.11

comments - Nucleation problems indicated by an initially slow rate followed by a rapid increase in rate.

Ti7: 50 ml bombs, 307°C, 25 ml of 0.5 m KCl, 1.0 g Gkaol.

time, hours	pH
2.00	3.59
4.17	3.50
7.33	3.48

comments - Problems with seal, seven of ten bombs loaded leaked.

Ti8: 50 ml bombs, 307°C, 25 ml of 1.0 m KCl, 1.0 g Gkaol.

time, hours	pH
1.92	3.54
4.45	3.51
11.00	2.98
23.67	2.46

comments - Nucleation problems indicated by an initially slow rate followed by a rapid increase in rate.

Ti9: 50 ml bombs, 290°C, 25 ml of 2.0 m KCl, 1.0 g Gkaol.

time, hours	pH
2.00	3.50
5.00	3.36
8.00	3.23
11.00	3.12
13.75	3.06
23.00	2.63

comments - Nucleation problems indicated by an initially slow rate followed by a rapid increase in rate.

Ti10: 50 ml bombs, 289°C, 25 ml of 2.0 m KCl, 1.0 g Gkaol and 0.25 g Indian ruby muscovite (Irmusc) SA = 1.20 m^2/g.

time, hours	pH
0.25	3.52
2.00	3.22
3.50	3.10
4.00	3.11
5.00	3.03
7.75	2.95
11.08	2.84
23.00	2.64
72.00	2.21
72.00	2.20
167.75	2.06

comments - Begin good rate data, the decrease in pH with time indicates that the kaolinite --> muscovite/illite reaction is occurring.

Ti11: 50 ml bombs, 289°C, 25 ml of 1.0 m KCl, 1.0 g Gkaol and 0.25 g Irmusc.

time, hours	pH
1.00	3.64
3.92	3.36
6.00	3.28
9.08	3.16
20.50	3.01
31.00	2.89
71.50	2.65
167.00	2.45
167.00	2.43

comments - Good rate data.

Ti12, 13: 50 ml bombs, 289°C, 25 ml of 0.5 m KCl, 1.0 g Gkaol and 0.25 g Irmusc.

time, hours	pH
1.50	3.64
4.50	3.38
8.87	3.26
11.50	3.24
22.25	3.18
71.50	2.93
167.00	2.77
167.00	2.76

comments - Good rate data.

Ti14: 50 ml bombs, 289°C, 25 ml of 4.0 m KCl, 1.0 g Gkaol and 0.25 g Irmusc.

time, hours	pH
1.00	3.29
1.00	3.28
2.95	3.02
5.00	2.88
7.83	2.68
18.08	2.21
25.72	2.00
91.00	1.52

comments - Problems with KCl precipitation due to the high salt concentration.

Experiments conducted to try to determine the rate of the reverse reaction.

Ti15: 50 ml bombs, 289°C, 25 ml of 0.5 m KCl, 0.1 N HCl and 0.1 N HCl, 1.0 g Gkaol and 0.25 g Irmusc.

0.5 m KCl, 0.1 N HCl		0.1 N HCl	
time, hours	pH	time, hours	pH
4.00	1.63	4.00	1.37
23.00	1.60	23.00	1.55
69.50	1.61, 1.64	96.02	1.67
145.92	1.68	145.92	1.67

comments - pH increased with time, KCl in solution seems to inhibit reaction.

Ti16: 50 ml bombs, 289°C, 25 ml of 0.001 m HCl, 1.0 g Gkaol.

time, hours	pH
3.83	3.33
23.00	3.34
69.50	3.33

comments - pH of the solution remains constant, ICP data given in text.

Ti17: 50 ml bombs, 307°C, 25 ml of 2.0 m KCl, 1.0 g Gkaol and 0.25 g Irmusc.

time, hours	pH
2.50	3.08
3.75	3.02
5.00	2.94
6.75	2.70
8.00	2.58
12.00	2.44
20.25	2.18
61.00	1.91
118.50	1.80

comments - good rate data.

Ti18: 50 ml bombs, 289°C, 25 ml of 0.01 and 0.1m HCl, 1.0 g Gkaol.

0.01m HCl		0.1 m HCl	
time, hours	pH	time, hours	pH
3.00	2.16	3.00	1.14
24.00	2.16	24.00	1.16
		48.00	1.21

comments - pH of the solution remains constant, ICP data given in text.

Ti19: 50 ml bombs, 307°C, 25 ml of 0.5 m KCl, 1.0 g Gkaol and 0.25 g Irmusc.

time, hours	pH	Si, ppm	Al, ppm
1.13	3.54	n.d.	n.d.
2.50	3.41	n.d.	n.d.
3.00	3.34	187.9	2.98
3.75	3.28	n.d.	n.d.
5.00	3.21	n.d.	n.d.
6.167	3.23	n.d.	n.d.
9.00	3.13	208.0	2.32
12.08	3.06	n.d.	n.d.
15.63	3.00	225.6	2.01
23.75	2.92	n.d.	n.d.
99.00	2.76	126.6	2.48
266.50	2.55	146.2	3.22

n.d. - not determined
comments - Not used in rate analysis; Silica concentration decreased with time after 16 hours, probably due to formation of a kspar or amorphous phase.

Ti20: 50 ml bombs, 307°C, 25 ml of 0.1 m HCl, 1.0 g Gkaol and 0.25 g Irmusc.

time, hours	pH
2.50	1.40
4.00	1.27
6.67	1.36
19.59	1.46

comments - pH of solution unstable and constantly changing; kspar identified in run products by x-ray diffraction.

Ti21: 50 ml bombs, 307°C, 25 ml of 0.1 and 0.01 m HCl, 0.5 g Gkaol and 3.0 g Irmusc.

0.1 m HCl		0.01 m HCl	
time, hours	pH	time, hours	pH
3.00	1.43	3.00	2.87
7.25	1.40	7.25	2.98
47.17	1.62	22.83	3.24
		47.17	3.35

comments - pH of solution unstable and constantly decreasing with time after quench; kspar identified in run products by x-ray diffraction.

Ti22: 50 ml bombs, 307°C, 25 ml of 0.001 and 0.0001 m HCl, 0.5 g Gkaol and 2.0 g Irmusc.

0.001 m HCl		0.0001 m HCl	
time, hours	pH	time, hours	pH
4.25	4.58	4.00	5.07
20.00	4.40	20.00	5.61
		122.50	5.03

comments - pH of solution unstable and constantly decreasing with time after quench; kspar identified in run products by x-ray diffraction.

Ti23: 50 ml bombs, 307°C, 25 ml of 0.0001 and 0.00001 m HCl, 0.5 g Gkaol, 0.5 g Bq and 2.0 g Irmusc.

0.0001 m HCl		0.00001 m HCl	
time, hours	pH	time, hours	pH
2.15	5.40	2.15	5.41
4.00	5.26	4.00	5.41
7.75	5.10	7.75	5.42
		18.50	5.37

comments - pH of solution fairly constant.

Ti24: 50 ml bombs, 307°C, 25 ml of 0.01 m HCl and 0.5KCl, 0.5 g Gkaol, 0.5 g Bq and 2.0 g Irmusc.

time, hours	pH
1.50	2.27
3.25	2.27
8.00	2.26
22.00	2.28

comments - pH of solution fairly constant.

Ti25: 50 ml bombs, 275°C, 25 ml of 2.0 m KCl, 1.0 g Gkaol and 0.25 g Irmusc.

time, hours	pH
2.00	3.41
4.00	3.31
7.08	3.21
10.00	3.10
13.00	3.02
23.50	2.86
29.92	2.82
167.50	2.40
217.25	2.32

comments - good rate data.

Ti26: 50 ml bombs, 275°C, 25 ml of 0.5 m KCl, 1.0 g Gkaol and 0.25 g Irmusc.

time, hours	pH
2.92	3.67
4.50	3.58
7.17	3.50
10.92	3.43
20.66	3.37
118.00	3.12

comments - good rate data.

Ti27: 50 ml bombs, 275°C, 25 ml of 0.0001 and 0.00001 m HCl, 0.5 g Gkaol, 0.5 g Bq and 2.0 g Irmusc.

0.0001 m HCl		0.00001 m HCl	
time, hours	pH	time, hours	pH
0.75	5.66	0.75	6.69
1.67	5.90	1.67	6.00
3.00	5.67	19.50	5.61
19.50	5.69		
19.50	5.64		

comments - pH data erratic.

Ti28: 50 ml bombs, 250°C, 25 ml of 2.0 and 0.5 m KCl, 1.0 g Gkaol and 0.25 g Irmusc.

2.0 m KCl		0.5 m KCl	
time, hours	pH	time, hours	pH
2.25	3.48	5.75	3.62
5.75	3.43	92.75	3.42
17.75	3.20	264.75	3.31
92.75	2.95		
188.00	2.77		
264.75	2.70		

comments - good rate data.

Ti29: 50 ml bombs, 250°C, 25 ml of 0.0001 and 0.00001 m HCl, 0.5 g Gkaol, 0.5 g Bq and 2.0 g Irmusc.

0.0001 m HCl		0.00001 m HCl	
time, hours	pH	time, hours	pH
1.00	5.88	1.00	6.13
23.00	5.54	23.00	5.44
69.50	5.48	69.50	5.44
74.00	5.22		

comments - pH data decreasing with time.

Experiments **Ti30** - **Ti33** were run with variable ratios of kaolinite to muscovite surface areas to test the effect of muscovite and kaolinite surface areas on the overall rate.

Ti30: 50 ml bombs, 289°C, 25 ml of 2.0 m KCl, 1.0 g Gkaol and 1.0 g Irmusc.

time, hours	pH
1.75	3.11
3.50	2.77
7.75	2.49
10.75	2.46
18.00	2.28

Ti31: 50 ml bombs, 289°C, 25 ml of 2.0 m KCl, 0.25 g Gkaol and 0.25 g Irmusc.

time, hours	pH
3.50	3.24
5.00	3.15
7.00	3.04
9.00	2.94
20.00	2.67

Ti32: 50 ml bombs, 289°C, 25 ml of 2.0 m KCl, 4.0 g Gkaol and 0.25 g Irmusc.

time, hours	pH
2.00	2.92
5.00	2.79
7.00	2.78
20.00	2.52

Ti33: 50 ml bombs, 289°C, 25 ml of 2.0 m KCl, 1.0 g Gkaol and 2.0 g Irmusc.

time, hours	pH
1.500	2.98
3.50	2.57
5.25	2.43
7.00	2.41
7.08	2.35
9.00	2.28

Teflon 1a: 25 ml, 93°C, 20 ml 0.5 m KCl, 1.0 g Gkaol and 0.25 g Irmusc.

time, hours	pH
115.5	3.82
283.75	3.96
501.5	4.14
4104.0	3.75
4104.0	3.84

comments - pH data fairly constant, long term experiments leaked slightly (≈ 5%), SEM revealed characteristic fibrous illite in 4104 hour experiments, this experiment confirms the low temperature synthesis of muscovite/illite.

Teflon 1b: 25 ml, 93°C, 20 ml 0.0001 m HCl, 0.5 g Gkaol and 2.0 g Irmusc.

time, hours	pH
115.5	5.11
283.75	5.08
501.5	5.12
4104.0	4.90

comments - long term experiment leaked slightly (≈ 5%), The reverse reaction (muscovite --> kaolinite) attempted but pH data fairly constant in **Teflon 1b -1d.**

Teflon 1c: 25 ml, 93°C, 20 ml 0.00001 m HCl, 0.5 g Gkaol and 2.0 g Irmusc.

time, hours	pH
115.5	5.16
283.75	5.10
501.5	5.13
4104.0	4.88

comments - pH data fairly constant, long term experiments leaked slightly (≈ 5%).

Teflon 1d: 25 ml, 93°C, 20 ml 0.0001 m HCl, 0.5 g Gkaol, 0.5 Bq and 2.0 g Irmusc.

time, hours	pH
115.5	5.11
283.75	5.12
501.5	5.20
4104.0	4.94

APPENDIX II

ENTROPY COEFFICIENTS

Entropy values for minerals can be estimated by using multiple linear regression (similar to the ΔG_f^o and ΔH_f^o models) by using the relation $S^o = \Sigma\, n_i\, s_i$ (25 minerals). The determined coefficients and residuals are given in the two tables that follow.

S_i (J/mol K) coefficient of each polyhedra.

Polyhedral unit	S_i coefficient	Standard Error Est.
Al_2O_3(4)	61.76	3.29
Al_2O_3(6)	33.04	4.47
$Al(OH)_3$(6)	77.80	3.38
SiO_2(4)	41.89	0.93
MgO(6)	27.08	1.77
$Mg(OH)_2$(6)	37.20	4.73
CaO(6)	47.23	1.48
CaO(8-Z)	32.08	1.76
Na_2O(8)	102.44	7.21
Na_2O(Z)	73.80	5.22
K_2O(8-12)	149.39	6.34
H_2O	49.10	1.69
FeO(6)	51.03	1.51
$Fe(OH)_2$(6)	83.94	2.22

Comparison of S°(measured) versus S°(predicted) for the 25 minerals used in the multiple linear regression model and the associated errors.

Mineral	S°(measured)	S°(predicted)	Residuals	% Residual
1 Kaolinite	203.05	198.52	4.53	2.23
2 Muscovite	306.4	305.13	1.27	0.41
3 Margarite	263.64	266.66	-3.02	1.15
4 Talc	260.8	258.90	1.90	0.73
5 Pyrophyllite	239.4	241.44	-2.04	0.85
6 Phlogopite	319.66	322.59	-2.93	0.92
7 Sanadine	232.90	231.24	1.66	0.71
8 Low albite	207.40	207.76	-0.36	0.17
9 Anorthite	199.30	192.76	6.54	3.28
10 Nepheline	124.35	123.99	0.36	0.29
11 FeSiO3	93.05	92.92	0.13	0.14
12 Fayalite	148.32	143.95	4.37	2.94
13 Tremolite	274.45	272.39	2.07	0.75
14 Diopside	143.09	142.93	0.16	0.11
15 Merwinite	253.13	252.55	0.58	0.23
16 Grossular	255.97	254.95	1.02	0.40
17 Grunerite	360.90	362.62	-1.72	0.48
18 Greenalite	304.4	302.69	1.81	0.59
19 Minnesotaite	350.8	353.56	-2.76	0.79
20 Clinoenstatite	67.86	68.96	-1.10	1.62
21 Forsterite	95.19	96.04	-0.85	0.89
22 Prehnite	292.74	298.01	-5.27	1.80
23 Natrolite	359.73	359.42	0.31	0.09
24 Mesolite	363.00	363.94	-0.94	0.26
25 Scolecite	367.42	366.80	0.62	0.17
			Average =	0.88

1, 4, 6, 7, 8, 9, 10, 11, 12, 13, 14, 15, 16, 20, and 21 Robie et al. (1978), 2, and 5 Krupka et al. (1979), 3, and 22 Hemingway et al. (1982), 17, 18, and 19 Miyano and Klein (1983), 23, 24, and 25 Johnson et al. (1983)

The vita has been removed from the scanned document